Modelling the ballast water distribution in the Arctic Ocean

by

Ingrid Linck Rosenhaim

A thesis submitted in partial fulfilment
of the requirements for the degree of

Doctor of Philosophy in Geosciences

Approved Dissertation Committee

Prof. Dr. Rüdiger Gerdes
(Jacobs University Bremen, Alfred Wegener Institute)
Prof. Dr. Laurenz Thomsen
(Jacobs University Bremen)
Prof. Ralf Brauner
(Jade University of Applied Sciences, Elsfleth)
Dr. Andreas Herber
(Alfred Wegener Institute)
Dr. Hiroshi Sumata
(Norwegian Polar Institute, Tromsø, Norway)
Dr. Kathrin Riemann-Campe
(Alfred Wegener Institute)

Date of Defense: March 29th, 2021

Department of Physics & Earth Sciences

Abstract

Ballast water is essential for a ship's safe navigation. It regulates maneuverability, trim, and compensates for weight changes during loading and unloading of cargo. Nevertheless, ballast water is considered one of the main vectors for the transfer of aquatic organisms worldwide. These transferred organisms can survive the voyage and ballast water discharge, reproduce and become invasive to the host environment, harming the local ecosystems and human health. With the decrease of sea ice extent in the Arctic seas, shipping has been increasing in the region, and it is expected to keep growing.

The aim of this study is to identify areas along the main Arctic shipping routes, where discharge of ballast water represents the risk of contamination to the local ecosystem. In order to examine quantitative assessment of the risk, a series of passive tracer experiments by a regional coupled ocean-sea ice model, NAOSIM (North Atlantic/Arctic Ocean Sea Ice Model) was conducted. The ballast water tracer is discharged in the model at selected real ship positions from 2013.

Analysis of ship-track density showed that, numerous vessels had their navigation routes on the continental shelf, in waters 200 m deep or less, and that navigation was restricted to the Atlantic end of the Northeast Passage for most of the year. Only during summer and beginning of autumn the Northeast Passage was navigated on its complete length.

The model results showed that the ballast water tracer starts to accumulate at the end of spring, with concentration increasing during summer and autumn. In the west Spitsbergen sector, the tracer is mainly transported polewards by the West Spitsbergen Current until it encounters the cold East Greenland Current, which then carries the tracer southwards. Water recirculation between south Spitsbergen and Bear Island creates an area of ballast water tracer accumulation. In the Barents Sea sector, the ballast water tracer starts to form accumulation south of Novaya Zemlya at the end of spring. Tracer concentration increase during summer and autumn. In autumn, a third area of ballast water tracer accumulation starts in the south Kara Sea, near the Kara Gate.

The Lagrangian particle trajectories demonstrated that organisms could be advected by the ocean surface currents to coastal ecosystem while presenting different pathways from the tracer. The ballast water tracer flow is mainly controlled by the currents and are highly seasonal. However, tracer mixing is enhanced by the turbulent horizontal flow and vertical convection, being dependent on the mixed-layer seasonality. Eddy kinetic energy is correlated to mixing of ballast water tracer, and to the displacement of particles along the trajectory pathways. Areas of ballast water tracer accumulation are indicators of high propagule pressure of non-indigenous species, increasing the chances of survival, reproduction, and establishment as invasive species.

Since September 2017, vessels navigating the Arctic waters should comply with the IMO Ballast Water Management Convention guidelines. It is expected that most vessels will be soon equipped with an on-board ballast water treatment system. Until then, vessels are required to perform mid-ocean ballast water exchange before arrival at the destination port.

Table of Content

Motivation

The Arctic Ocean and its shelf seas have been experiencing changes due to the warming climate. The sea ice cover is decreasing in extent and volume, compromising the habitats of different native species like polar bears as well as algae that grow underneath the sea ice. However, thinner and less sea ice is an advantage for shipping. The Arctic shipping routes are shorter connections between the North Atlantic and the Pacific Oceans than the routes crossing the Suez or Panama Canals. With an increase in the number of vessels navigating the Arctic shipping routes, the risk of aquatic invasions by non-indigenous species increases, and other threats like environmental contaminations by toxins, hydrocarbons, oil spills, and pathogens transferred within the ships' ballast water, too.

Several studies exist that are concerned with the transfer and introduction of non-indigenous organisms via ballast water, in regions like the Great Lakes and the continental shelves of North America's east and west coast. Other studies are species-specific due to their capability to harm the host environment and outcompete native species, cause economic and human health problems, and disrupt native fauna [*Griffiths et al.*, 1991]. Some studies are based on in situ experiments that use dyes to observe the dispersion and dilution rates of ballast water and associated organisms after discharge. For example, the study performed by *Wells et al.* [2011], releasing Rhodamine-WT dye and magnetic-attractive particles in the semi-enclosed Goderich Harbor in Ontario, Canada. There are also studies that use ocean circulation models to perform numerical simulations of the dispersion and mixing rate of ballast water after discharge. For example, *Larson et al.* [2003] simulated the spread of organisms discharged with the ballast water on specific areas destined for ballast water exchange at the coast of British Columbia and the adjacent offshore waters of the Washington coast. *Brickman* [2006] developed a semiquantitative risk assessment model for the dispersion of organisms discharged with ballast water during the exchange processes on shelf seas. The model simulated ballast water exchange along navigational tracks of the Scotian Shelf and Gulf of Maine, east coast of Canada.

In recent years, ship traffic in the Arctic routes has increased, despite the harsh climate and sea ice presence. The main maritime routes of the Arctic Ocean have been sea ice-free during more extended periods in summer, turning these northern connections between the North Atlantic and the Pacific Ocean more attractive to shipping. To date, numerical simulations concerning the dispersion of ballast water after discharge are abundant in temperate regions. Still, little to none has been done involving the Arctic Ocean and its shelf seas.

The study developed for this thesis starts closing this knowledge gap via numerically simulations of the spread of ballast water discharged by commercial vessels navigating the Arctic Ocean. Specifically, for this study a passive tracer is implemented in the North Atlantic/Arctic Ocean-Sea Ice Model NAOSIM [*Fieg et al.*, 2010; *Köberle and Gerdes*, 2003]. Ballast water discharge is numerically simulated based on a ship dataset containing information of vessel locations in the Arctic realm. This thesis's main objective is to identify areas of the Arctic shipping routes where ballast water discharge presents the risk of contamination to costal ecosystem.

This thesis is structured as follows: Chapter 1 presents the main characteristics of the Arctic Ocean, introduces the topic of ballast water and a short description of the Ballast Water Management Convention, and reviews the concept of non-indigenous and invasive species with examples. Chapter 2 outlines the objectives of the present study, describes the ship dataset and the applied regional ocean model NAOSIM, and lastly describes the experiments setup. Chapter 3 presents the results of ballast water tracer distribution, flow, and accumulation in the main sectors of the Northeast Passage. Chapter 4 presents the diagnostic results of individual particle advection and the influence of the eddy variability of the velocity field on the advection of particles and ballast water tracer mixing. Lastly, Chapter 5 presents a summary of the results presented in this thesis and an outlook for further investigations.

Chapter 1. Introduction

This chapter presents an overview of the Arctic Ocean and its characteristics, introduces the ballast water topic, and gives a short description of the Ballast Water Management Convention. It reviews the concept of non-indigenous and invasive species, presenting examples of known non-indigenous organisms in the Arctic and other regions of the globe.

1.1 Arctic Ocean

The Arctic Ocean is a relatively small (ca. 9.4 x 10^6 km^2 [*Rudels*, 2009]) enclosed ocean with extensive shelf areas and two deep central basins. It is separated from the North Atlantic by the Greenland-Scotland Ridge (ca. 500-850 m deep) and surrounded by the landmasses of Europe, Asia, and North America, and comprises the Greenland Sea, the Iceland Sea, and the Norwegian Sea, also called the Nordic Seas [*Jakobsson et al.*, 2004; *Rudels*, 2009; 2015]. It lies almost entirely north of the polar circle and occupies most of the area north of 66°33'N (Figure 1.1).

The two large basins form the deep Arctic Ocean, the Eurasian and the Amerasian basins, which are separated by the Lomonosov Ridge (at a depth of ca. 1600 m), that divides the deep-water masses. The Gakkel Ridge splits the Eurasian Basin into the Nansen and Amundsen basins. The Amerasian Basin is divided by the Alpha-Mendeleyev Ridge complex into the Makarov and Canada basins. The deepest is the Amundsen Basin, reaching ca. 4500 m deep. The other three basins have maximum depths of about 4000 m [*Jakobsson et al.*, 2004; *Rudels*, 2015].

Almost 53% of the Arctic Basin consists of shelf seas, composed by the wide and shallow shelf seas as the Barents Sea (200-300 m), the Kara Sea (50-100 m), the Laptev Sea (<50 m), the East Siberian Sea (<50 m) and the Chukchi Sea (50-100 m), and the narrow shelves north of North America and Greenland [*Rudels*, 2009; 2015]. The Arctic Ocean is connected to the North Atlantic by the Fram Strait and the Barents Sea, across the Greenland-Scotland Ridge and through the Canadian Arctic Archipelago, by the Baffin Bay and the Davis Strait, and to the North Pacific through the Bering Strait.

Atlantic waters enter the Arctic Ocean through the 2600-m-deep Fram Strait and the ca. 200-m-deep Barents Sea. The Fram Strait is the only passage that allows for water masses exchange in both ways (Atlantic-Arctic and Arctic-Atlantic). Outflows of Arctic waters occur through Fram Strait and the shallow (150-230 m) and narrow channels of the Canadian Arctic Archipelago. Most of the Arctic Ocean water masses are of Atlantic origin, but it also receives low-salinity Pacific waters through the shallow (50 m) and narrow (85 km) Bering Strait [*Jakobsson et al.*, 2004; *Rudels*, 2009; 2015].

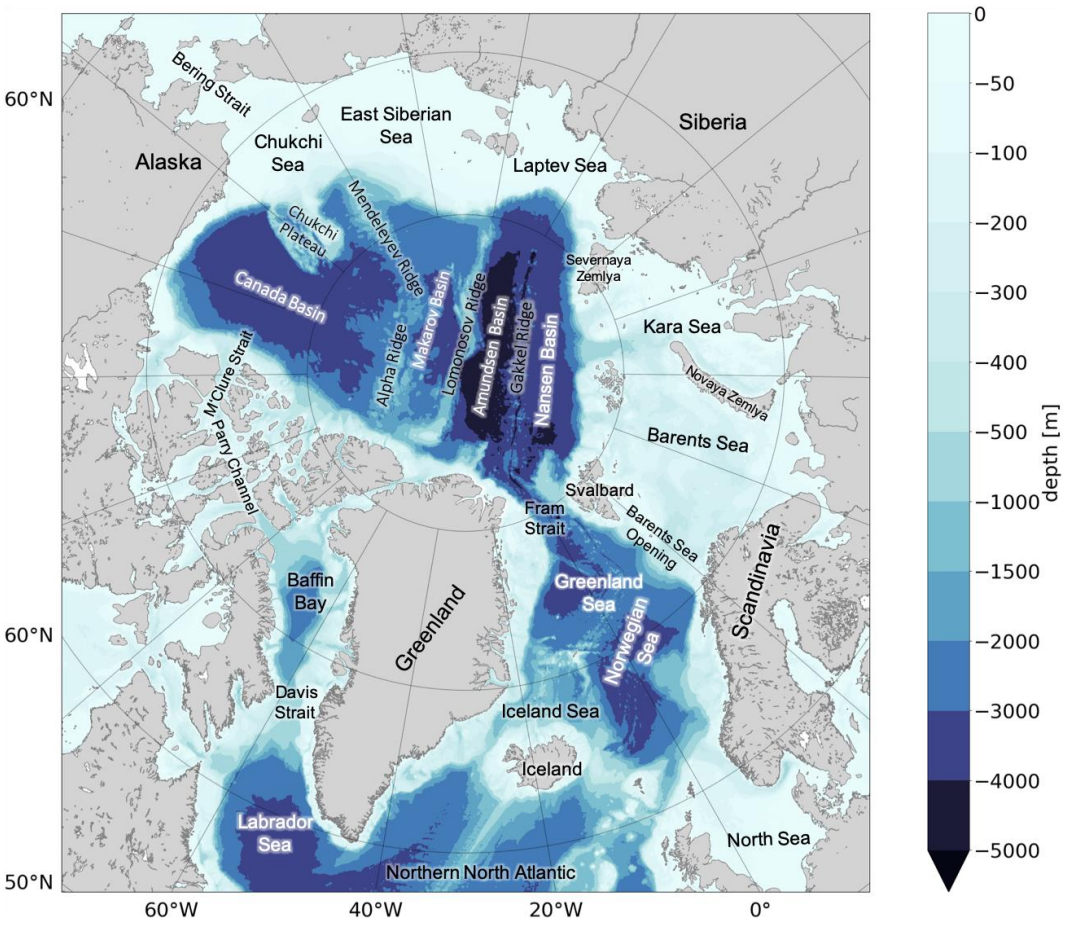

Figure 1.1: Arctic Ocean topography and geography features. The bathymetry is from the ETOPO1 Global Relief Model [*Amante and Eakins*, 2009].

The Arctic Ocean is salinity stratified. The stability of the upper layer suppresses mixing with the water beneath and allows the uppermost layer to be cooled to freezing temperature. In winter, sea ice forms and perseveres during the year in the central Arctic

Ocean (over the deep basins) [*Rudels*, 2015]. Salt rejection during freezing induces convection, taking high-salinity water down and bringing to the surface 'low-salinity' water. The melting and freezing cycle produces a low-salinity layer independent of other freshwater sources. The runoff of Siberian rivers is large enough to isolate the heat in the Atlantic water layer from the surface. That contributes to the formation and growth of sea ice, also on the continental shelves [*Aagaard et al.*, 1981; *Rudels*, 2009; 2015].

The polar mixed layer and the halocline are sustained by freshwater input from river runoff, sea ice melt, and the inflow of low-salinity water through the Bering Strait. The Canada Basin has the lowest surface salinity and the thickest halocline in the Arctic Ocean. In *Rudels* [2009] five vertical layers of the Arctic Ocean are simplistically distinguished. The upper one is the polar mixed layer followed by the halocline, the Atlantic layer, the intermediate waters, and the deep and bottom waters layer.

The polar mixed layer is the ca. 50 m thick upper layer, that is homogenized during winter due to sea ice formation, brine rejection, and haline convection. During summer, the uppermost 10-20 m becomes diluted due to sea ice melting. In the Canadian Basin, the salinity ranges between 30 and 32.5, and in the Eurasian Basin, between 32 and 34. The halocline extends from 100 to 250 m, where the salinity increases with depth, and the temperature remains close to freezing. The salinity range is between 32.5 and 34.5 [*Rudels*, 2009].

The Atlantic layer is 400-700 m thick. In this layer, the potential temperature remains above 0 °C, and the salinity range is between 34.5 and 35. Below the Atlantic water is the intermediate water layer. It circulates freely across the Lomonosov Ridge. Its potential temperature range is between -0.5 and 0 °C, and the salinity range between 34.87 and 34.92. The deep and bottom waters of the Canadian Basin have a salinity range between 34.91 and 34.96, and the potential temperature varies between -0.55 and -0.5 °C. The salinity of deep and bottom waters of the Eurasian Basin range between 34.92 and 34.945, and the temperature between -0.97 and-0.5 °C [*Rudels*, 2009].

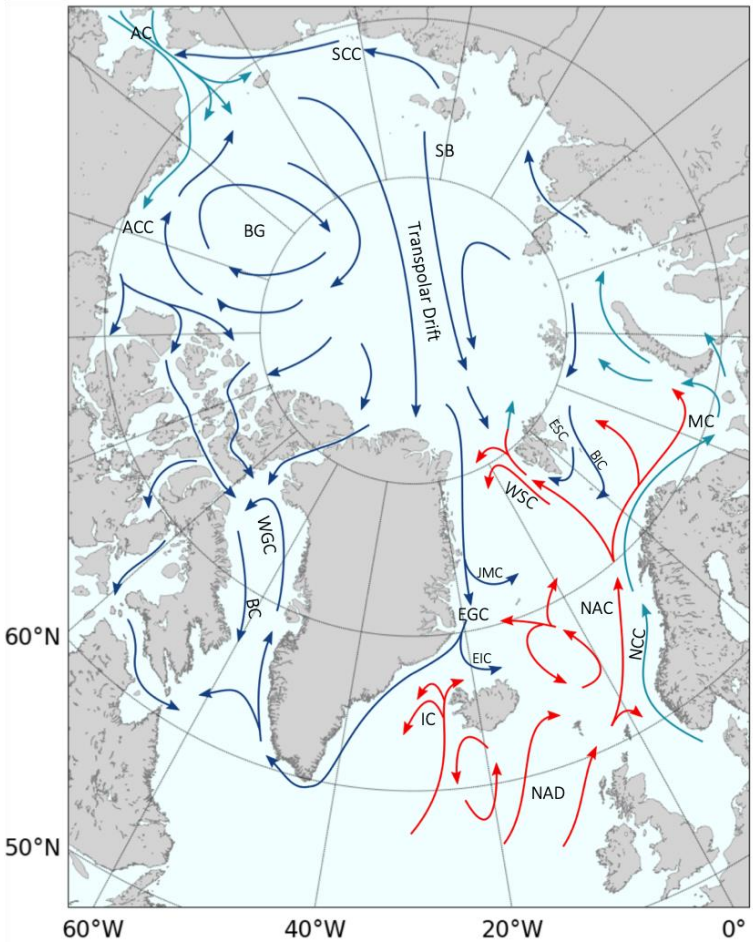

Figure 1.2: Arctic Ocean surface circulation. Red arrows indicate the warm Atlantic waters, the blue arrows the cold and less saline polar and arctic currents, and the greenish arrows represent the low salinity and transformed waters. The figure is based on [Rudels, 2009] and [Kovács, 2019]. AC: Anadyr Current; ACC: Alaskan Coastal Current; BC: Baffin Island Current; BIC: Bear Island Current; BG: Beaufort Gyre; EGC: East Greenland Current; EIC: East Iceland Current; ESC: East Spitsbergen Current; IC: Irminger Current; JMC: Jan Mayen Current; MC: Murman Current; NAD: North Atlantic Drift; NAC: Norwegian Atlantic Current; NCC: Norwegian Coastal Current; SB: Siberian Branch (of the Transpolar Drift); SCC: Siberian Coastal Current; WGC: West Greenland Current; WSC: West Spitsbergen Current.

The surface water circulation and ice motion are predominantly induced by the wind forcing. The Sea Level Pressure (SLP) over the Amerasian Basin and North Atlantic are particularly relevant to the interannual variability of the ocean surface current system [*Proshutinsky and Johnson*, 1997; *Rudels et al.*, 2004]. The upper-ocean circulation has two characteristic patterns: an anticyclonic gyre in the Canadian Basin, known as the

Beaufort Gyre, and a Transpolar Drift (TPD), which carries waters from the Canadian Basin and the Siberian shelves towards the Fram Strait

The Arctic Ocean waters are mainly from the North Atlantic flowing through the Norwegian Sea within the Norwegian Atlantic Current (NAC). When the latter reaches the Barents Sea Opening, between Bear Island and Norway, the current splits. Part flows north as the West Spitsbergen Current (WSP) into Fram Strait, and part flows together with the Norwegian Coastal Current (NCC) into the Barents Sea. A small volume of Pacific water enters the Arctic through Bering Strait within the Anadyr Current (AC), providing less saline and less dense waters that occupy the upper layers of the Canada Basin [*Rudels*, 2019].

Outflow of Arctic waters occur within the East Greenland Current (EGC) in Fram Strait. The EGC transport most of the sea ice export and part of the freshwater export, and great part of the returning and now transformed Atlantic water. The West Greenland Current (WGC), which is a continuation of part of the EGC, that flows north entering Baffin Bay, joining waters that flow south through the Canadian Arctic Archipelago and flowing south as the Baffin Island Current (BC). Part of the EGC crosses Davis Strait and join the BC, flowing south into the Labrador Sea [*Rudels*, 2019]. Figure 1.2 presents a schematic of the mean surface currents of the Arctic Ocean.

1.2 Arctic Sea Ice

The sea ice covered polar oceans occupy ca. 7% of our planet. They are essential as they provide suitable temperatures for human life, and are an important component of the climate system and ocean circulation [*Comiso and Hall*, 2014; *Wadhams*, 2000].

Solar radiation received at low latitudes and absorbed by the ocean is transported by shallow ocean currents towards the poles. In the polar oceans, this warm shallow water is then cooled down by the cold atmosphere above, leading to sea ice formation and increase of the salinity. The water becomes denser, sinks, and leads to deep-water masses formation. The process described above is one of the main drivers of the thermohaline circulation [*Aagaard and Carmack*, 1989; *Mauritzen and Häkkinen*, 1997].

Sea ice is a thin, fragile, and dynamic solid layer that serves as a boundary between two large fluid bodies, i.e., the ocean and the atmosphere. It insulates the ocean from the cold polar atmosphere reducing the outgoing longwave radiation from the ocean and limiting the convective heat exchange [*Weeks and Ackley*, 1986].

Due to its bright color and together with snow cover, the sea ice has a high albedo reflecting ca. 80-90% of shortwave radiation. In comparison, open seawater has low albedo and reflects only ca. 10% of the shortwave solar radiation [*Wadhams*, 2000].

Sea ice starts forming when the seawater surface is cooled down by the cold atmosphere to temperatures below the freezing point, which depends on the salinity. Seawater, with a salinity of 34, has freezing temperatures below -1.86 °C [*Petrich and Eicken*, 2010]. The heat stored by the ocean is then conducted to the atmosphere, and individual sea-ice crystals grow. During the process of sea ice formation, salt is trapped in brine pockets, and as the sea ice grows, these brine pockets are expelled from the sea ice within brine channels directed downwards [*Wadhams*, 2000]. The salt from the growing sea ice is released into the ocean contributing to the densification of the surface seawater. Denser surface water leads to convection in the upper layers of the ocean, contributing to the global circulation. When sea ice melts, it returns freshwater to the ocean, creating a stable stratification of the upper ocean layers [*Brandon et al.*, 2010]. The sea ice has, generally, a much lower salinity than the seawater.

Sea ice experiences an annual cycle of growth and melt, and is subjected to horizontal transport and deformations. The freezing of seawater and melting of sea ice are periodic responses to the seasonal variation of shortwave radiation and air temperature. In the Arctic Ocean, the maximum sea ice extent is usually reached in February-March, and the minimum extent of sea ice is reached in September (Figure 1.3) [*Comiso*, 2010; *Meier et al.*, 2014].

Arctic sea ice forms in an enclosed ocean and is restricted by the Eurasian, the American, and Greenland landmasses. The high latitude Arctic sea ice generally receives less insolation and presents more deformed ice due to the surrounding landmasses [*Dieckmann and Hellmer*, 2010]. As a consequence of pressure imposed by atmospheric systems, sea ice can drift for long distances. Surface winds can cause divergence and

convergence of sea ice floes, which contribute to changes in sea ice extent and thickness [*Köberle and Gerdes*, 2003].

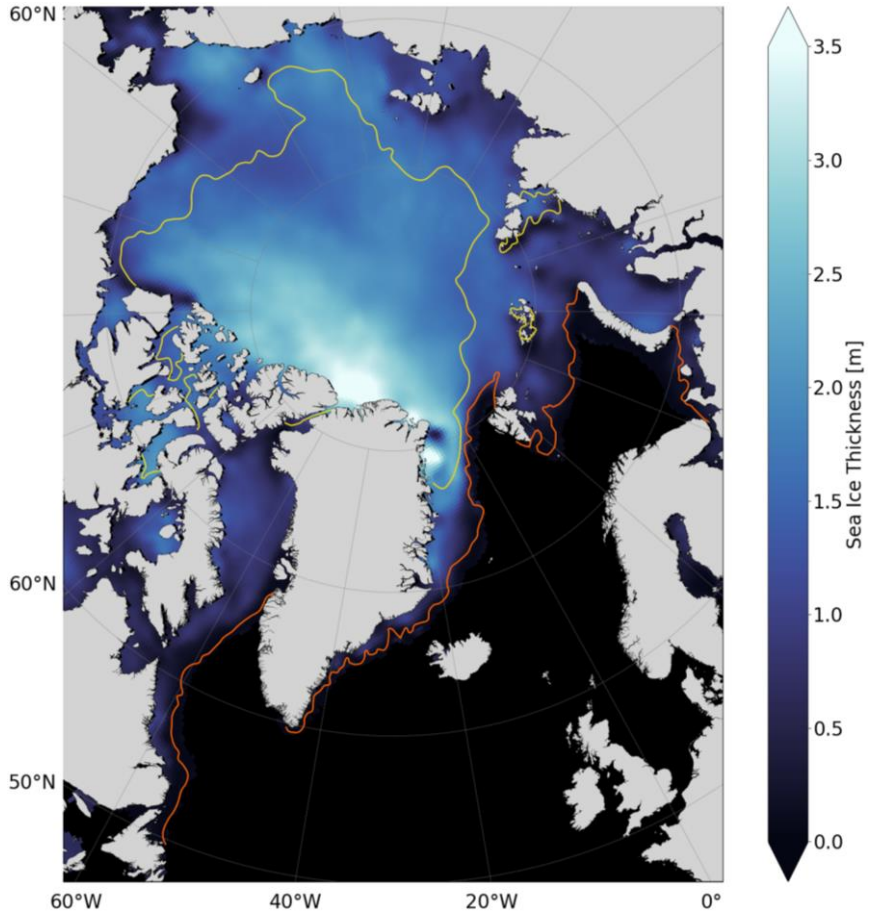

Figure 1.3: Average sea ice thickness. The orange line represents the mean maximum sea ice extension in March 2013, and the yellow line represents the minimum mean sea ice extension in September 2013. Sea ice thickness data are from CryoSat2-SMOS product [Ricker et al., 2017] and sea ice extension data are calculated from sea ice concentration AMSR2 from Meereisportal[1] [Spreen et al., 2008]. Minimum and maximum average sea ice are individually presented in Figure A.01 of the Appendix.

The sea ice cover consists of perennial and seasonal ice. Perennial ice is defined as the sea ice that survived at least one summer and represents the sea ice cover during the minimum extent [*Comiso*, 2002; *Comiso and Hall*, 2014]. Seasonal ice is defined by the

[1] meereisportal.de

ice that forms during the current winter and melts by the end of summer [*Comiso et al.*, 2017].

As the sea ice melt and retreats, the high-albedo sea ice surface is replaced by the low-albedo ocean surface; this enhances the absorption of solar radiation and increases the warming of the surface water. In turn, this will increase the melting of sea ice, forming positive feedback of the sea ice retreat [*Perovich et al.*, 2008].

The Arctic sea ice extent is declining at a rate of ca. 3.8% per decade, while the perennial sea ice cover (older and thick ice) is declining at a rate of ca. 11.5% [*Comiso and Hall*, 2014]. In 2012 the Arctic sea ice reached its record minimum extent (Figure 1.4).

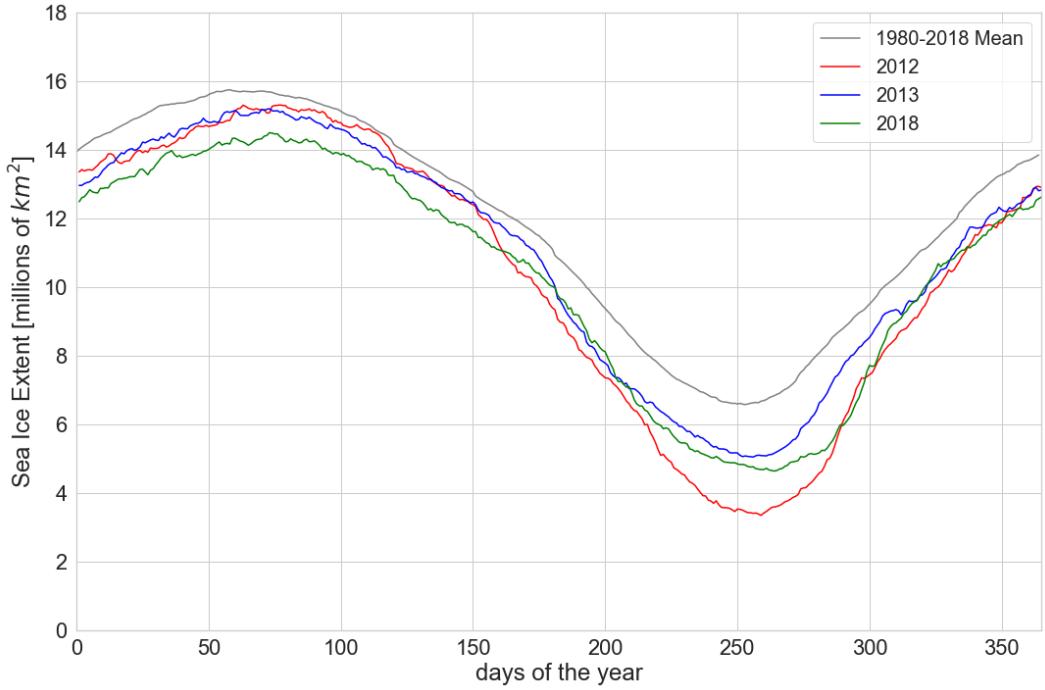

Figure 1.4: Arctic Sea Ice Extent. The Arctic sea ice extent corresponds to the area of ocean with at least 15% of sea ice. The gray line represents the mean sea ice extent between 1980 and 2018; the red line corresponds to the sea ice extent during 2012, with the record minimum; the blue line represents the sea ice extent during 2013; the green line represents the sea ice extent during 2018. The data used in this figure is a product of the NSIDC NASATeam algorithm [*Stroeve and Meier*, 2018].

Reductions of sea ice, in extent and thickness, cause disturbances to the ecosystem, especially in the Arctic, as it acts as a platform for human activities (e.g., hunting,

traveling), is the habitat for many marine mammals (e.g., polar bears, seals), and algae. On the other hand, the sea ice is an obstacle for shipping and other commercial operations in the Arctic Ocean (e.g., offshore structures, port facilities, exploitation of natural resources from the seafloor) [*Ho*, 2010].

The reduction of sea ice cover has additional environmental consequences. It will lead to increase of primary production, and to shifts of northward boundaries to many organisms and taxa [*Arrigo et al.*, 2008; *Lenoir et al.*, 2011; *Perry et al.*, 2005]. It is expected to increase the inflow of warm Atlantic currents into the Arctic, transporting propagules along coastal ecosystems [*Ruiz and Hewitt*, 2009] facilitating exchanges of North Atlantic and Pacific species. Sea ice reductions will also cause the opening of the Arctic waterways for extended periods, increasing the length of the navigation season. That can increase the vessel traffic in the Northwest and Northeast Passages, increasing the chances of non-indigenous species introductions through ballast water and or attached to ship hulls.

1.3 Arctic Shipping

Maritime transportation in the Arctic region is still limited during most of the year due to sea ice cover. As the sea ice retreats during summer, some of the Arctic waterways are free of sea ice and present a faster and shorter connection between the North Atlantic and the Pacific Ocean. *Miller and Ruiz* [2014] estimated a yearly increase of ca. 25% of shipping in the Arctic until 2040. Further reductions of sea ice will enable the Arctic Ocean to become a short route between Europe, East Asia, and North America [*Jing et al.*, 2012].

1.3.1 Arctic Shipping Routes

Northeast Passage

The Northeast Passage is a long corridor that runs from Norway, along the north coast of Russia, to the Bering Strait (Figure 1.5), connecting the North Atlantic to the Pacific Ocean. The Northeast Passage is composed of all the marginal seas of the Eurasian Arctic, i.e., the Barents Sea, the Kara Sea, the Laptev Sea, the East Siberian Sea, and the

Chukchi Sea. The Northeast Passage is part of the Northern Sea Route and makes up ca. 90% of it [*Lu et al.*, 2014; *Ostreng et al.*, 2013].

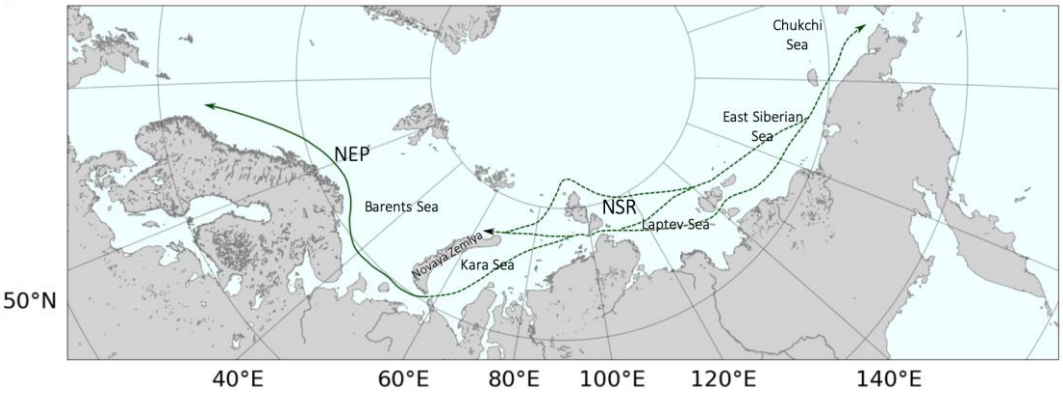

Figure 1.5: The Northeast Passage and the Northern Sea Route. The dashed line represents the waterways that compose the Northern Sea Route, and the solid line, together with the dashed lines, represents the Northeast Passage.

Northern Sea Route

The Northern Sea Route is the Russian part of the Northeast Passage, and lies within Russia's exclusive economic zone (EEZ). This route was used by the former Soviet Union as an international trade route, mainly to transport supplies to the northern communities. It was opened for non-Russian vessels in 1991. The Northern Sea Route stretches from Novaya Zemlya in the Kara Sea to the Bering Strait [*Council*, 2009; *Khon et al.*, 2010].

It is composed of a series of sailing corridors, and the sea ice conditions define the final navigational course. This route covers ca. 2,200 to 2,900 nautical miles of icy waters. The Northern Sea Route comprises the Eurasian Arctic marginal seas, i.e., the Kara Sea, the Laptev Sea, the East Siberian Sea, and the Chukchi Sea. These marginal seas are connected by straits that run through three archipelagos, the Novaya Zemlya, the Severnaya Zemlya, and the New Siberian Islands. The eastern sector of the route has the shallowest shelf seas (e.g., the East Siberian Sea is ca. 58 m deep, and the Chukchi Sea is ca. 88 m deep), and that affect the size, volume, and the draft of vessels that navigate these straits [*Brubaker and Østreng*, 1999; *Ostreng et al.*, 2013].

Northwest Passage

The Northwest Passage is a collection of possible routes through the waterways of the Canadian Arctic Archipelago (Figure1.6) and connects the North Atlantic to the North Pacific Ocean [*Wilson et al.*, 2004]. It consists of different routes, of which the majority are through the southern part of the archipelago, braking off from the Parry Channel, and one through Hudson Strait [*Ostreng et al.*, 2013]. In a westward way, the shortest route (ca. 2200 nautical miles long) crosses the whole length of the Parry Channel (composed by the Lancaster Sound, Barrow Strait, and the Viscount Melville Sound), through the M'Clure Strait, to the Beaufort Sea and Bering Strait. This route and the one that turns southward in the Prince of Wales Strait, are suitable for deep-draft vessels. The other routes that turn southwards from the Parry Channel are shallow or have complex currents, which make some unsuitable for shipping [*Lu et al.*, 2014; *Ostreng et al.*, 2013; *Pharand*, 2007].

Figure 1.6: Northwest Passage. The black lines indicate the different channels that compose the Northwest Passage.

Like the Northeast Passage, the Northwest Passage is composed of a series of channels. The decision through which channel the route will go, depends on the sea ice conditions. These routes cover distances between ca. 2,200 to 3,000 nautical miles. Thus, the Northwest Passage is a transportation corridor connecting the Baffin Bay on the east to the Beaufort Sea on the west [*Council*, 2009; *Ostreng et al.*, 2013].

.

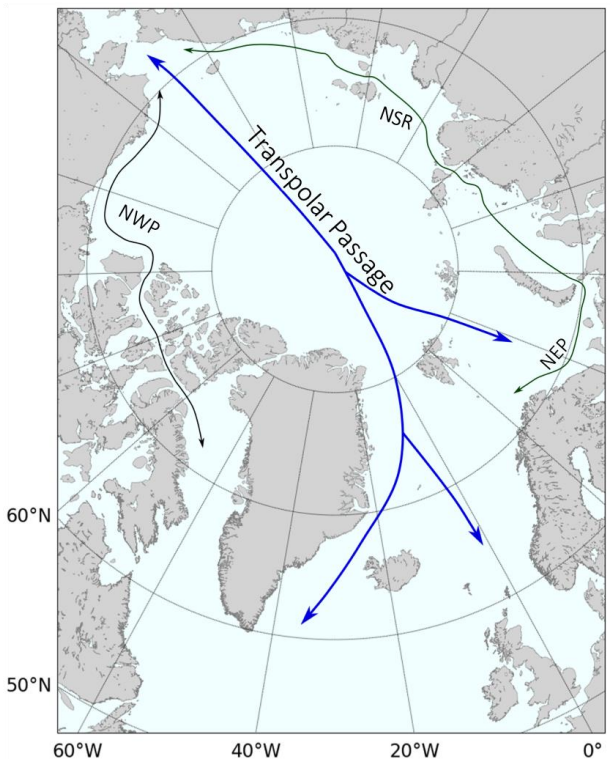

Figure 1.7: Transpolar Sea Route or Transpolar Passage. The blue line indicates possible routes for the Transpolar Sea Route in a scenario of an ice-free Central Arctic Ocean.

Transpolar Sea Route or Transpolar Passage

The Transpolar Sea Route is any route outside of national jurisdiction in the Arctic Ocean (Figure 1.7). It covers all waters that make the high seas and regions where freedom of navigation applies. This definition applies to two sections; the first is the Central Arctic Basin, where states have no jurisdiction apart from flag state[2] jurisdiction exercised in their ships and crews. The second includes all areas that are beyond the territorial seas of 12 nautical miles, and within the outer limits of 200 nautical miles of the exclusive economic zone (EEZ). This second sector is a belt of 188 nautical miles in extension measured outwards from the outer limits of the territorial seas. In this belt, the coastal state rights and obligations mix with the rights and obligations of all the other states. The shortest distance across the Central Arctic Basin is 2,100 nautical miles, from the Bering Strait across the North Pole to the Fram Strait. All other possible transits within the central Arctic Ocean

[2] Flag state refers to the country where the ship is registered.

are longer [*Ostreng et al.*, 2013]. Due to sea ice cover year-round, the Transpolar Passage across the North Pole is not yet suitable for many vessels.

1.3.2 Traffic types

Ship traffic is divided into three different types: destination, transit, and internal traffic. Each traffic type is described below.

Destination traffic

To destination traffic belongs the vessels that come from outside the Arctic to load or unload cargo to or from the region. These vessels have at least one port call inside the Arctic region [*Guy and Lasserre*, 2016; *Luitjens*, 2015].

Transit traffic

Vessels that enter and leave the Arctic region without making a port call are listed under transit traffic [*Luitjens*, 2015]. Those vessels are not associated with any port activities of the region, using the Arctic routes only as a short cut linking southern ports [*Guy and Lasserre*, 2016].

Internal traffic

Vessels that travel only inside the Arctic connecting the northern regions constitute the internal traffic. It concerns the transportation of supplies needed by local communities [*Guy and Lasserre*, 2016].

1.4 Ballast Water

Historically, ballast was any solid material (e.g., sand, rocks, cobble, iron) that was brought on board a vessel to regulate stability, increase the draft, maintain stress loads within acceptable limits, and change the trim. With the introduction of steel-hull vessels in the mid-nineteenth century, the loading of water as ballast in cargo holds or designated tanks had shown to be simpler and more efficient, and water then became the ballast of choice. Ballast water is pumped in and out to maintain safe operations through a voyage,

to compensate for weight changes during loading and unloading of cargo at port, and due to fuel and water consumption (figure 1.8) [*David*, 2015].

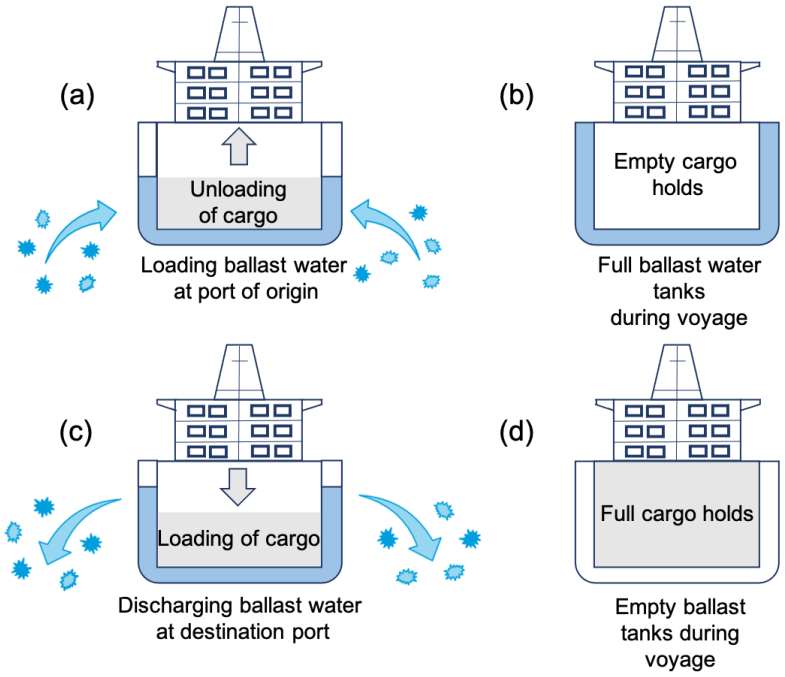

Figure 1.8: Illustration of vessel's ballast procedures during voyage. (a) Unloading of cargo at port, and loading of ballast water into tanks; (b) empty cargo holds and full ballast water tanks; (c) loading of cargo at port and unloading of ballast water; (d) full cargo holds and empty ballast water tanks. Adapted from [*Luitjens*, 2015].

As necessary ballast water is for safe and efficient shipping operations, it may pose serious ecological, economic, and health problems. Ballast water is one of the main vectors for the transfer of non-indigenous species. It contains a diverse collection of organisms, e.g., bacteria, phytoplankton, zooplankton, ranging in sizes from nanometers to centimeters, and in different life stages (e.g., eggs, cysts, larvae) [*Brickman*, 2006; *Brickman and Smith*, 2007]. The transferred organisms may survive, establish a reproductive population, and become invasive in the new environment. They may outcompete native species and even multiply into pest proportions (e.g., due to lack of predators) [*DiBacco et al.*, 2012; *Scriven et al.*, 2015]. Ballast water may also contain heavy metals, dissolved hydrocarbons, and other pollutants, anthropogenic contaminants, and

toxins that may reach water bodies eventually and may be harmful to aquatic ecosystems [*Endresen et al.*, 2004; *Jing et al.*, 2012; *Ruiz et al.*, 2000; *Tamburri et al.*, 2002].

Microorganisms and nutrients from estuarine and coastal waters can be taken on board as water is pumped into the ballast tanks. Planktonic microorganisms can survive the voyage in the ballast tanks and potentially become invasive to the environment where the ballast water is discharged, during loading of cargo at port or during mid-ocean exchange operations [*Emami et al.*, 2012; *Jing et al.*, 2012].

Wildlife and human health may be affected by the epidemiology of waterborne diseases as a result of spread via ballast water of pathogens and other microorganisms [*Ruiz et al.*, 2000; *Takahashi et al.*, 2008]. These organisms are capable of surviving harsh conditions in cysts, spores, and resting stage forms [*Gregg and Hallegraeff*, 2007].

In 1992, *Vibrio cholerae* was detected in the ballast water of five ships docked in the Gulf of Mexico. The ballast water was loaded in regions infected with cholera and posed significant epidemic threats to the communities where the ballast water was discharged [*McCarthy and Khambaty*, 1994]. *Vibrio cholerae* O1 and O139 was found in 93% of the ballast water of vessels arriving in the Chesapeake Bay [*Ruiz et al.*, 2000]. *Escherichia coli*, which is common in warm-blooded organisms and are capable of causing food poisoning in humans, was found to be disseminated via ballast water [*Ichikawa et al.*, 1992; *Jing et al.*, 2012; *Ruiz et al.*, 2000]. Shellfish poisoning and respiratory illness are some of the health threats that are caused by algae bloom associated with phytoplankton introductions via ballast water [*Epstein*, 1995; *Hallegraeff and Bolch*, 1992; *Jing et al.*, 2012].

The International Maritime Organization (IMO) recognized the importance of preventing the spread of non-indigenous species and developed a series of voluntary guidelines with the intent to reduce the introduction of unwanted marine organisms. The "International Convention for Control and Management of Ships Ballast Water and Sediments" (BWM Convention[3]) was adopted by the IMO on February 13th, 2004, and

[3] http://www.imo.org/en/About/Conventions/ListOfConventions/Pages/International-Convention-for-the-Control-and-Management-of-Ships'-Ballast-Water-and-Sediments-(BWM).aspx

entered into force on September 8th, 2017, one year after several states representing at least 35% of the world's merchant shipping tonnage have endorsed the Convention. To the date when the BWM Convention entered into force, the number of contracting states was 63, representing 68.51% of the world's merchant shipping tonnage.

1.4.1 Ballast Water Management Convention

The BWM Convention includes a series of technical requirements and standards for the control and management of ballast water in its guidelines. It requires that all vessels in international traffic manage their ballast water and sediments to standards defined in the guidelines, and according to a ship-specific ballast water management plan. From September 8th, 2017 onwards, it is required that all vessels carry a ballast water record book and an international ballast water management certificate. The member states have the option to take additional measures that are subjected to standards established in the convention and to IMO guidelines.

One of the main elements in the ballast water guidelines, is the recommendation to perform a mid-ocean exchange (regulation D-1). The regulation D-1 says that ballast water mid-ocean exchange should, "whenever possible, be conducted at least 200 nautical miles away from the nearest land and in waters at least 200 m deep[4]". In the regulation D- 1, it is also stated that vessels should not be subjected to a significant trip diversion, and ballast water exchange should be performed with an efficiency of 95% of volume exchange. Figure 1.9 illustrates the areas in the Arctic Ocean, where the waters are shallower and deeper than 200 m.

Another important element from the ballast water guidelines is the ballast water performance standard (regulation D-2). Regulation D-2 sets the concentration limits of viable organisms that are allowed in the ballast water during the discharge at port. The guidelines also state that mid-ocean exchange could be used to meet the concentration limits described in regulation D-2. Mid-ocean exchange is believed to reduce the risk of

[4] http://www.imo.org/en/About/Conventions/ListOfConventions/Pages/International-Convention-for-the-Control-and-Management-of-Ships'-Ballast-Water-and-Sediments-(BWM).aspx

introduction of non-indigenous species by discharging most of the coastal species in the ballast tanks into the open ocean, where the salinity is usually not tolerated by brackish and freshwater organisms, and replacing those with open ocean species that are not likely to survive in brackish or freshwater of destination ports [*DiBacco et al.*, 2012; *Taylor et al.*, 2002]. Studies have already shown that mid-ocean exchange is not always entirely effective at eliminating all coastal organisms. It depends on the vessel type, voyage duration, the exchange method, port location (estuarine, river or marine ports), and species composition [*DiBacco et al.*, 2012].

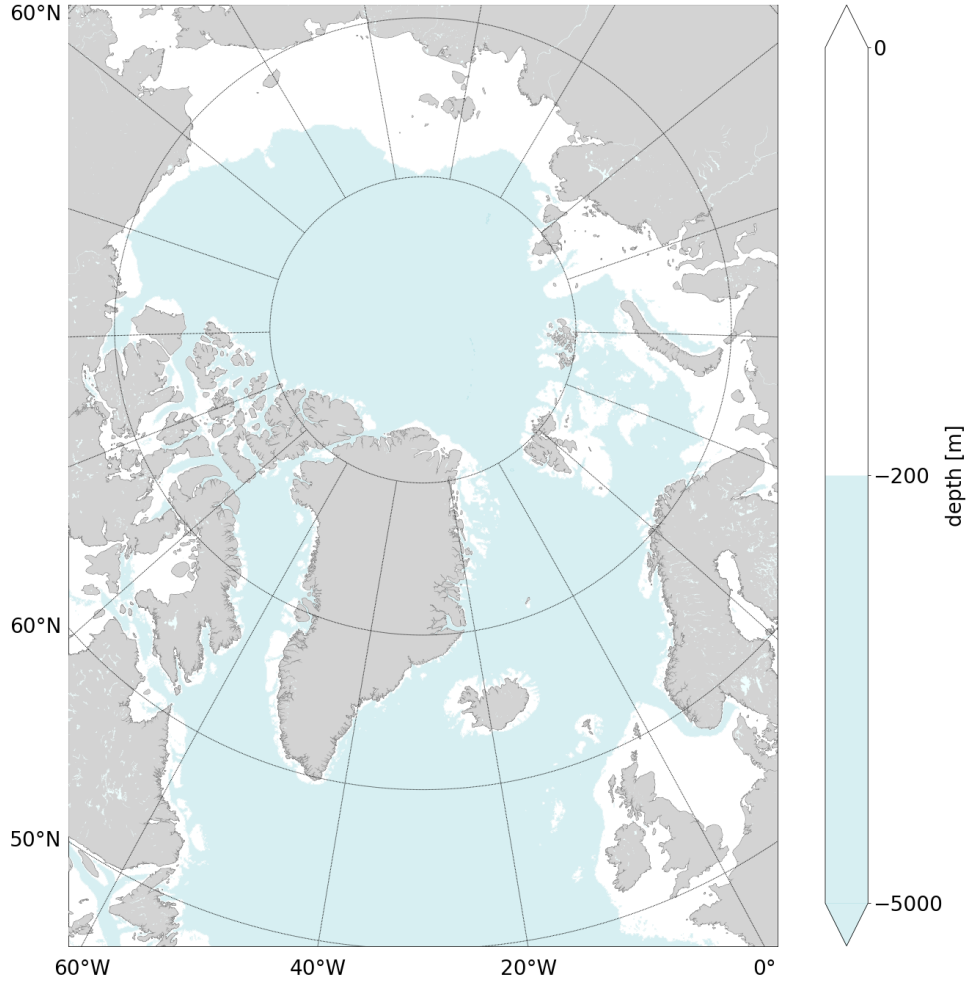

Figure 1.9: Water depth. The map illustrates the areas of the Arctic Ocean with waters shallower (white) and deeper (blue) than 200 m.

Eventually, all vessels should meet the ballast water treatment standard, which should be according to specific renewal surveys, and most vessels will, eventually, be requested to install an on-board ballast water treatment. However, studies have shown that ballast water treatment systems are not always effective. For example *Stehouwer et al.* [2015] compared ballast water treatment systems based on UV radiation, electrochlorination, and chlorine dioxide. Their results presented higher concentrations of phytoplankton due to re-growth after treatment. *Liebich et al.* [2012] found similar outcomes. On the other hand, other studies showed that a combination of different ballast water management methods is more efficient in eliminating unwanted organisms (e.g., *Briski et al.* [2013]).

The IMO defines ballast water management as any mechanical, physical, chemical, and biological method and processes that are used individually or in combination to remove or prevent the uptake or discharge of harmful aquatic organisms within ballast water [*David et al.*, 2015].

Ballast water treatment systems can be sorted as mechanical separation of water and organisms by filtration and centrifugal separation, physical treatment, which involves thermal systems and UV radiation, and chemical treatments, which make use of biocides, electrolysis, or electrochlorination and is usually generated on board. The treatment of the ballast water can be applied in different stages, i.e., pre-treatment, treatment, and residual control (neutralization). Some systems are applied as ballast water is pumped into the ballast water tanks (e.g., by filtration), others require treatment also at ballast water discharge, and others are applied only during voyage [*David and Gollasch*, 2015; *Luitjens*, 2015]. The ballast water management systems must be approved by the IMO and attend the Guidelines for Approval of Ballast Water Management Systems.

The Polar Code (International Code for Ships Operating in Polar Waters[5]) acknowledges that the Regulations D-1, regarding ballast water exchange, and D-2, regarding ballast water performance standards, are considered appropriate for the Arctic region.

[5] https://www.imo.org/en/OurWork/Safety/Pages/polar-code.aspx

1.5 Non-Indigenous Species

The IMO Guidelines G7 define non-indigenous species as any organism that is outside of its native region, intentionally or unintentionally transported by humans or by natural processes. Other definitions limit the term to only human-mediated transports. However, not all non-indigenous species have negative impacts on the host environment [*Gollasch et al.*, 2015].

Species that harm the host environment are commonly referred to as invasive species. They may disturb interactions between species, threaten the diversity or abundance of native species, and can cause local species extinction leading to a negative impact on the food web [*Mack et al.*, 2000]. In other words, invasive species may threaten the ecological stability of the ecosystem, and have a negative impact on economic (e.g., aquaculture) and recreational activities that are dependent on these ecosystems, and can be harmful to human health [*Deschutter et al.*, 2018; *Gollasch et al.*, 2015; *Ruiz et al.*, 1997]. After an invasive species established a population, it can be difficult and expensive to eliminate it from the invaded ecosystem [*Molnar et al.*, 2008; *Thresher and Kuris*, 2004].

The BWM Convention defines Harmful Aquatic Organisms and Pathogens (HAOP) as any aquatic organisms or pathogens that, if introduced into marine ecosystems, estuaries, or freshwater courses, may create hazards to the environment, human health, resources, reduce biological diversity, or interfere with other uses of such areas [*Gollasch et al.*, 2015].

1.5.1 Examples of aquatic non-indigenous and invasive species

Some of the well-known and documented aquatic non-indigenous and invasive species are presented below.

Rhopilema nomadica Galil, Spanier & Ferguson, 1990. Its preferred common name is nomad jellyfish, but it is also known as the Red Sea jellyfish. *R. nomadica* is native to the east coast of Africa and the Red Sea. It was introduced to the Mediterranean Sea through the Suez Canal in the late 1970s spreading along the Levantine coast, from Egypt to Turkey and Greece. During summer, huge swarms spear along those shores disrupting

coastal fisheries, clogging the nets, making it difficult the sorting of catches, as it is capable of delivering a painful sting [*CABI*, 2020; *Galil et al.*, 2015].

Dreissena polymorpha (Pallas, 1771). Its common name is zebra mussel, and it is known as the most aggressive freshwater invader worldwide. It is native to the drainage basins of the Black, Caspian, and Aral Seas. *D. polymorpha* expanded its range during the nineteenth century, westwards to western Europe, United Kingdom, and North America, where it was introduced via ballast water to the waterways of the Great Lakes and all major rivers east of the Rocky Mountains, causing multiple economic impacts on fisheries, aquaculture, water attractions and aquatic transport [*CABI*, 2020; *Griffiths et al.*, 1991].

Mnemiopsis leidyi A. Agassiz, 1865. Its preferred common name is sea walnut, but it is also known as North American comb jelly (Figure 1.10a). It is native to the Atlantic coast of North and South America, where it lives over a wide range of salinity and temperature. It was introduced to the Black Sea in the early 1980s via ballast water, from where it spread to the Sea of Azov, to the Sea of Marmara, and the eastern Mediterranean. It was identified in the Caspian Sea in 1999. In 2005 it was recorded in the Adriatic Sea, and in 2006 was the first time recorded in the North Sea and Baltic Sea [*CABI*, 2020]. The sea walnut (comb jelly) is considered one of the main reasons for the collapse of fish stocks in the Black Sea, where the anchovy fisheries have almost disappeared by 1994 [*Kideys*, 2002].

Carcinus maenas (Linnaeus, 1758). The preferred common name is European shore crab (Figure 1.10b), but it is also known as European green crab. It is native to the European sector of the Atlantic Ocean, the western Baltic Sea, and West Africa to Mauritania, and it was widely introduced to Australia and North America, and recently to East Asia, South America, and South Africa. *C. maenas* has the potential to significantly alter any ecosystem it invades [*Gregory and Quijón*, 2011; *Klassen and Locke*, 2007], and it is blamed for the collapse of the softshell clam industries in Maine. It feeds on many organisms, including clams, oysters, mussels, marine worms, and small crustaceans; food is not a limiting agent for this species. This species tolerates a wide range of environmental conditions, and it is able to spread by natural and human-mediated vectors. In its larval stages, it may be taken on with ballast water, and it can survive as plankton for up to 90

days, and be dispersed by ocean currents along the coast, spreading from invaded regions to new ones[6] [*CABI*, 2020].

Figure 1.10: Examples of invasive species. (a) *Mnemiopsis leidyi* A. Agassiz, 1865. Image by Karl Van Ginderdeuren[7], licensed under CC BY-NC-SA 4.0; (b) *Carcinus maenas* (Linnaeus, 1758). Image by Hans Hillewaert[8], licensed under CC BY-SA 3.0; (c) *Pseudodiaptomus marinus* Sato, 1913. Image by Karl Van Ginderdeuren[9], licensed under CC BY-NC-SA 4.0. All images are from World Register of Marine Species (WoRMS), accessed on August 27th, 2020.

Pseudodiaptomus marinus Sato, 1913. It is a small egg-carrying copepod (Figure 1.10c). Its natural habitat is the estuarine environment of the Northwest Pacific. This species is highly adaptive to environments with unfavorable conditions as it tolerates a large range of salinity and temperature [*Sabia et al.*, 2015]. The spread of the species is mainly due to shipping activities. The *P. marinus* has been recorded in the Adriatic Sea [*de Olazabal and Tirelli*, 2011; *Lučić et al.*, 2015], in the French coast [*Brylinski et al.*, 2012], in the German Bight, in the Netherlands, and at the Belgian part of the North Sea [*Deschutter et al.*, 2018; *Jha et al.*, 2013], and in the Iberian Peninsula [*Albaina Vivanco et al.*, 2016; *CABI*, 2020].

[6] https://wsg.washington.edu/crabteam/greencrab/

[7] https://creativecommons.org/licenses/by-nc-sa/4.0.
WoRMS image – http://www.marinespecies.org/aphia.php?p=image&tid=106401&pic=64765.

[8] https://creativecommons.org/licenses/by-sa/3.0/deed.en.
WoRMS image – http://www.marinespecies.org/aphia.php?p=image&tid=107381&pic=662

[9] https://creativecommons.org/licenses/by-nc-sa/4.0.
WoRMS image – http://www.marinespecies.org/aphia.php?p=image&tid=360352&pic=74201.

The North Sea has a high number of invasions, ca. 60% of the invasive species identified in this ecosystem are known to harm many species and the ecosystem itself [*Molnar et al.*, 2008].

1.5.2 Invasive species in the Arctic seas

Historically, the Arctic region is considered an area of low risk of biological invasions. It has limited access and harsh environmental conditions that, together with reduced food resources, limit the dispersal, survival, growth, and reproduction of many species [*Chan et al.*, 2019; *Ruiz and Hewitt*, 2009; *Vermeij and Roopnarine*, 2008]. However, due to a warming climate and an increase in human activities, the Arctic region is now under threat of biological invasions [*Chan et al.*, 2019; *Miller and Ruiz*, 2014; *Ricciardi et al.*, 2017].

The retreat of sea ice in recent years is opening the region for shipping, tourism, exploration of resources, and hence, increasing the potential of human-mediated introductions of non-indigenous species [*Chan et al.*, 2019]. Further reductions in the extent of sea ice might enable the Arctic Ocean to be used as a major shipping route between Europe, East Asia, and North America, generating new possibilities for introductions of non-indigenous species to the region, having negative consequences for some of the native biota, and may provide suitable conditions for more southern species [*Chan et al.*, 2019; *Jing et al.*, 2012; *Vermeij and Roopnarine*, 2008; *Wilson et al.*, 2004; *Wisz et al.*, 2015].

Some high-latitude ecosystems may be already suitable for temperate species, and successful establishment might be possible once the propagule supply is sufficient [*Chan et al.*, 2019; *de Rivera et al.*, 2011]. Further warming of the Arctic may enhance the suitability of its coastal regions for temperate species [*Chan et al.*, 2019; *Goldsmit et al.*, 2018; *Ware et al.*, 2014]. Until recently, only a few invasive species have been identified in Arctic waters, research, and knowledge of its native species are limited [*Jing et al.*, 2012; *Petersen*, 1999].

Chan et al. [2019] identified 54 introduction events of 34 unique non-indigenous species in the Arctic Ocean. Iceland was found to have the highest number of introductions

(26% of the total). The Barents and Norwegian Seas have the second-highest number (20% at each). Large numbers of introductions lead to a high number of non-indigenous species establishments and imply that these regions are vulnerable to biological invasions due to the diversity and abundance of species introduced. As these regions are transitioning from a cold Arctic to a warm Atlantic-dominated climate regime, they are also becoming more suitable for temperate species [*Chan et al.*, 2019; *Lind et al.*, 2018].

Chan et al. [2019] also found that the Kara Sea, the East Siberian Sea, and the Beaufort Sea had only a single introduction event each, and these introductions resulted in successful establishment. In most regions of the Northwest Passage and the Canadian Arctic Archipelago, they found only a small number of introductions, and none presented established populations of non-indigenous species. Most of the source regions are the Northeast Atlantic (39%), the Northwest Pacific (29%), the Northeast Pacific (16%), the Northwest Atlantic (14%), and the Arctic Sea (2%) [*Chan et al.*, 2019].

Non-indigenous species belonging to seven different phyla have the status of established in the Arctic seas, as identified by *Chan et al.* [2019]. Examples of the established species belonging to each phylum are briefly described below.

Phylum Arthropoda have ten different established species of shrimp and crab. For example, the snow crab, sp. *Chionoecetes opilio* (O. Fabricius, 1788), found to be established in the Barents Sea. It is a benthic predator, feeding on crustaceans, polychaetes, and fish [*Jørgensen and Spiridonov*, 2013; *Kaiser et al.*, 2018], competing with benthic species and bottom-feeding fish [*Haug et al.*, 2017; *Kaiser et al.*, 2018]. Another example is the Japanese skeleton shrimp sp. *Caprella mutica* Schurin, 1935 established in the North Sea. It can displace native caprellids, and affect feeding of native fishes and aquaculture operations [*Katsanevakis et al.*, 2012].

Phylum Chlorophyta have one established species; the algae green sea fingers sp. *Codium fragile subsp. fragile* (Suringar) Hariot, 1889, established in the Iceland Shelf.

Phylum Chordata have five different established species in the Arctic seas. For example the pink salmon sp. *Oncorhynchus gorbuscha* (Walbaum, 1792); and the sea grapes sp. *Molgula manhattensis* (De Kay, 1843), which belong to the subphylum Tunicata. Both species have established populations in the Norwegian Sea.

Phylum Mollusca have on species with established population in the Barents Sea, the Mediterranean mussel, sp. *Mytilus galloprovincialis* Lamarck, 1819.

Phylum Ochrophyta have four species with established populations in the Arctic seas. One example is the sp. *Stephanopyxis turris* (Greville) Ralfs, 1861. This species is established in the Iceland Shelf. Another example is the sp. *Sargassum muticum* (Yendo) Fensholt, 1955, its common name is wireweed and has established population in the Norwegian Sea.

The phylum Platyhelminthes have one species with established population in the Norwegian and Barents Sea. The sp. *Gyrodactylus salaris* Malmberg, 1957, known as the salmon killer.

Phylum Rhodophytahave three species with established populations in the Arctic region. One is commonly named the Japanese red seaweed, sp. *Bonnemaisonia hamifera* Hariot, 1891, which has established population in the Iceland shelf. The second is the sp. *Dasysiphonia japonica* (Yendo) H.-S.Kim, 2012, which common name is the algae siphoned japan weed, and have established population in the Norwegian Sea; and the third is the algae, sp. *Dumontia contorta* (S.G.Gmelin) Ruprecht, 1850, with established population in the Beaufort Sea.

The valid scientific and common names, as well as the short descriptions of each species, were collected from two online sources. The primary online source used in this chapter is the World Register of Marine Species [*Horton et al.*, 2017]. The other online source is the Invasive Species Compendium [*CABI*, 2020].

1.6 Summary

The Arctic Ocean has, in the last decades, experienced strong reductions of its sea ice extension, especially during summer. With the decrease of the sea ice cover, and increase of the sea-ice free season length, even if only for a small number of days to a few weeks, the Arctic region becomes a shorter corridor for vessels navigating between Atlantic and Pacific ports.

With an increase of the number of vessels navigating the Arctic routes, the risks of non-indigenous species finding a faster way to Arctic ecosystems increases, and with it,

the number of possible invasions by those species. Due to climate change, it is expected that, in the future, many non-indigenous species will find a new home in what is today a harsh environment.

Before the BWM Convention and its guidelines were created with the request for ballast water mid-ocean exchange, aquatic invasions were mostly a port-to-port problem. The mid-ocean exchange strategy changed this pattern, which became a coastal problem.

Most navigation tracks are on the continental shelf, and vessels are not required by the convention to make a large trip diversion to perform ballast water mid-ocean exchange. Consequently, most of the ballast water exchange is performed on the continental shelf. For vessels navigating the Arctic Routes, it may be dangerous to leave the continental shelf area to perform ballast water mid-ocean exchange, due to the presence of sea ice further offshore.

Due to the effects of climate change, the Arctic sea surface temperature is expected to increase, as sea ice decreases. This can lead to shifts on the invasion dynamics in the northern hemisphere, increasing the opportunities in the Arctic seas for propagules that are naturally transported by warmer currents, and for human-mediated organisms due to shipping and shoreline development as a consequence of mineral exploration.

Temperature range is a known limiting factor for many species, but as temperature rises, especially in the Arctic, it is expected that these changes will affect the environmental resistance to invasions. With rising of the sea surface temperatures, it is likely that many native and non-indigenous species, in response to the changes in sea surface temperature, may expand their northern boundaries. Decreases on sea ice extension may increase the possibility for exploration of natural resources. As an example, vessels starting their voyage from European ports in the North Sea, will possibly do with empty cargo and full ballast tanks, increasing the opportunities for non-indigenous species like the *P. marinus* (calanoid copepod), already established in the North Sea, to be introduced into the coastal seas of the Arctic, where it may establish and reproduce, becoming an Arctic invasive species.

The North Sea is nowadays the host environment of over 80 non-indigenous species [*Jing et al.*, 2012; *Reise et al.*, 1998]. Many of those species might present a threat to become invaders in coastal areas of the Arctic Ocean, like the coastal seas along the

Northeast Passage. With reduction on sea ice extent, and increase of Atlantic warm water inflow into the Barents Sea, many species that nowadays are established in the North Sea, and already show resilience and strong tolerance to low temperature and high salinities, might find an opportunity to migrate and establish themselves in the Arctic coastal ecosystems.

The presence of sea ice for most of the year on the Arctic shelf seas limit the number of vessels navigating its routes. As these waters are expected to have a longer sea-ice free season, it is also expected that the number of ships in the Arctic routes will increase, as well as the opening of the Transpolar Passage for navigation during the summer.

Many vessels still do not have on-board ballast water treatment systems, and are still required to comply with the ballast water mid-ocean exchange procedures before arriving at the destination port. In the future, it is expected that all vessels will be equipped with ballast water treatment system, and will only be a question of how effective this treatment system will be in the cold polar waters.

Even if in the future, all vessels shall have an on-board treatment system, there are other contaminants that may be discharged, whether intentionally or accidentally (e.g., oil spills, leaching of active antifouling compounds, sewage, greywater), and it might cause different ecosystem disturbances that might generate consequences to invasion resistance.

Chapter 2. Objectives and methods

The present chapter outlines the objectives of this study to fill in the knowledge gap of ballast water distribution in the Arctic Ocean. A description of the ships' dataset that is used in the model simulations is given. The applied ocean-sea ice model NAOSIM is presented and followed by a description of the ballast water tracer.

2.1 Objectives

This thesis's main objective is to identify areas along the main Arctic shipping routes, where the discharge of ballast water may present the risk of contamination to the local ecosystem. The introduction of non-indigenous organisms and the presence of pathogens, or toxins transported within the ballast water, may harm the ecosystem where it is discharged. In order to fulfill the main objective of this thesis, the same was divided and set as follows:

1. Identify the ballast water tracer's flow after discharge in the ocean model's surface layer and areas of possible accumulation.

After discharge, the ballast water tracer is governed by the ocean circulation calculated in the model. Multiple tracer release points provide tracer material that is carried by the ocean currents also to coastal areas. As coastal areas are the habitat of many species, it can also become a new habitat to non-indigenous species, or be harmed by pathogens or toxins that ballast water may contain. Tracer accumulation can indicate an increase in the propagule pressure (i.e., the number of non-indigenous individuals released into an ecosystem [*Lockwood et al.*, 2005]), which is often recognized as a factor of opportunity for non-indigenous species to reproduce and form populations in the host environment.

2. Identify particle pathways as a proxy for neutrally buoyant organisms that are transported by the surface currents as an effect of advection, and analyze the influence of the surface eddy kinetic energy field on tracer and particle dispersion.

Different types of organisms have different buoyancy and swimming behaviors. By following particle trajectories advected by the surface currents, it is possible to identify pathways through which neutrally buoyant non-indigenous organisms, pathogens, and contaminant particles, can be transported. Turbulence is responsible for mixing processes in the surface layer and through the water column. Eddy kinetic energy is the energy associated with the turbulence of the flow of a fluid. It is expected to influence the mixing range and thus the flow of the ballast water tracer.

2.2 Ship positions dataset

Luitjens [2015] put together a ship dataset using Automatic Identification System (AIS) data kindly provided by the Environmental Research and Development department of DNVGL[10]. The AIS data contain information transferred during voyages, such as vessel identification, vessel type, position, course, and speed. For the ship dataset, *Luitjens* [2015] selected the information on vessel type, date and time of the transmission, and geographical coordinates (latitude and longitude). Due to the ships' identification's confidentiality, the dataset's vessels are identified by the respective ship type. The dataset is built with the above information of four ship types: bulk carrier, tanker, general cargo, and roll-on/roll-off, that performed destination traffic in the Arctic region in 2013. In that year, 378 vessels among the four ship types of the dataset navigated in the Arctic region. From those, 202 performed destination traffic. These vessel types are selected because they generally carry a homogeneous amount of cargo, and therefore a homogenous amount of ballast water between ports of origin and destination.

Bulk carries, or bulkers, are used to carry dry cargos as grain ore, timber, or coal. These vessels only have one deck divided into several holds. Bulker is among the vessels which carry the largest volumes of ballast water [*Luitjens*, 2015]. Tankers are vessels that carry liquid cargos inside of tanks. The most common loads are crude oil, refined oil products, liquefied gases, and different beverages (e.g., orange juice and wine). Tankers

[10] Det Norske Veritas – Germanischer Lloyd.

often arrive at the loading port without cargo, and the ballast water is discharged during cargo load operations [*Luitjens*, 2015].

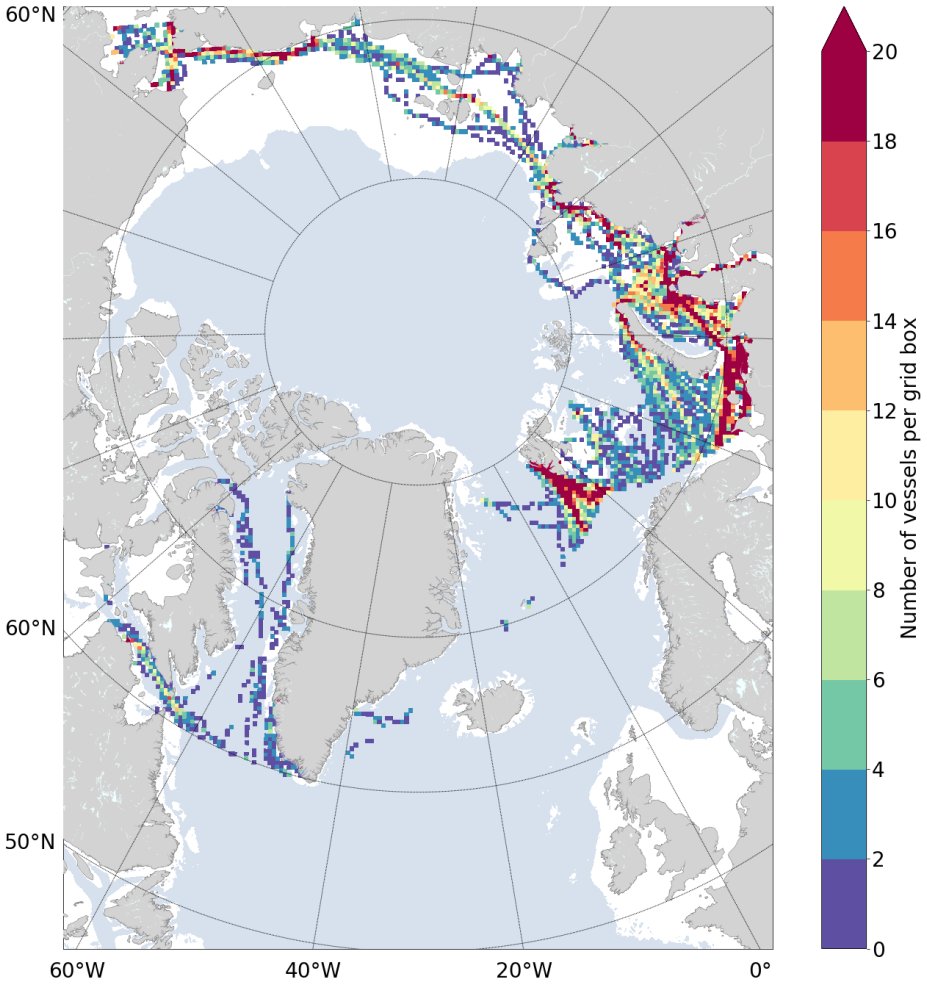

Figure 2.1: Ship-track density in the Arctic Ocean in 2013. The ship-track density is computed with the vessel positions of the dataset for destination traffic in the Arctic Ocean in 2013. For visualization of the ship-tracks, the grid used in this figure belongs to the ¼ degree resolution version of NAOSIM. Adapted from [*Rosenhaim et al.*, 2019].

General cargo vessels usually carry conventional cargos packed or unpacked by cranes, inside cartons, or bags. These ships have many decks that allow for a diversity of cargo carried to multiple destinations on the same journey [*Brodie*, 2014; *Luitjens*, 2015]. Ro/Ro, or roll-on/roll-off vessels, carry cargo that is driven on board. Cargo usually is cars,

trucks, with or without containers, and trains. The cargo is stored and secured inside the vessel on several decks [*Luitjens*, 2015; *Van Dokkum*, 2003].

For this study, a sub-dataset is created with the ship positions located inside the model domain. The sub-dataset comprises 165 vessels and contains information on ship type, geographical coordinates, and transmission date. With the sub-dataset vessel positions, a ship-track density is calculated according to the number of vessels that navigated through the model grid coordinates and presented in Figure 2.1.

2.3 North Atlantic/Arctic Ocean-Sea Ice Model – NAOSIM

The North Atlantic/Arctic Ocean-Sea Ice Model (NAOSIM) is a regional coupled ocean-sea ice model developed at the Alfred Wegener Institute Helmholtz Center for Polar and Marine Research [*Köberle and Gerdes*, 2003]. NAOSIM derives from the Geophysical Fluid Dynamics Laboratory modular ocean model, MOM-2 [*Pacanowski*, 1995]. The ocean model is coupled with a dynamic and thermodynamic sea ice model. The dynamic part of the sea ice model is based on *Hibler* [1979], while the thermodynamic processes are implemented as in *Semtner* [1976]. Advection of tracers is treated by the flux-corrected transport scheme (Gerdes et al., 1991), known by its low implicit diffusion while avoiding overshooting of advected quantities as described in *Köberle and Gerdes* [2003], among other details of the model. The 1/12-degree version of NAOSIM was developed from the ¼ degree version of the model, and differences between the fine-resolution model (FRM, with 1/12-degree grid), and the high-resolution model (HRM, with ¼ degree grid) versions of NAOSIM are given by [*Fieg et al.*, 2010]. NAOSIM has been applied to many studies of tracer dispersion (e.g., *Gerdes et al.* [2001]; *Gerdes et al.* [2003]; *Karcher et al.* [2012]; *Kauker et al.* [2003].

The FRM-NAOSIM is the model version applied in the study developed in this thesis. It has a horizontal resolution of 1/12° and 50 vertical levels that range from 10 m thickness in the upper 220 m (22 levels) to 366 m thickness in the lowest grid box at the maximum depth of 5316.75 m. The model grid is a rotated spherical grid with its equator matching the geographical 30°W/150°E meridian. NAOSIM's rotated grid avoids the high

costs of numerical calculations near the pole, and it produces nearly equidistant grid cells [*Fieg et al.*, 2010].

Figure 2.2: NAOSIM model domain. The model covers the northern North Atlantic and the Nordic Seas from 50°N to the Bering Strait.

The forcing used by NAOSIM consists of atmospheric data calculated from NCEP/NCAR Reanalysis Core 1 [*Kalnay et al.*, 1996] from its restart date in January 1990 onwards. The model simulations of the 1/12-degree version started using January 1990 potential temperature and salinity fields from a hindcast simulation of the ¼ degree version as initial conditions. The ¼ degree model was forced with daily atmospheric fields, and the simulation was from 1948 onwards. The forcing data are specifically daily means of two

meters air temperature, dew point temperature, wind speed, surface wind stress, cloud cover, and precipitation [*Fieg et al.*, 2010]. The model domain covers the northern North Atlantic and the Nordic Seas from 50°N onwards, and it covers the whole Arctic Ocean to the Bering Strait (Figure 2.2).

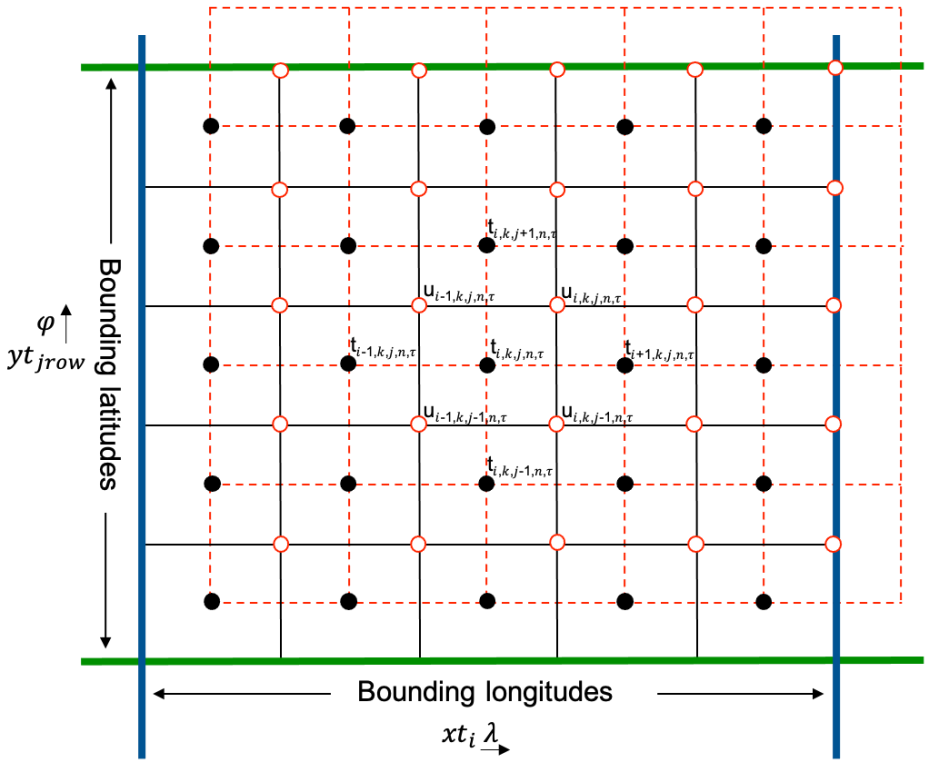

Figure 2.3: NAOSIM grid cell arrangement on a horizontal longitude-latitude surface.The T cells are represented by the black lines and the T grid points by the black dots. The U cells are represented by the red dashed lines and the U grid points by the red-white dots. Adapted from [*Pacanowski*, 1995].

In NAOSIM, the river and coastal runoffs are implemented as a virtual salt flux distributed over the first three vertical layers (i.e., 30 m). That compensates for insufficient vertical mixing of the freshwater near river mouths and gives a more realistic distribution of the Arctic Ocean's salinity in the model [*Fieg et al.*, 2010]. The ocean open boundary conditions are formulated following *Stevens* [1991]. The temperature and salinity data are restored with a 7-day time constant to the Levitus climatology [*Levitus and Boyer*, 1994; *Levitus et al.*, 1994] at the points of inflow. At the outflow points, the advection of tracers

and radiation of waves are allowed. The current simulations' initial conditions are from a model run from 1948 to 1990 from a model simulation with the HRM NAOSIM.

NAOSIM's grid system is a rectangular Arakawa staggered B grid [*Bryan*, 1969]. It comprises T cells and U cells. Within each T cell is a T grid point that represents the location of tracer quantities. Similarly, each U cell holds a U grid point representing the location of the meridional and zonal velocity components [*Pacanowski*, 1995].

In a horizontal surface at a depth level k, the grid points and cells are arranged so that a grid point U is located at the northeast vertex of the cell T, and the grid point T is located at the southwest vertex of the cell U (Figure 2.3). The horizontal staggered grid system is the same in all vertical levels between the surface and the bottom ocean domain. Unlike the horizontal grid, the NAOSIM grid is not staggered vertically, which means that all T cells and W cells have the same depth within index k [*Pacanowski*, 1995].

2.4 Methods

2.4.1 Experiment-One

This study is based on three assumptions: (1) each vessel from the sub-dataset makes one call to the destination port per month; (2) it enters the Arctic Ocean without cargo and full ballast tanks; and (3) those vessels perform ballast water exchange along the voyage path before arriving at the destination port. Since the ballast water convention states that ships should not be subjected to a significant trip diversion to perform ballast water exchange, it is assumed that ballast water is exchanged, by many vessels, in waters shallower than 200 m deep. This assumption is preceded by the ship-track density (Figure 2.1) where most of the navigation tracks are on waters shallower than 200 m.

From each ship of the sub-dataset, one position is selected per month to simulate the ballast water distribution throughout a year. Figure 2.4 illustrates the selected positions for the ballast water discharge in the model simulations.

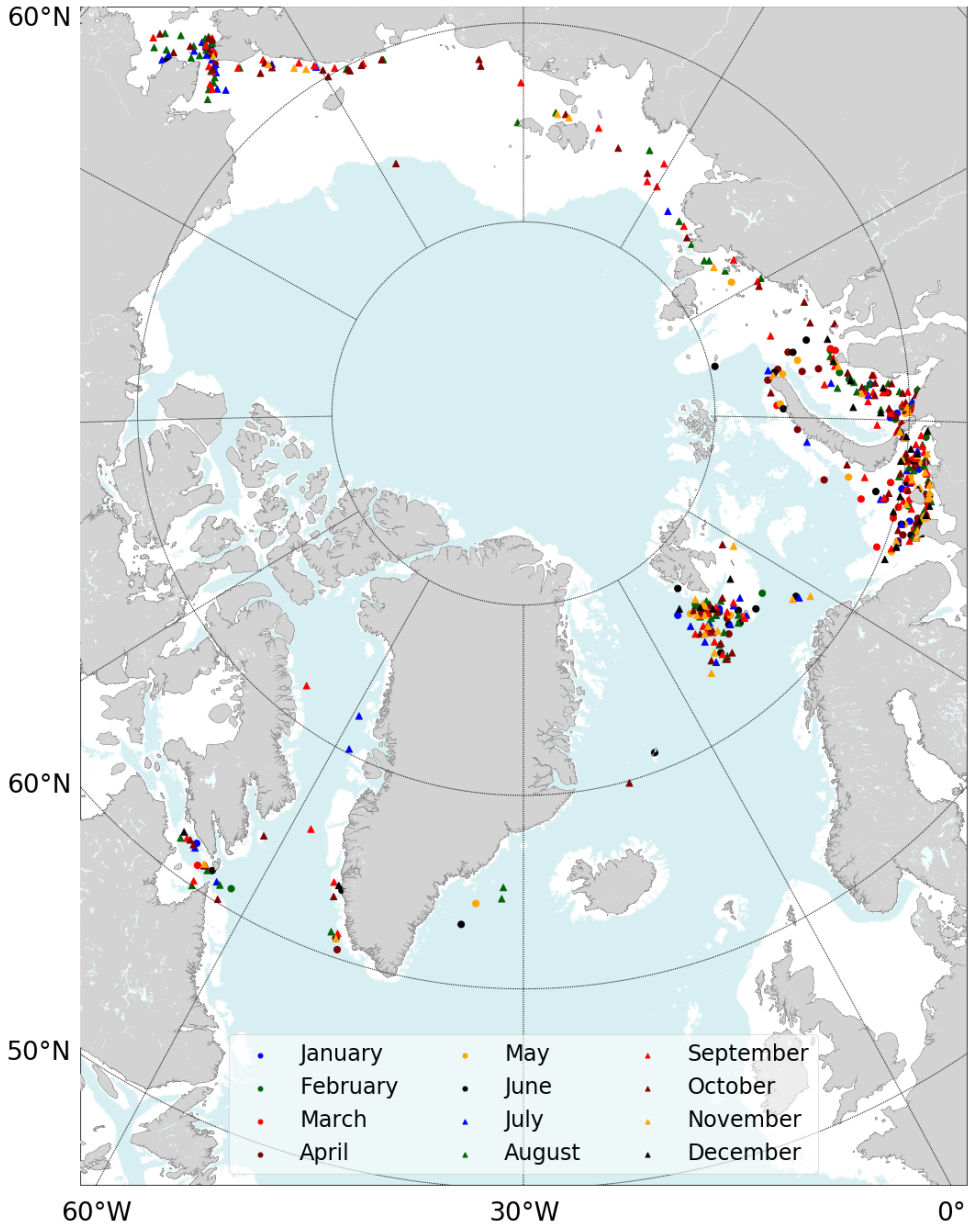

Figure 2.4: Positions of ballast water tracer discharge for the model simulations. The white areas represent waters shallower than 200 m deep Adapted from [*Rosenhaim et al.*, 2019].

For the ballast water simulations, a passive and conservative tracer is implemented into the model NAOSIM. The term "passive" means that the tracer does not contribute to the density of the ocean, whereas its flow is fully governed by the advection-diffusion and convective mixing processes of the ocean model. The ballast water tracer is discharged in the model NAOSIM according to the transmission dates of the ship positions selected from

the sub-dataset. As the sub-dataset contains only vessel information for the year 2013, no ballast water tracer is released in the model before January and after December 2013. The model simulations are carried out through 2013 with ballast water tracer discharge, and two months into 2014 without any ballast water tracer discharge.

Every ship position, selected for the release of ballast water tracer, corresponds to a unique horizontal model grid box. On these selected positions, the ballast water tracer is released in the surface layer for 24 hours and according to the transmission date of each vessel position. Tracer concentration at release is set to one. In the real world, ballast water exchange may take between 12 and 36 hours and is commonly performed during the voyage. That would cover larger distances than the horizontal scale of one model grid box. Hence the approach of releasing the tracer for 24 hours and in one grid box per vessel position is preferred.

The dataset does not contain information on the amount of ballast water carried by each vessel and whether it performed ballast water exchange or had an onboard treatment system.

2.4.2 Experiment-Two

This model experiment has ballast water tracer discharge in only two selected positions. One ship position is located in the Barents Sea, south of Novaya Zemlya, and the second ship position is located southwest of Spitsbergen. The tracer release points of this experiment are illustrated in Figure 2.5.

This experiment is designed to calculate the time needed for the ballast water tracer to mix into different concentration thresholds (e.g., 0.01, 0.05, until 0.50), in the selected areas. To collect this information, the ballast water tracer is discharged in the model once in the beginning of the month and the model simulation is carried for the length of three months with no further tracer release. This simulation is repeated for each month of 2013, with model initialization with zero ballast water tracer concentration over the entire model domain.

Figure 2.5: Ballast water tracer release points of Experiment-Two. The red points southwest of Spitsbergen and south of Novaya Zemlya mark where the ballast water tracer is discharged during the model simulations in Experiment-Two. The water depth is illustrated by white, representing waters shallower than 200 m, and blue representing waters deeper than 200 m. Adapted from [*Rosenhaim et al.*, 2019].

2.4.3 Experiment-Three

An offline particle tracking experiment is designed to identify the pathways of particles that are advected by the surface currents and work as proxy for neutrally buoyant organisms discharged in ballast water and transported by the surface ocean currents.

A particle pathway is described by following its trajectory, i.e., by following the location or position of $x = (x_0, x_1, x_2, \dots x_n)$ of the ocean particle as a function of time, where x_0 is the initial position of the particle trajectory. The trajectory pathway of a particle is given by integrating

$$x = \int_0^T \boldsymbol{u}\, dt \qquad \text{Equation 2.1}$$

where x is the trajectory, $\boldsymbol{u}$ is the two-dimensional velocity field (u and v), dt is time, and T is the total time period of the trajectory [*Olbers et al.*, 2012; *Wolfram and Ringler*, 2017].

For this experiment, a python script is written to compute the particle trajectories using only the horizontal surface velocity field. Vertical movements and the consequent position in a different regime of mean and fluctuating horizontal currents are not considered.

To compute the trajectories, the saved velocity components (u and v) from the model simulations conducted in Experiment-One (described previously in section 2.4.1) are used. In that experiment, the ballast water tracer is released in the model at the selected ship positions of the sub-dataset (described above in section 2.2).

The particle trajectories are computed for two different time intervals of mean velocities, daily and five days. The time interval daily (1-day) are the saved velocities from the model simulations. The time interval of five days (5-days) is the result of the offline computation averaging daily velocities over five days, and are both treated here as total velocities. Each time interval is used to compute particle trajectories for two seasons, winter and summer. Winter consists of January, February, and March, and summer of July, August, and September.

By following equation 2.1, the distances in u and v directions from x_0 to x_n are computed, returning the next particle position along the trajectory pathway. The trajectories' starting points correspond to selected ship positions from the sub-dataset, and are chosen to match the ballast water tracer releases in the model simulations. There are two possibilities for the particle trajectories to end: either the trajectory computation reaches the end of the time frame pre-defined for the trajectory, or the next computed particle location is on land.

The velocity field is composed of the mean and the fluctuating components,

$$\boldsymbol{u} = \overline{\boldsymbol{u}} + \boldsymbol{u}' \qquad \text{Equation 2.2}$$

Where $\overline{\boldsymbol{u}}$ is the mean velocity field and $\boldsymbol{u}'$ is the deviation from that mean [*Vallis*, 2017]. In this experiment, $\overline{\boldsymbol{u}}$ is a time mean over the finite period of a month, and $\boldsymbol{u}$ is the daily velocity field from the saved model output. Here, the $\boldsymbol{u}'$ is also referred to as perturbation velocity.

Monthly mean velocities are computed offline by averaging the daily velocities of each month. The monthly mean velocities are used to compute the perturbation (time-varying) velocity by being subtracted from the daily (total) velocity. The perturbation velocity is then later used for the surface eddy kinetic energy computations.

The total kinetic energy (TKE) can be decomposed into the mean kinetic energy (MKE) and the eddy kinetic energy (EKE) [*Wang et al.*, 2020]. The eddy kinetic energy is

the energy associated with the turbulent part of the flow and is computed from the perturbation velocity (or fluctuation component) as follows:

$$EKE = \frac{1}{2}(u'^2 + v'^2) \qquad \text{Equation 2.3}$$

Daily eddy kinetic energy is computed from the daily perturbation velocity. For the analysis of eddy kinetic energy along the particle trajectories computed with the 5-days velocity field, daily eddy kinetic energy is further averaged over five days.

2.5 Brief theoretical review

2.5.1 Eddy Kinetic Energy

Eddy kinetic energy (EKE) is the energy associated with the turbulent part of a fluid flow. It is commonly described as the kinetic energy of the time-varying component of the velocity field [*Martínez-Moreno et al.*, 2019]. The eddy kinetic energy is calculated by subtracting the mean velocity values from the total velocity returning the perturbation velocity values represented by u' and v' in equation 2.2.

The ocean surface eddy kinetic energy field is highly affected by the wind. The applied wind stress to the ocean surface gives the energy necessary to maintain the oceanic kinetic energy, which is directly associated with the flow of fluid parcels and the necessary amount of shear to produce mixing [*Ferrari and Wunsch*, 2009]. The eddy kinetic energy stirs tracers and momentum along density surfaces (i.e., in the mixed layer); it does not generate overturns (or convection) and mixing across density surfaces [*Ferrari and Wunsch*, 2009]. The maximum and minimum eddy kinetic energy values are indicators of sources and sinks of energy in the ocean [*Richardson*, 1983]. Eddy activity is usually represented using eddy kinetic energy [*Talley*, 2011]. NAOSIM does not resolve eddies. However, in this study, the eddy kinetic energy is computed to visualize the turbulent mixing of the ballast water tracer in the ocean model and the effects of turbulent flow on the displacement of particles.

2.5.2 Mixing

Mixing is a result of 'stirring' caused by turbulent flow and eddies. The ocean is stably stratified, and vertical displacement of water parcels works against the buoyancy force, requiring more energy than horizontal mixing. Turbulent mixing is stronger along surfaces of constant density compared to vertical mixing across surfaces of constant density. Vertical mixing, is responsible for changes in the ocean's vertical structure and controls the rate at which deep-water eventually reaches the surface [*An Open University Course*, 1989; *Ferrari and Wunsch*, 2009; *Roy-Barman and Jeandel*, 2016].

The ocean surface layer is forced directly by wind stress, heat, and freshwater exchanges (buoyancy). Sufficiently large wind stress creates turbulence that mixes the upper layers of the ocean, creating a substantially uniform density layer or mixed layer. Buoyancy loss through the sea surface (heat and freshwater) increases the density of the top of the surface layer, causing it to overturn to a greater depth with similar density. This overturn is usually called convection, a mixing process where heavy and light fluid parcels are exchanged towards homogeneity of the water column. Heat and freshwater gain decrease the density at the top of the upper surface layer and create a more stably stratified profile [*Ferrari and Wunsch*, 2009; *Talley*, 2011].

Shallow and coastal waters, when the tidal currents are fast enough and the waters are shallow enough, will present an entirely mixed water column. At the end of winter, due to a long time of cooling and deepening of the mixed layer and increase of its density, the thickest mixed layers occur [*Talley*, 2011]. Since ballast water ballast water is released in the experiments described above, mostly in shallow shelf seas, vertical mixing is an important process influencing the ballast water flow in this study.

2.5.3 Particle trajectories

It is common in observational oceanography to use tracer release experiments to study the surface and subsurface ocean currents. Conservative chemicals are typically used to mark distinct water masses to infer mixing rates and advective pathways [*Wagner et al.*, 2019].

Ocean general circulation models are valuable tools for studying water masses, tracers, and pollution dispersion pathways. Ocean models complement the sparse observational oceanographic data [*Wagner et al.*, 2019].

Two different approaches can be used to identify water masses and tracers' pathways on ocean models: (1) online representation and (2) offline representation. The online representation uses a passive tracer with concentrations determined by the resolved circulation, transport processes of advection and diffusion, and parameterized mixing, as the mixed layer processes like convection. The offline representation uses saved model output and Lagrangian particle trajectories [*Blanke and Raynaud*, 1997; *Kelly et al.*, 2018]..

The particle trajectory is calculated by updating the particle position in space and time according to the saved mean velocities, which does not require the full model to be rerun. In the offline approach, the parameterized mixing processes are unrepresented. Only the effects of advection are considered, a disadvantage of the method [*Kelly et al.*, 2018]. However, the turbulent mixing processes are described by horizontal turbulent flow (and eddies) and by vertical mixing.

Chapter 3. Ballast water discharge along Arctic shipping routes

This chapter analyzes the ballast water tracer flow and accumulation at two essential areas of the Northeast Passage. It discusses how ocean circulation influences the tracer distribution through different seasons. The chapter starts with a summary of the ship-track density. It is followed by a description of the chosen areas of study. Results, discussion, and conclusions are presented. The results presented here are published in *Rosenhaim et al.* [2019].

3.1 Ship density in the Arctic Ocean

The highest density of vessels in 2013, as shown in the previous chapter in Figure 2.1, are observed along the Northeast Passage, especially the Barents and Kara Seas, and west and south of Spitsbergen, throughout the whole year. Since the number of ships is closely connected to contamination risks by ballast water and polluted water, this study's focus is the spreading of the ballast water tracer from these two main areas. Complementary figures illustrating the monthly ship-track density are presented in the Appendix (Figures A.02, A.03, and A.04).

In total, 165 vessels compose the sub-dataset of ship positions. Many of these vessels make multiple voyages to the Arctic region during a year. Consequently, the ballast water tracer is released 499 times in the model, distributed along one year of simulations.

The number of vessels in the Arctic, as the number of ballast water tracer discharge, during winter is small and increases towards the summer. This increase in the number of vessels navigating the Arctic routes has a strong connection to the contamination risks through ballast water and polluted water. The number of ballast water tracer discharge in the model simulations for each month is presented in Figure 3.1.

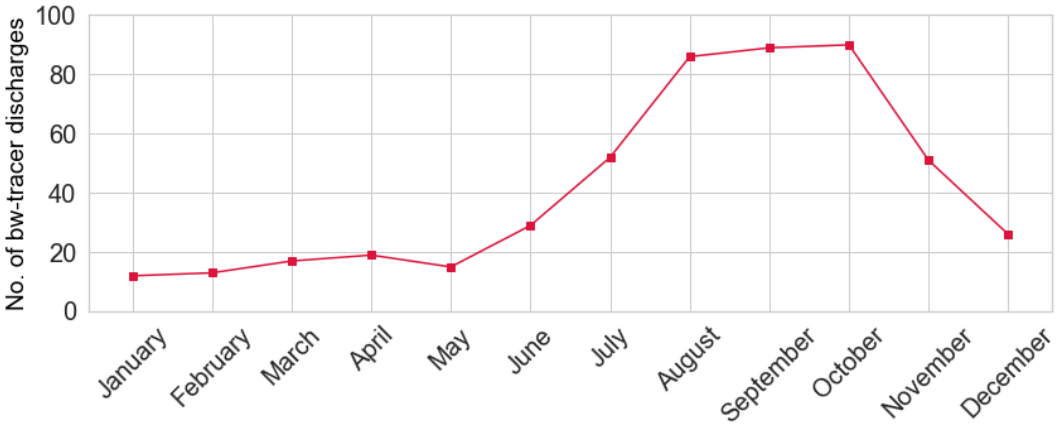

Figure 3.1: Number of monthly ballast water tracer discharge events along the year 2013 in the whole model domain.

The estimated volume of ballast water discharged by ships performing destination traffic in the Arctic region in 2013, is approximately 13 million m^3 [*Luitjens*, 2015].

3.2 Study areas

For the analysis of ballast water tracer dispersion after discharge, two main areas of the Northeast Passage have been chosen due to their high ship traffic density throughout the whole year. The chosen areas are the south Barents and Kara Seas, and the west and south of Spitsbergen. The following sections describe the main oceanographic features of the chosen areas.

3.2.1 West and south Spitsbergen sector

Spitsbergen is the eastern boundary of Fram Strait, which is the only deep strait connecting the North Atlantic and the Arctic Ocean (ca. 2600 m deep). The Fram Strait has two main current systems: the East Greenland Current (EGC), that carries cold and fresher water and sea ice from the Arctic basin southwards to the subpolar North Atlantic, and the West Spitsbergen Current (WSC), that carries warm Atlantic Water northwards into the Arctic Ocean [*Rudels et al.*, 1999; *Saloranta and Haugan*, 2001] (Figure 1.2 – Chapter 1). The area south of Spitsbergen and north of Bear Island is mainly characterized by water recirculation [*Loeng et al.*, 1997].

3.2.2 Barents and Kara Seas sector

The Barents and Kara Seas are part of the shallow Arctic Continental shelf seas. The Barents Sea has a maximum depth of ca. 500 m and an average depth of 230 m [*Drinkwater*, 2011].

The Barents Sea hydrology is characterized by the warm and saline Atlantic Water inflow from the south and the cold and fresher water inflow from the Arctic [*Loeng and Drinkwater*, 2007]. The sea ice cover in the Barents Sea is characterized by strong seasonality, with maximum cover occurring in March and April [*Drinkwater*, 2011]. The ocean surface currents flow from the Barents Sea, through the Kara Gate into the Kara Sea, and they vary seasonally with a strong flow during winter and a weaker flow during summer [*Loeng et al.*, 1997].

The Kara Sea has water depths of less than 200 m, except for the two canyons in the north and east, the Novaya Zemlya Trough. It receives one-third of the total freshwater discharged in the Arctic basin, having consequences for the stratification of the Arctic Ocean [*Aagaard and Coachman*, 1975; *Hanzlick and Aagaard*, 1980]. Water is exchanged through the Kara Gate on the west, and it has open boundaries to the Arctic Ocean in the north and to the Siberian shelves in the east [*Volkov*, 2002].

3.3 Results

3.3.1 General flow

The spreading of the ballast water tracer discharged in the continental shelf seas follows the surface currents directly forced by the wind. In contrast, the flow of the ballast water tracer discharged in the western Spitsbergen area, which is deeper than the continental shelf seas, is strongly influenced by the two main currents of the Fram Strait, i.e., the West Spitsbergen Current and the East Greenland Current.

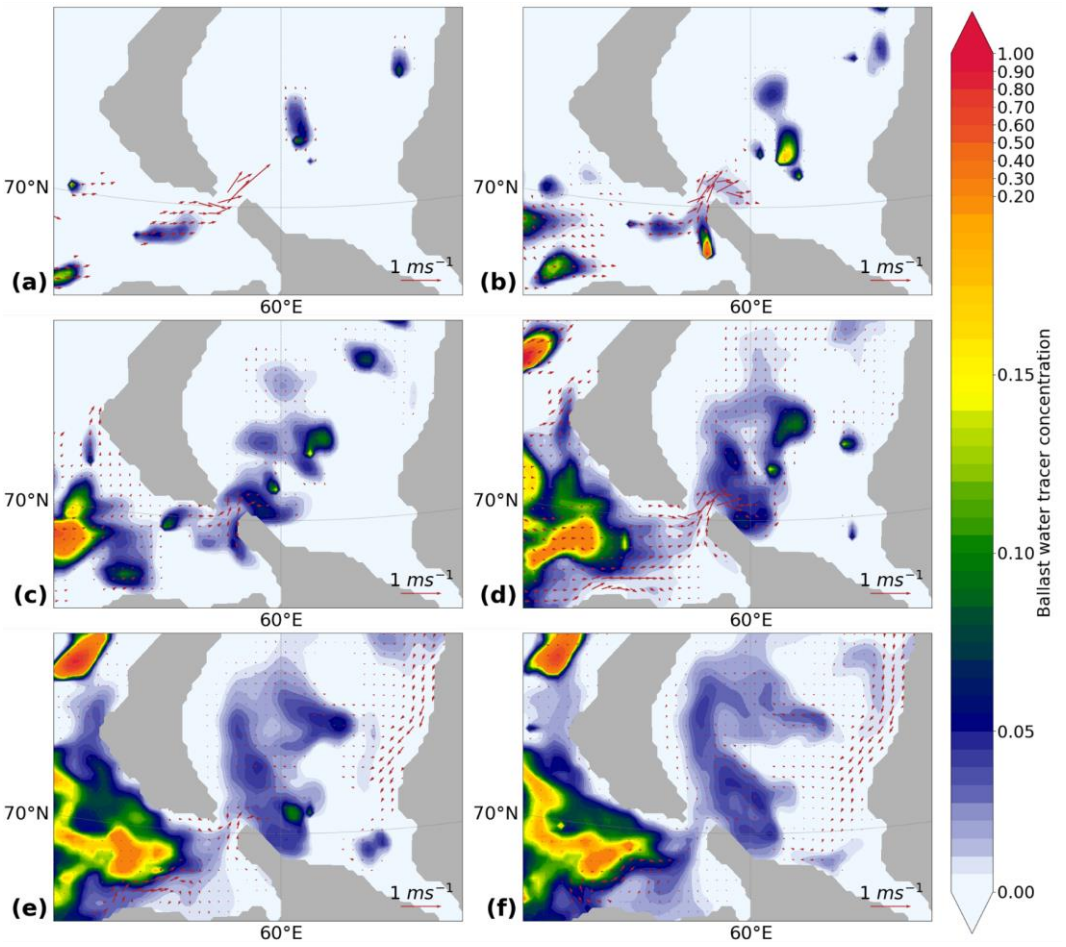

Figure 3.2: Flow of the ballast water tracer and the surface currents in the Barents Sea sector. The figure shows the monthly mean ballast water tracer concentration (colored shades) and the model simulation's surface currents (red arrows) from 2013. The panels refer to (a) January, (b) February, (c) March, (d) April, (e) May, and (f) June.

3.3.2 Barents Sea sector

During winter months (January, February, and March), the discharged ballast water tracer presents an eastwards main flow, from south of Novaya Zemlya in the Barents Sea and through the Kara Gate, into the Kara Sea. At the beginning of March, the tracer persists southwest of Novaya Zemlya, remaining there through spring (April, May, and June) and most of the summer (July, August, and September). Part of the accumulated ballast water tracer in the southern Barents Sea starts to flow through the Kara Canal and into the Kara Sea in August (mid-summer). It begins to accumulate in the eastern side of the Kara Gate, south Kara Sea. Figure 3.2 illustrates the monthly averages of ballast water

tracer and ocean surface currents from January to June, and Figure 3.3 illustrates the monthly averages of ballast water tracer and ocean surface currents from July to December.

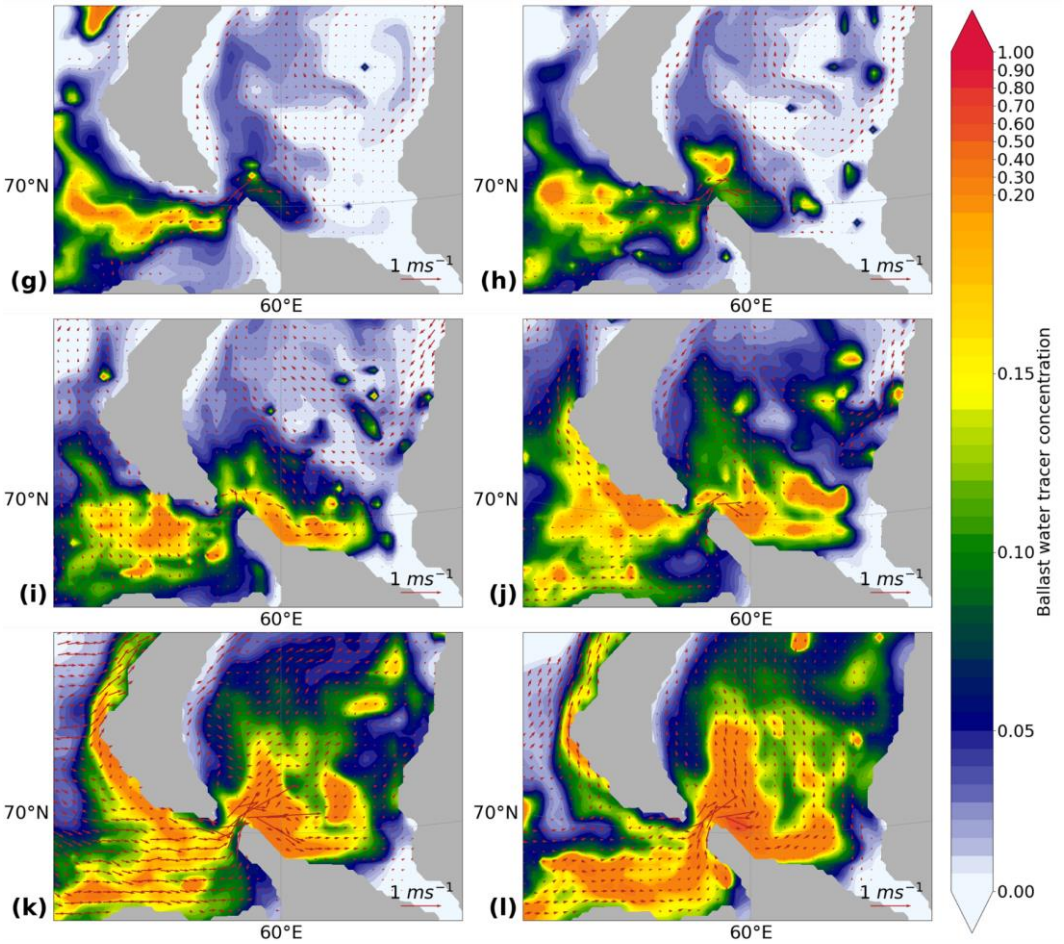

Figure 3.3: Flow of the ballast water tracer and the surface currents in the Barents Sea sector. The figure shows the monthly mean ballast water tracer concentration (colored shades) and the model simulation's surface currents (red arrows) from 2013. The panels refer to (g) July, (h) August, (i) September, (j) October, (k) November, and (l) December.

At the end of September, part of the ballast water tracer that starts to accumulate during spring and summer in the southwest of Novaya Zemlya flows northwards, reaching the island's southwest coast (Figure 3.3i and j). Through autumn (October, November, and December), there is an increase of ballast water tracer accumulation on the southern Kara Sea. In both, south Barents Sea and the south Kara Sea, the model output for winter 2014 (i.e., January and February, Figure 3.4) shows large areas with high tracer concentration.

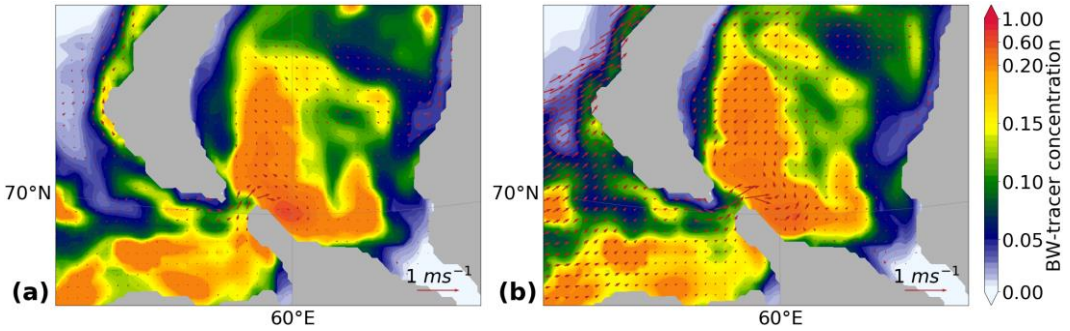

Figure 3.4: Ballast water tracer concentration in 2014. The figure shows the monthly mean values of the ballast water tracer concentration (colored shades) and the model simulation's surface currents (red arrow). The panels refer to (a) January and (b) February 2014.

During winter or colder months, the ballast water tracer is carried to deeper layers as a consequence of vertical convective displacement in the water column. In some places, it reaches the continental shelf floor (Figure 3.5). In contrast, during summer or warmer months, the tracer remains in the surface layers, between the surface and 20 m deep, due to stable stratification of the water column and a shallower mixed-layer (Figure 3.6).

According to the model results, spring and summer are the most favorable seasons for the tracer to accumulate in the southern Barents Sea sector. In contrast, the tracer accumulation in the south Kara Sea started during summer and persisted through autumn and the next winter. Furthermore, the ballast water tracer concentrations reached at the accumulation areas during summer and autumn showed a persistent pattern through autumn and the next winter (January and February 2014).

As the model simulations progress into autumn, the ocean surface currents become stronger, and the flow from the Barents Sea into the Kara Sea accelerates. Due to the strengthened flow through the Kara Canal, the ballast water tracer concentration increases in the area, indicating tracer accumulation on the canal's east side. Most of the tracer forming this accumulation area was previously released in the southern Barents Sea, specifically on the southwest of Novaya Zemlya. The extended model simulations into the next winter (January and February 2014) show the ballast water tracer had concentration values of 0.60 in both sites, still two months after the last ballast water tracer discharge in the model.

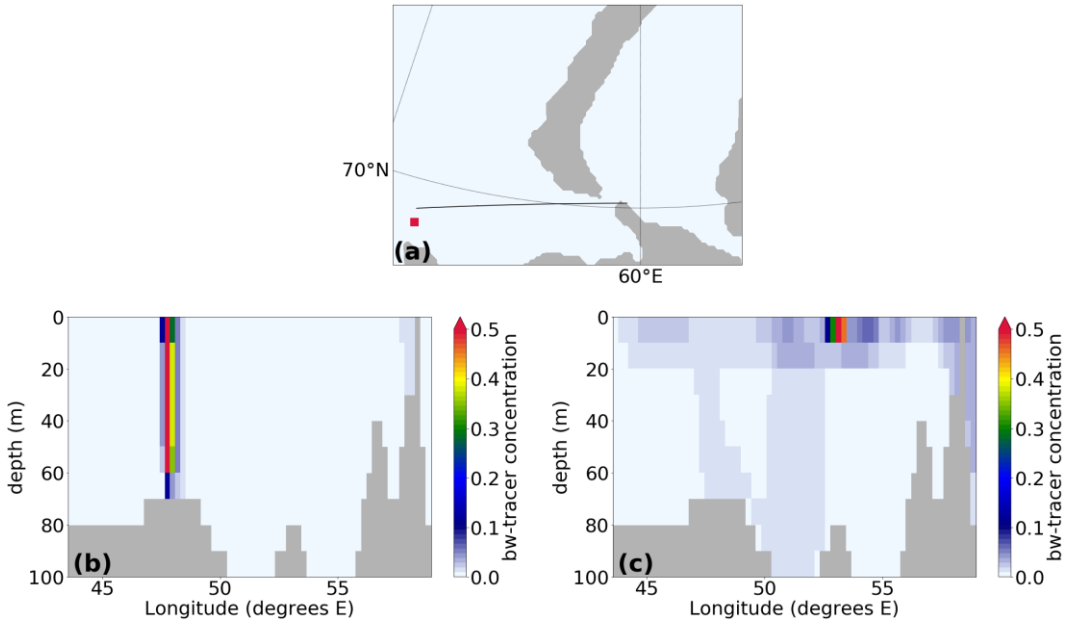

Figure 3.5: Vertical sections of the Barents Sea sector south of Novaya Zemlya. The black line in (a) shows the location of the sections. In winter (b), the ballast water tracer is carried to deeper layers by convection. In contrast, in summer (c), the ballast water tracer stays at the surface layer due to the water column's stratification. Adapted from [*Rosenhaim et al.*, 2019].

At the beginning of January 2014, the ballast water tracer concentration in the southern Kara Gate is up to ca. 0.50, and tracer is transported from the southern Barents Sea to the southern Kara Sea. As the simulations progress through the month, the direction of the surface currents changes, and the flow is then from the Kara Sea into the Barents Sea. As a result, the ballast water tracer concentration drops to ca. 0.15 and less in the Kara Gate (Figures A.05 and A.06 in the Appendix). Through January 2014 simulations, the surface currents frequently changed direction. The atmospheric circulation strongly influences the surface currents in this area.

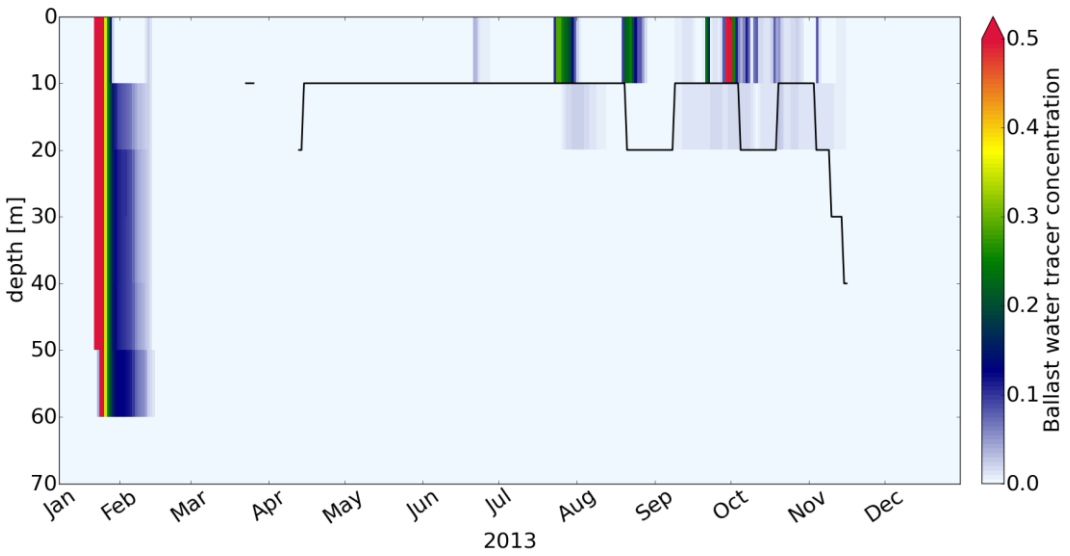

Figure 3.6: Vertical displacement of tracer and mixed-layer depth in the Barents Sea sector. The figure presents the evolution along the simulation year of the ballast water tracer in one model grid coordinate (indicated as a red square in Figure 3.5a). The black line represents the bottom of the mixed-layer depth. Adapted from [*Rosenhaim et al.*, 2019].

During the first half of February 2014, the surface currents flow from the Barents Sea to the Kara Sea. By mid-month, the currents change direction for a few days and then back to the Barents Sea's main flow to the Kara Sea. The ballast water tracer concentration in the Kara Gate remained with concentration values less than 0.15 through February.

The ballast water tracer flows resultant from the model simulations in the Barents, and Kara Seas sector showed consistency with the ocean surface circulation described by [*Loeng et al.*, 1997]. The authors mention that the seasonality of the water fluxes may be strongly related to the wind field's seasonality. During summer, the wind is expected to be mostly calm, while during winter, stronger winds are expected to prevail.

3.3.3 Spitsbergen sector

The ballast water tracer, discharged in the west Spitsbergen sector, flows northwards, following the direction of the West Spitsbergen Current (WSC) until the current reaches the Arctic basin, and it encounters the East Greenland Current (EGC) that carries the tracer southwards along the east coast of Greenland.

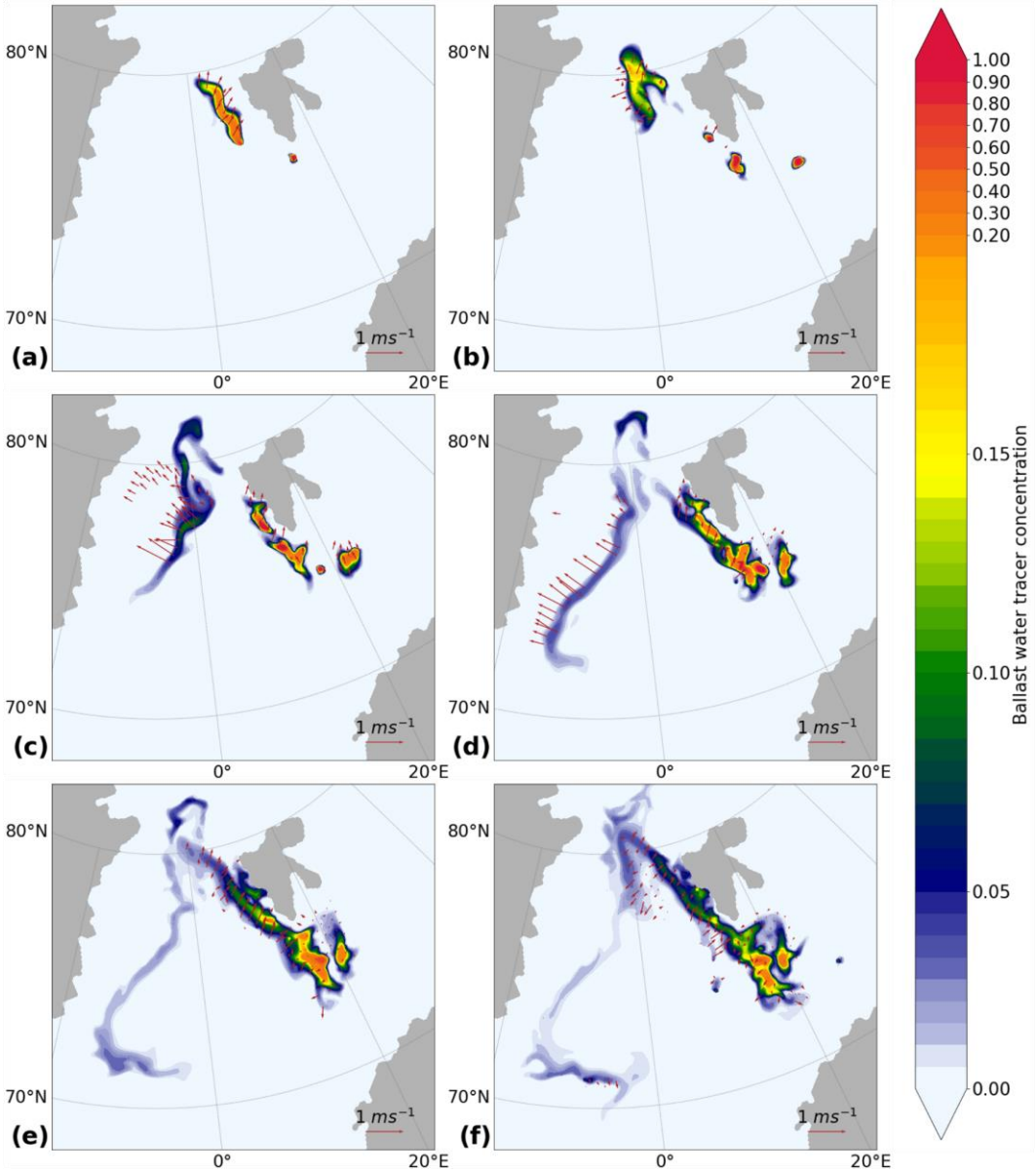

Figure 3.7: Flow of the ballast water tracer and the surface currents in the Spitsbergen sector. The figure shows the monthly mean ballast water tracer concentration (colored shades) and the surface currents of the model simulation (red arrows) from 2013. The panels refer to (a) January, (b) February, (c) March, (d) April, (c) May, and (f) June.

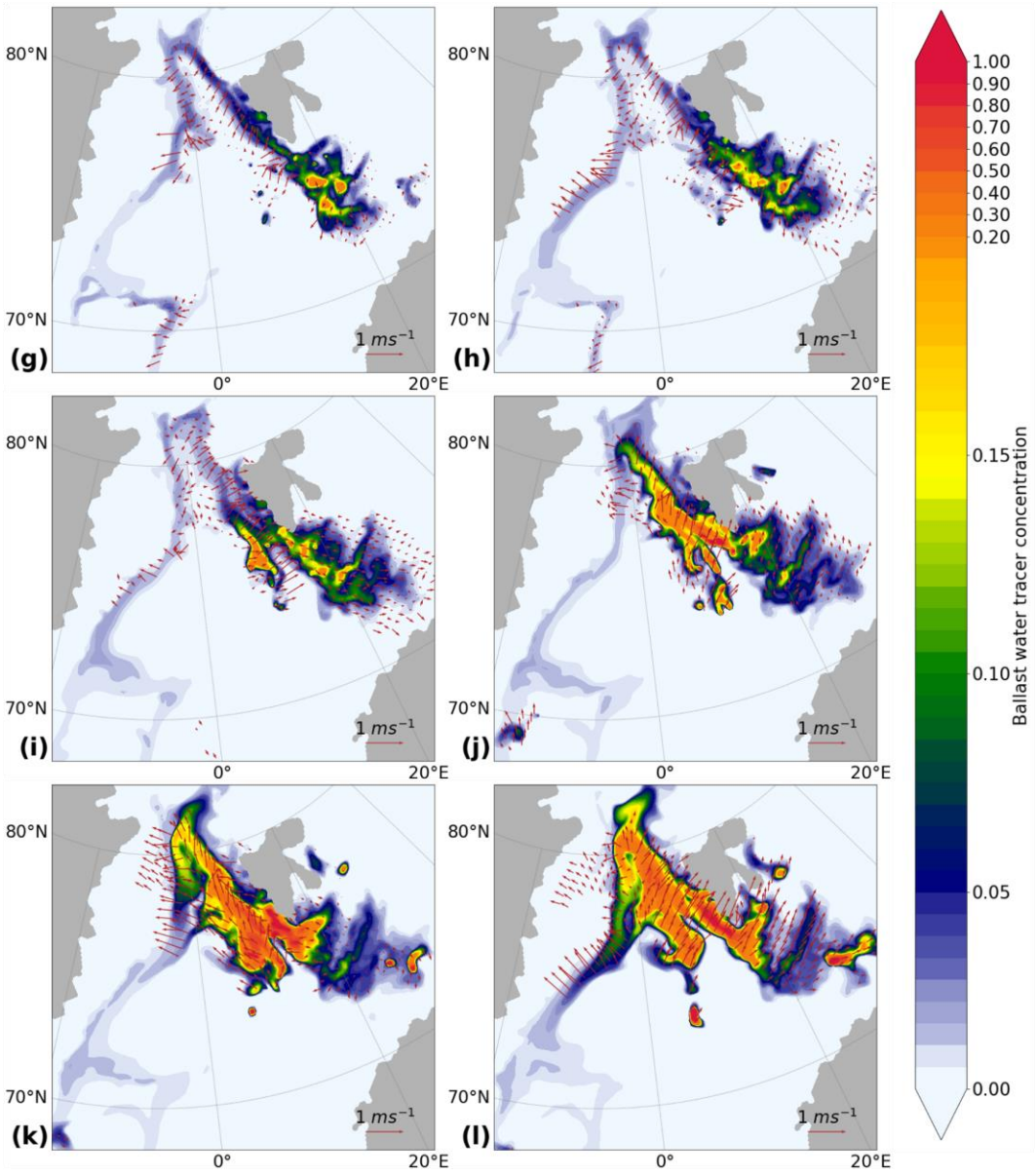

Figure 3.8: Flow of the ballast water tracer and the surface currents in the Spitsbergen sector. The figure shows the monthly mean ballast water tracer concentration (colored shades) and surface currents of the model simulation (red arrows) from 2013. The panels refer to (g) July, (h) August, (i) September, (j) October, (k) November, and (l) December.

Accumulation of ballast water tracer started during spring in the area between the southern tip of Spitsbergen and Bear Island. In these areas, high tracer concentration (ca. 0.50) persisted through the simulation year due to new tracer release in the vicinity (Figure 3.7 and 3.8). The area's topographic features as the Bear Island Bank and the Storfjord Sea channel contribute to the accumulation of ballast water tracer.

The model results of January and February 2014, two months after the last ballast water tracer release in the model simulation, shows that the tracer concentration in the areas south of Spitsbergen and along the main currents in the Fram Strait remained considerably high (Figure 3.9). Ballast water tracer released in this region in winter, due to convection, reached depths of 250 to 300 m. On the other hand, the ballast water tracer discharged during warmer months stayed on the upper layers (upper 20 m) due to strong stratification of the water column (Figure 3.10 and 3.11).

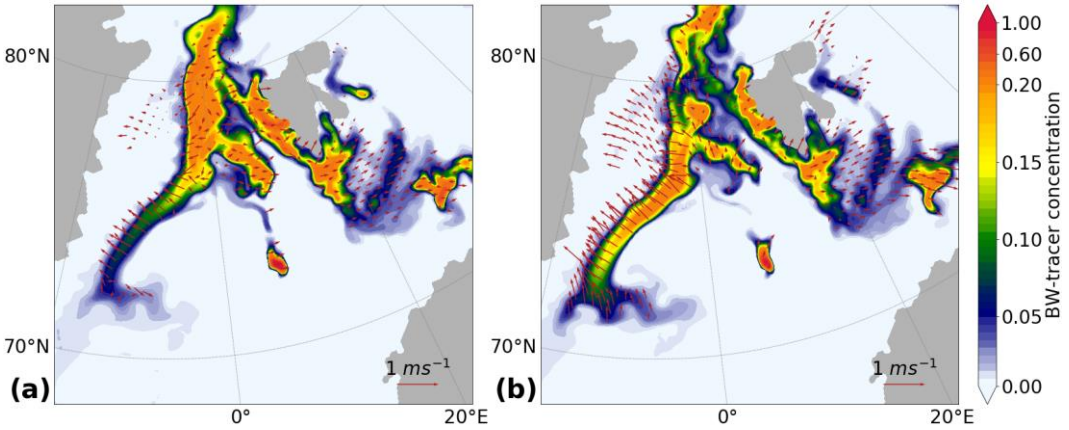

Figure 3.9: Ballast water tracer concentration in 2014. The figure shows the monthly mean values of the ballast water tracer concentration (colored shades) and the model simulation's surface currents (red arrows) from 2014. The panels refer to (a) January and (b) February 2014.

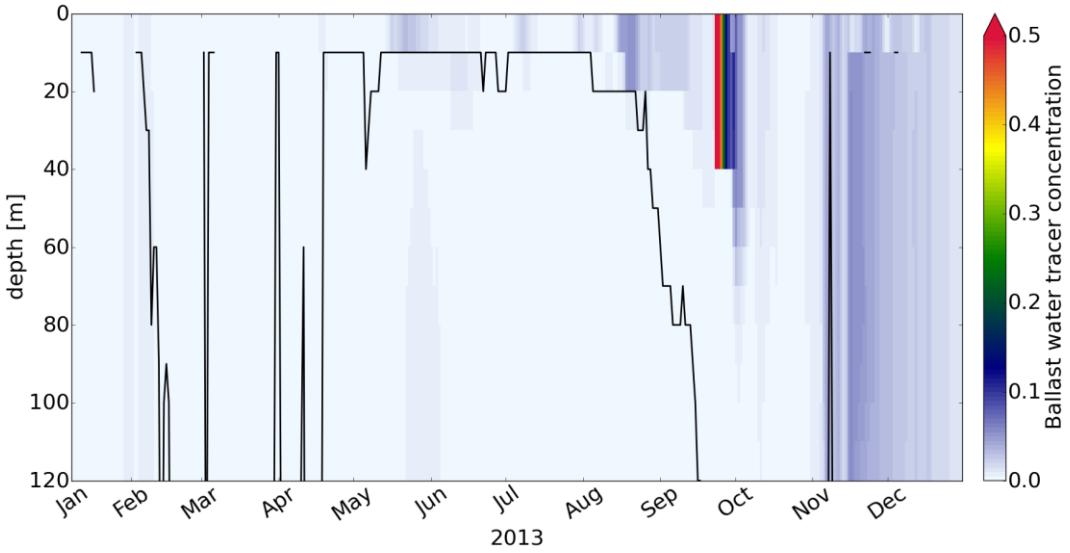

Figure 3.10: Vertical displacement of tracer and mixed-layer depth in the Spitsbergen sector. The figure presents the evolution along the simulation year of the ballast water tracer in one model grid coordinate (indicated as a red square in Figure 3.11a). The black line represents the bottom of the mixed-layer depth. Adapted from [*Rosenhaim et al.*, 2019].

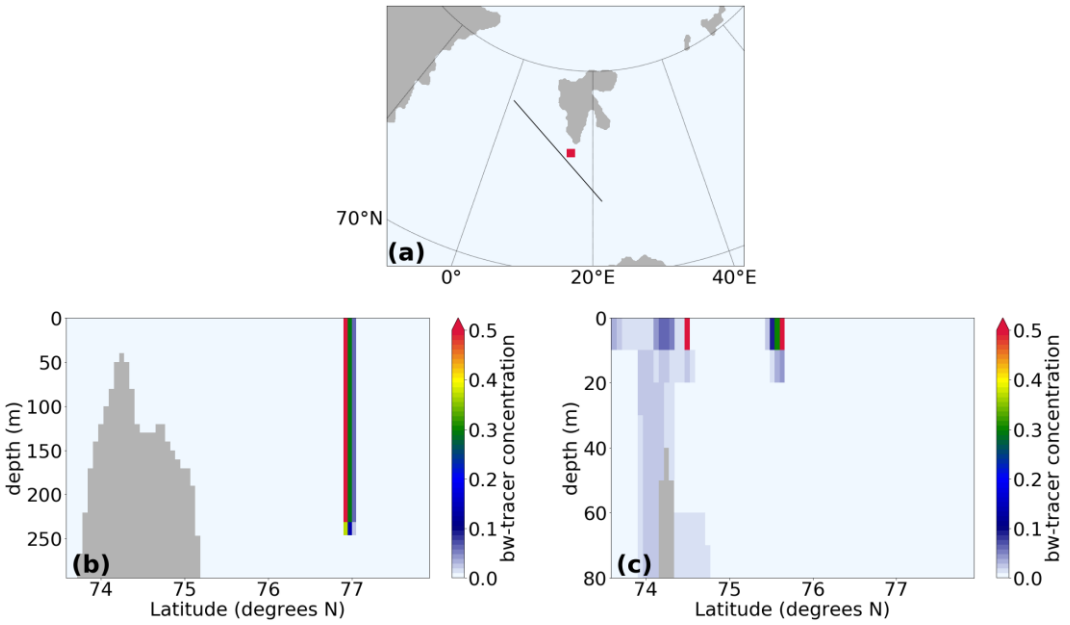

Figure 3.11: Vertical sections of the west Spitsbergen sector. The black line in (a) shows the location of the sections. In winter (b), the ballast water tracer is carried to deeper layers by convection. In summer (c), the ballast water tracer stays at the surface layer due to the stratification of the water column. Please, note the different y-ranges in panels b and c. Adapted from [*Rosenhaim et al.*, 2019].

3.3.4 Experiment-Two

In Experiment-Two ballast water tracer is released in only two ship positions. One in the Barents Sea south of Novaya Zemlya and the other at southwest of Spitsbergen as described in section 2.4.2. The monthly reinitialization of the ballast water tracer in the Barents Sea showed that the tracer takes more than 20 days to disperse and mix with the seawater and reach a concentration of 0.01. The only exceptions are the model simulations of January and November, where the tracer reached 0.01 of concentration in less than 20 days. As presented in Figure 3.12, ballast water tracer released in May, June, and July takes 80, 72, and 42 days, respectively, to reach a concentration value equal to 0.01 in the Barents Sea.

Unlike the Barents Sea, the ballast water tracer released in the west Spitsbergen sector in January takes 54 days to reach concentrations of 0.01. In February, it takes 42 days. The tracer released in June and July reached concentrations of 0.01 after 44 and 46 days, respectively (Figure 3.13). To reach concentration thresholds of 0.05 or higher, all tracer simulations in the west Spitsbergen sector take less than 20 days.

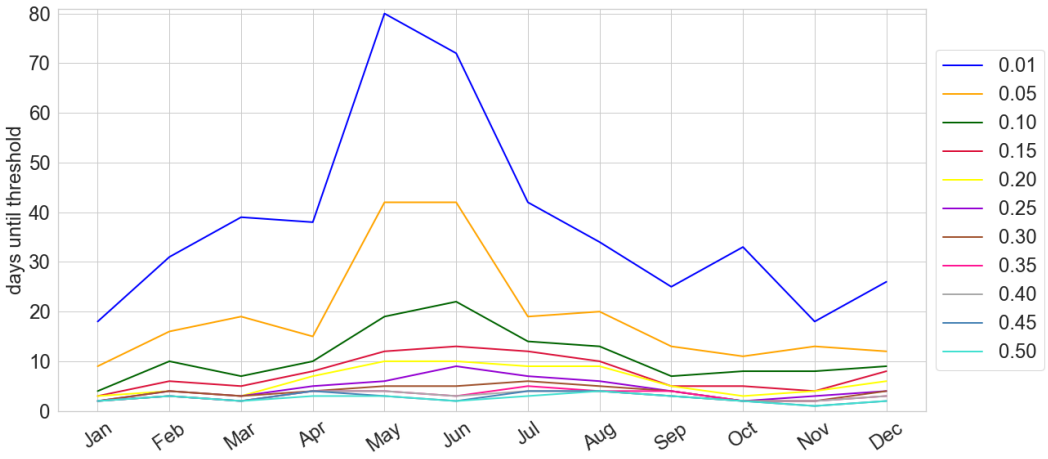

Figure 3.12: Experiment-Two – ballast water tracer released in the Barents Sea sector. The figure shows the results of the ballast water tracer monthly reinitialization experiment. Each of the chosen thresholds of tracer concentration is represented by a different color in the figure. The blue line represents the 0.01 tracer concentration threshold and shows that during spring and the beginning of summer, the ballast water tracer takes relatively long to completely mix with the surrounding ocean water. Adapted from [*Rosenhaim et al.*, 2019].

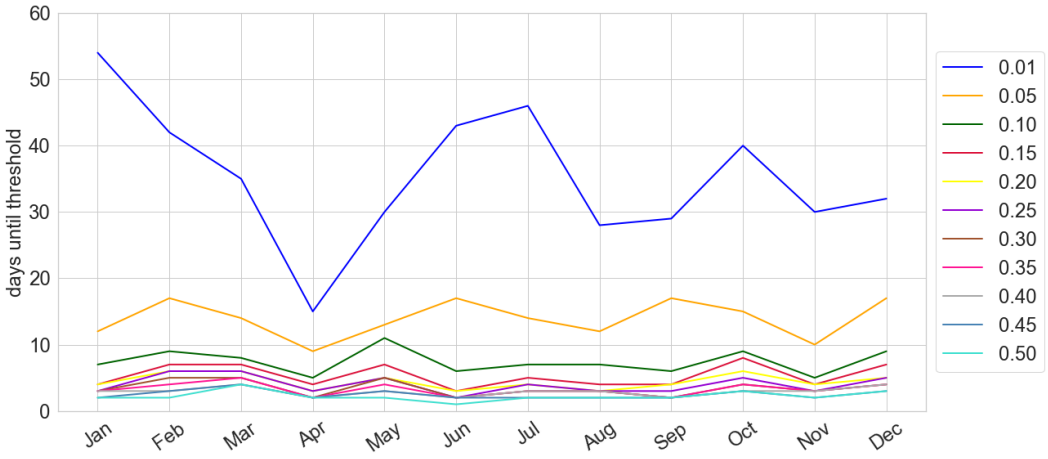

Figure 3.13: Experiment-Two – ballast water tracer release southwest of Spitsbergen. The figure shows the results of the ballast water tracer monthly reinitialization experiment. Each of the chosen thresholds of ballast water tracer concentration is represented by a different color in the figure. The orange line represents the 0.05 tracer concentration threshold and shows that in the west Spitsbergen sector, the ballast water tracer can mix with the surrounding ocean water in less than 20 days. Adapted from [*Rosenhaim et al.*, 2019].

Analysis of higher tracer concentration thresholds revealed that in the Barents Sea, south of Novaya Zemlya, the ballast water trace takes longer to reach different concentration thresholds, especially during May and June, compared to the tracer released on the southwest Spitsbergen sector.

3.4 Summary and discussion

For the simulation of the dispersion of ballast water discharged by vessels along the main Arctic shipping routes, a passive tracer is implemented in the 1/12-degree version of the regional coupled ocean-sea ice model NAOSIM. The model domain covers the whole Arctic Ocean, the Nordic Seas, and Northern North Atlantic.

Two areas are selected to analyze the ballast water tracer dispersion due to the year-round high density of commercial ship navigation. One area is the southern Barents Sea, connected to the Kara Sea through the Kara Canal, and the second area is the west and south of Spitsbergen.

In winter, the number of ballast water tracer discharged in the model simulations is small due to the small number of vessels navigating the Northeast Passage during this

season (Figure 3.1). The amount of tracer in the winter months is also small because the model simulations start in January (the first winter month) without previous tracer releases.

As the model simulations progress into spring and summer, the number of vessels that navigate the Arctic routes increases. Consequently, the number of ballast water tracer discharges increase in the model, leading to an increased risk of environmental contamination (e.g., by non-indigenous species, anthropogenic contaminants, pathogens, toxins, and polluted water).

Only a small part of the number of vessels navigating the Arctic shipping routes in 2013 is reflected in the model simulations. A total of 378 vessels of types bulker, tanker, general cargo, and ro/ro navigated the Arctic shipping routes in 2013; 202 performed destination traffic and the geographical coordinates of only 165 ships are used for the model simulations.

The number of vessels is expected to increase. As a result of model experiments, some studies suggest that the Northern Sea Route might experience a considerably longer navigable season [*Gascard et al.*, 2017]. *Miller and Ruiz* [2014] estimated an increase in the number of ships at a rate of ca. 20% per year in the Northern Sea Route. Furthermore, as the exploitation of natural resources in the Arctic realm increases, vessels with origin in European, American, and East Asian ports, shall enter the Arctic with a full load of ballast water.

Results of the ballast water model simulations shows that the flow of the ballast water tracer is strongly seasonal, especially in the Barents Sea sector, which shows a fast flow through the Kara Canal during winter and autumn, compared to the weak flow through the canal during spring and summer (Figures 3.2 and 3.3). Furthermore, during the most favorable seasons for shipping in the Northeast Passage, the number of vessels is larger. So, a correspondingly larger amount of ballast water tracer is released. These factors contribute to the seasonality of the ballast water tracer accumulation south of Novaya Zemlya and south of Spitsbergen.

Whether ballast water is exchanged and where is not known. Since a considerable number of vessels navigated on waters shallower than 200 m, as illustrated by Figure 2.1,

it is assumed that the vessels from the sub-dataset exchanged ballast water during the voyage and many on the continental shelf.

The model simulations showed that the ballast water tracer released in the Barents Sea accumulates in waters shallower than 200 m on both sides of the Kara Canal. The ballast water tracer released in the west Spitsbergen sector presented a northward flow, following the West Spitsbergen Current. As it encounters the East Greenland Current, the tracer is carried southwards along the east coast of Greenland, as illustrated by Figures 3.7 and 3.8.

The West Spitsbergen Current, a warm current with North Atlantic influence, and the East Greenland Current, a cold current with Arctic influence, are the two main currents of Fram Strait. These two currents are responsible for the ballast water tracer's flow towards regions deeper than 200 m. The area between Bear Island and Spitsbergen's southern tip, in the Barents Sea Opening, presented ballast water tracer accumulation due to water recirculation in this area [*Loeng et al.*, 1997; *Timofeev*, 1963].

The ballast water tracer spread and accumulation seasonality have important aspects like the wind and wind-driven currents, the water column's hydrostatic stability, and factors influencing the actual shipping intensity and location.

During winter and autumn, instabilities in the water column, which generate convection and vertical mixing, are due to more frequent and strong winds, cooling of the surface water by the cold atmosphere above, sea ice formation, and salt rejection. Vertical mixing causes homogeneity of the water column, and relatively high ballast water tracer concentrations are carried to deeper layers. When sea ice starts to melt in spring, it returns freshwater to the ocean surface, the open water starts to absorb more solar radiation, and the water column becomes more stable and stratified, as vertical convection ceases and horizontal mixing dominates. Due to the water column's stable stratification, the ballast water tracer during spring and summer tends to remain in the surface layers.

For the ballast water tracer discharged in the Barents Sea sector, a homogeneous water column means that the tracer can reach the continental shelf floor (Figure 3.5b). A stratified water column maintains the tracer in the upper 20 m with larger horizontal spreading and accumulation (Figure 3.5c).

In the west Spitsbergen sector, the ballast water tracer released in winter and autumn can reach depths between 200 and 400 m (Figure 3.11b). During spring and summer, the ballast water tracer remains in the upper 20 m of the water column due to stable stratification and is horizontally spread (Figure 3.11c). The main difference between the Barents Sea sector and the Spitsbergen sector is the maximum depth reached by the ballast water tracer during cold months. The Fram Strait has greater depths than the continental shelf seas. The ballast water tracer is carried by convective mixing to deeper levels and mixed with the surrounding waters before reaching the ocean floor.

The seasonality pattern of the ballast water tracer described above is illustrated by Figures 3.6 and 3.10, with a representation of the mixed-layer depth. *Loeng and Drinkwater* [2007] and *Rey* [2004] mention that the phytoplankton blooming season is strongly affected by the mixed-layer seasonality. Both studies show a schematic representation of phytoplankton's seasonal developments, and they point out that the peak of the phytoplankton bloom in the Barents Sea occurs in spring. Accumulation of the ballast water tracer started in spring, and the tracer reinitialization experiment shows that in spring, the ballast water tracer released in the southern Barents Sea takes longer to reach lower concentration thresholds, as illustrated in Figure 3.12. Thus, as the ballast water tracer concentration remains high during spring and summer, it indicates high risks of contamination by non-indigenous species and toxins to this Arctic ecosystem.

From the model simulations, three areas are identified where ballast water tracer present accumulation. One is located south of Spitsbergen, where the tracer reached concentrations of 0.60 in spring, remaining considerable high through summer, autumn, and the two winter months of 2014. The tracer in this area is trapped in the recirculation between the southern tip of Spitsbergen and Bear Island. The ballast water tracer that is transported by the two main currents of Fram Strait (WSC and EGC) presented a high concentration (approximately 0.40 to 0.60) during autumn and January-February 2014.

The second area of tracer accumulation is the southern Barents Sea. Here, the tracer concentration presents high values and started to accumulate during spring and summer due to the Kara Canal's seasonal weak water flux. The third area to present accumulation of ballast water tracer is the southern Kara Sea, on eastern side of the Kara Canal. This accumulation area is formed by the time-varying water flux through the canal, with tracer

previously discharged in the southern Barents Sea during summer and autumn (Figure 3.3i- l).

3.5. Conclusions

Using a regional ocean-sea ice model forced by actual atmospheric forcing, the spread and potentially harmful accumulation of ballast water discharged in the main Arctic shipping routes is simulated using ship tracks from 2013.

The ballast water tracer flow, accumulation, and amounts have strong seasonality due to weather conditions, sea ice presence, differences in vertical mixing, and the prevailing currents. The model simulation results presented high concentrations of ballast water tracer in deeper layers during winter and autumn due to convection and vertical mixing, responsible for the water column's homogeneity.

The water column's stable stratification influences accumulation during spring and summer of ballast water tracer south of Novaya Zemlya and south of Spitsbergen. Stratification prevents vertical mixing and suppresses convection during these seasons, keeping the ballast water tracer in the surface layers. No significant difference is observed, for the ballast water tracer released at the surface of waters deeper or shallower than 200 m, during warm months in the model results. Ballast water tracer accumulation started on the east side of the Kara Canal in autumn, mainly due to a temporal imbalance between tracer influx from the southern Barents Sea and drainage from the Kara Sea.

Accumulation of ballast water presents a risk to the ecosystem. It may provide a greater number of non-indigenous species and organisms, which might establish themselves in the new environment, and become invasive. Ballast water may also contain infectious pathogens. If sewage, oil spills, grey, and scrubber water are discharged together with ballast water, the local ecosystems' risks of contamination increase.

Chapter 4. Ballast water analysis via individual particle trajectories

The study previously described in Chapter 3 demonstrates the link between ballast water tracer concentration, distribution, and seasonality. The present chapter focuses on the advection of individual tracer particles. It investigates the influence of the eddy variability of the velocity field, measured by the eddy kinetic energy, on the advection of particles, ballast water tracer mixing, and the importance of tracer diffusivity to the ecosystem.

4.1 Results

The previous analysis in chapter 3 determines the influence of the seasonal cycle. Therefore, this chapter focuses on particle trajectories computed in winter and summer, too. The particle trajectories computed with the winter velocities have their start position west of the Kara Canal at 53°18’58” longitude and 69°26’14” latitude (or model coordinates i275 and j490, represented by the black square in Figure 4.1) on January 9th. The summer particle trajectories have their start position also west of the Kara Canal approximately 111 km further east compared to the winter starting point at 55°57’33” longitude and 69°36’49” latitude (i263 j489, represented by the black square in Figure 4.11), and the start date on July 17th. The model coordinates and starting dates are chosen to match the ballast water tracer releases in previous model simulations. As the particle trajectory is calculated, variables like ballast water tracer concentration, particle displacement from one position to the next, and eddy kinetic energy are computed at each particle position according to the time-averaged velocity field. The trajectories computed using the daily velocity field are here called 1-day trajectories, while the trajectories computed using the velocity field averaged over five days are here called 5-days trajectories, and the velocity field represented by $\overline{\boldsymbol{u}}$ refer to monthly means.

4.1.1 Winter trajectories

In general, particles move along slightly different trajectory pathways when computed with different time-averaged velocities, as shown in Figure 4.1. The reason behind is the different time frequencies that lead to loss of information of short time events during the computation of averages. The winter particle trajectories are in total 82 days long.

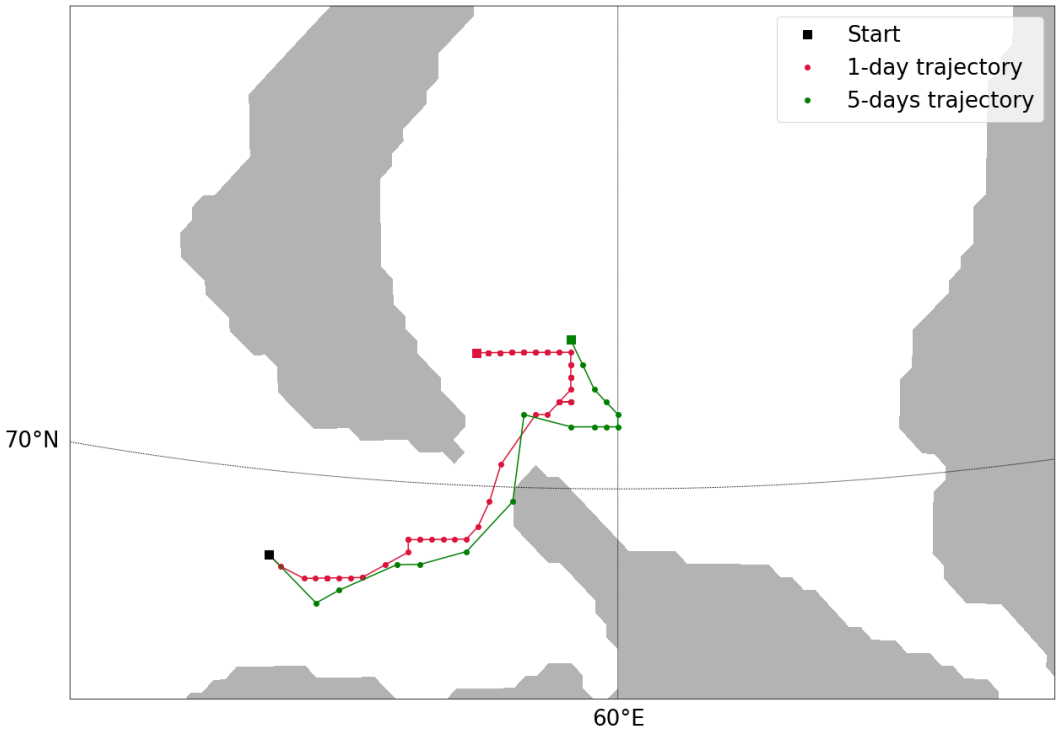

Figure 4.1: Winter particle trajectory pathways. The black square marks the initial position (i275 j490) of the trajectories, and the squares in the corresponding colors represent the end of the pathways.

By the end of March, none of the trajectories calculated with the winter velocities ends on land. The particle trajectory calculated with the 5-days velocities has a particle position at the southern coast in the Kara Canal (northwest Vaygach Island – not resolved by the model due to its resolution). The surface currents advect the particle through the canal and into the Kara Sea. This particle position is the nearest to land in the trajectory pathway.

Along the winter particle trajectory pathways, the highest values of eddy kinetic energy (EKE) are computed at the particle positions in the Barents Sea and Kara Canal. The particle displacements, from one position to the next, are also greater in the Barents Sea and Kara Canal. The eddy kinetic energy and the particle displacements of both trajectories in the Kara Sea are relatively small compared to the values computed in the Barents Sea.

The correlation between eddy kinetic energy values of both trajectories and the distance between the path-lines described by each trajectory is negative, demonstrating that closer path-lines result from higher eddy kinetic energy, i.e., strong turbulent flow. In contrast, lower eddy kinetic energy (or less turbulence), results in increased distance between the path-lines described by the trajectories (Figure 4.2).

Figure 4.2 presents the eddy kinetic energy values along both particle trajectories and the distance between the trajectories' path-lines. Tables 4.1 and 4.2 show the average eddy kinetic energy (EKE) and average particle displacement along each trajectory in the Barents Sea and the Kara Sea in winter, respectively.

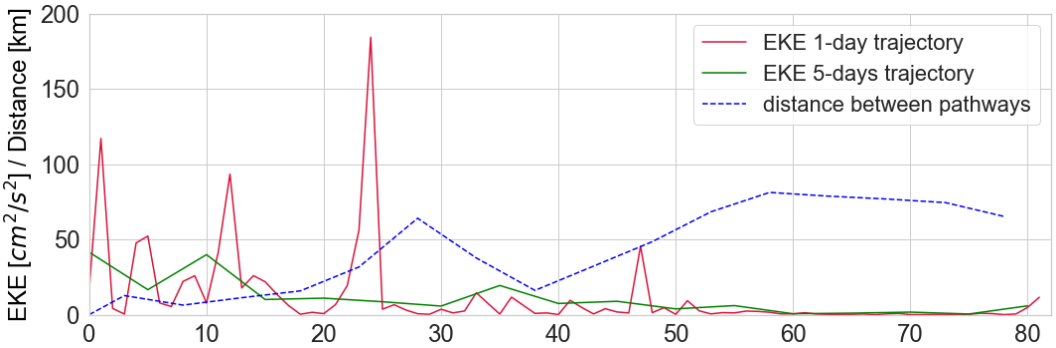

Figure 4.2: Winter Eddy kinetic energy values and distance between trajectory pathways. The figure shows the eddy kinetic energy values computed at each particle position along the winter particle trajectory pathway calculated with 1-day velocities (red line) and 5-days velocities (green line). The dashed blue line shows the distance between the two trajectory pathways.

The ballast water tracer concentration computed along the trajectory pathways experiences a fast reduction from its maximum concentration at the beginning of all winter trajectories, as shown in Figure 4.3. This reduction of tracer concentration is due to intense vertical mixing, typical for the wintertime. Since particle trajectories are calculated using

only the surface velocity field and show just the effect of horizontal advection on the particle displacement, the trajectory pathways do not follow the same path of the tracer. This difference between tracer and particle paths increases when the time-average with which the trajectory is calculated increases. The fast tracer concentration reduction indicates that the tracer is well mixed in the Barents Sea during winter, shortly after release.

Table 4.1 – Winter averaged values of eddy kinetic energy computed from 1-day and 5-days velocity field. The mean eddy kinetic energy corresponds to the time range listed in column two (after no. of days) indicating the part of the trajectory being in the Barents Sea, or the Kara Sea, or along the total trajectory.

EKE	**1-day trajectory**		**5-days trajectory**	
	Mean	After no. of days	Mean	After no. of days
Barents Sea	25.48	24	21.26	6
Kara Sea	3.18	57	5.50	10
Trajectory	11.92	82	11.07	17

Table 4.2 – Winter averaged values of particle displacements between its positions computed along 1-day and 5-day trajectory pathways. The displacement values correspond to the time range listed in column two (after no. of days) indicating the part of the trajectory being in the Barents Sea, or the Kara Sea, or along the total trajectory.

Particle Displacement	**1-day trajectory**		**5-days trajectory**	
	Mean	After no. of days	Mean	After no. of days
Barents Sea	8.77 km	24	36.36 km	6
Kara Sea	2.43 km	57	16.73 km	10
Trajectory	4.76 km	82	25.22 km	17

Table 4.3 shows the values of mean ballast water tracer concentration vertically integrated and only within the surface, computed at the particle positions in the Barents and

Kara Seas. The different concentrations stress the influence of vertical mixing on the ballast water tracer concentration.

Table 4.3 – Winter average values of ballast water tracer concentration along the 1-day and 5-days particle trajectories. The tracer concentration values are separately presented as vertical integral and within the surface layer. The time range correspond to the ones on table 4.1 and 4.2 (after no. of days), indicating the part of the trajectory being in the Barents Sea or the Kara Sea.

Ballast water tracer concentrations	**1-day**	**5-days**
Vertical integral of mean BW-tracer – Barents Sea	0.075	0.054
Vertical integral of mean BW-tracer – Kara Sea	0.0098	0.028
Mean BW-tracer in surface layer – Barents Sea	0.055	0.045
Mean BW-tracer in surface layer – Kara Sea	0.0019	0.0164

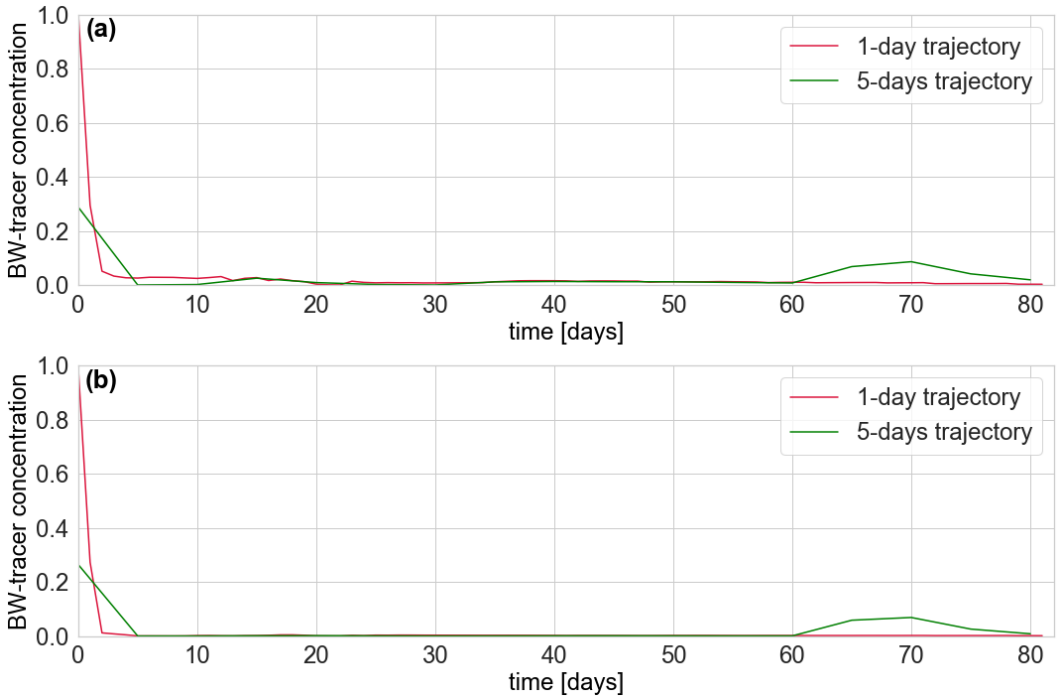

Figure 4.3: Ballast water tracer concentration along the winter trajectory pathways. The plot shows the (a) vertically integrated values of ballast water tracer concentration and (b) the ballast water tracer concentration within the surface layer, computed along the trajectories.

4.1.1.1 – Winter 1-day particle trajectories

In the particle trajectory calculated with 1-day velocities (u and v), the particle remains in the Barents Sea until day-23. It reaches the Kara Canal on day-24 (February 2nd), and on day-25, the particle arrives in the Kara Sea (Figure 4.6).

The highest value of eddy kinetic energy and the greatest particle displacements are computed on day-24 when the particle is at the center of the Kara Canal. As illustrated in Figure 4.4, the eddy kinetic energy in the Barents Sea (from day-0 to day-23) is higher than the eddy kinetic energy values in the Kara Sea (from day-25 to day-81). The particle displacement has the same tendency, demonstrating that the displacement of a particle from one position to the next, along the trajectory pathway, correlates to the eddy kinetic energy strength in wintertime.

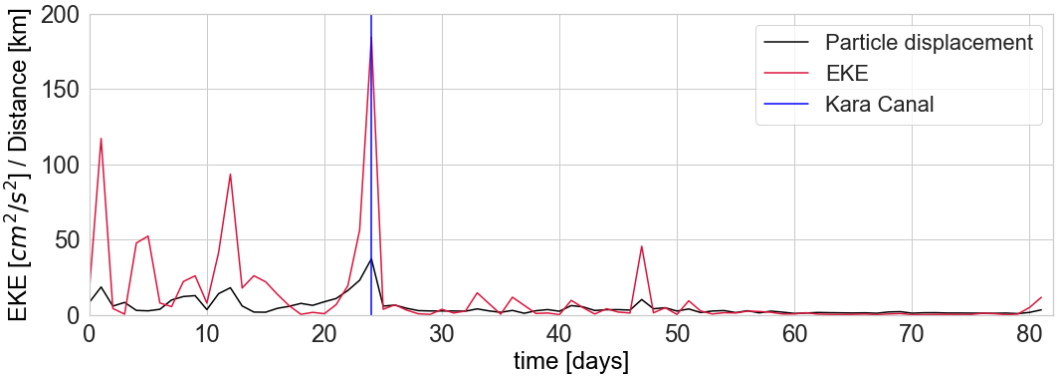

Figure 4.4: Particle displacements and eddy kinetic energy values along the particle trajectory computed with the winter 1-day velocity field. The blue vertical line indicates the particle position in the Kara Canal.

The large particle displacement from the Kara Canal to the next position in the Kara Sea is due to the velocity field (u and v). While the high value of eddy kinetic energy at the Kara Canal is due to the difference between the values of total velocity in u direction and its monthly mean ($\bar{u}$, Figure 4.5a), returning a high value of the perturbation velocity (u'). Figure 4.6 shows the particle trajectory on days 24 and 25, with the ballast water tracer concentration (Figure 4.6a,c), which in the Kara Canal is close to zero, and the eddy kinetic energy (Figure 4.6b,d) that has high values in the Kara Canal.

The ballast water tracer that remained in the ocean surface layer after release presents a substantial reduction of its concentration in the first four days of the experiment, reaching tracer concentration close to zero after 24 days (Figure 4.6a,c). Ballast water tracer with a low concentration on deeper levels is advected by deeper currents into the Kara Canal, keeping low concentrations of ca. 0.03 for a longer time.

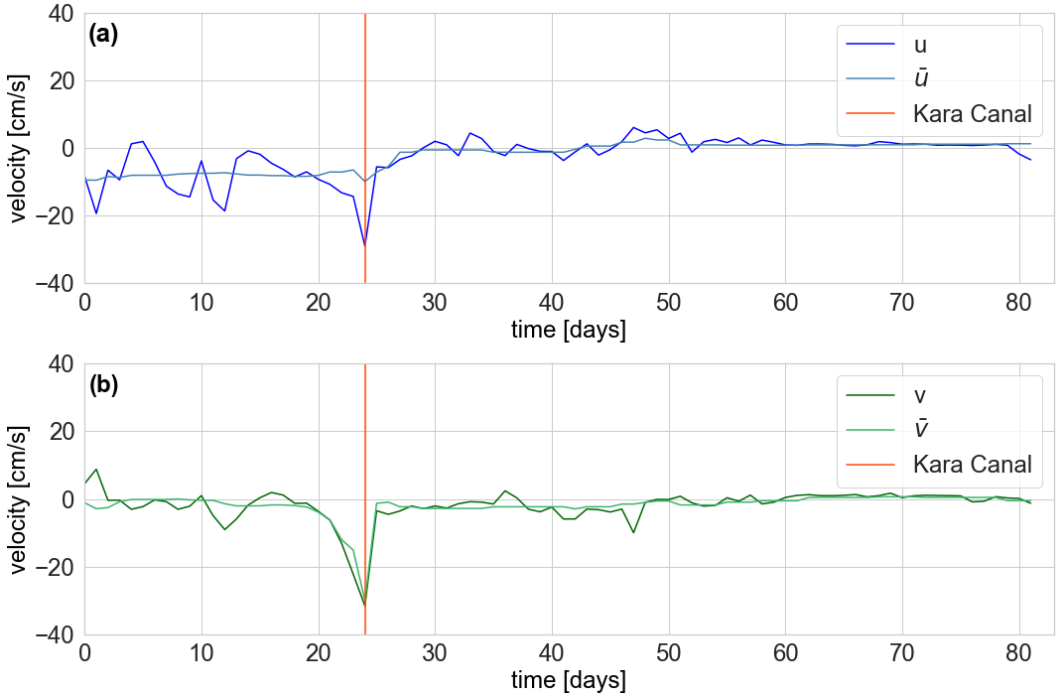

Figure 4.5: Velocities field (u and v) values computed along the particle trajectory calculated with the 1-day winter velocity field, and the respective monthly average values represented by $\bar{u}$ and $\bar{v}$. The vertical line indicates the particle position at the Kara Canal.

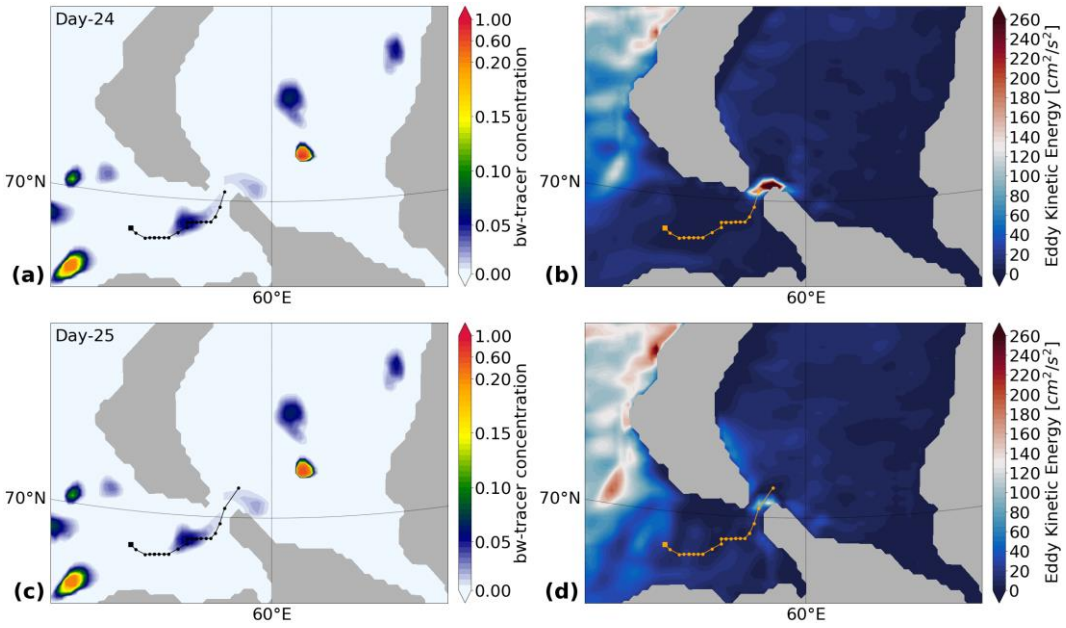

Figure 4.6: Ballast water tracer, eddy kinetic energy, and 1-day winter particle trajectory. The panels show the (a, c) ballast water tracer concentration (vertical integral values) and (b, d) surface eddy kinetic energy as background for the particle trajectory computed with the winter 1-day velocity field.

4.1.1.2 –Winter 5-days particle trajectory

In the particle trajectory computed with 5-days velocity field (u and v), the particle remains in the Barents Sea until day-25 reaches the Kara Canal on day-30, and arrives in the Kara Sea on day-35. The greatest particle displacements are computed while the particle is in the Barents Sea (on days 0, 10, and 20) and the Kara Sea on day-35 (Figure 4.7).

The ballast water tracer concentration in the particle position at the Kara Canal on day-30 is close to zero (Figure 4.3, green line). At this particle position, the eddy kinetic energy is low because the differences between the 5-days velocities (u and v) and the corresponding monthly means ($\bar{u}$ and $\bar{v}$) are relatively small, returning small values of perturbation velocities (u' and v') (Figure 4.8). Figure 4.9a shows the low concentration (around zero) of ballast water tracer in the Kara Canal and, Figure 4.9c shows ballast water tracer from another release, flowing to the Kara Canal, close to the coast. Figure 4.9 (b and d) illustrates the eddy kinetic energy in the area on both days.

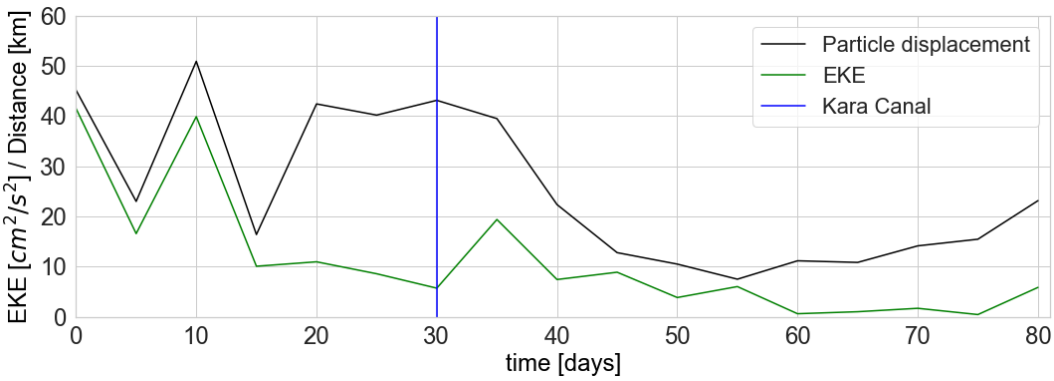

Figure 4.7: Particle displacement and eddy kinetic energy values along the particle trajectory calculated with the winter 5-days velocity field. The blue vertical line indicates the particle position at the Kara Canal.

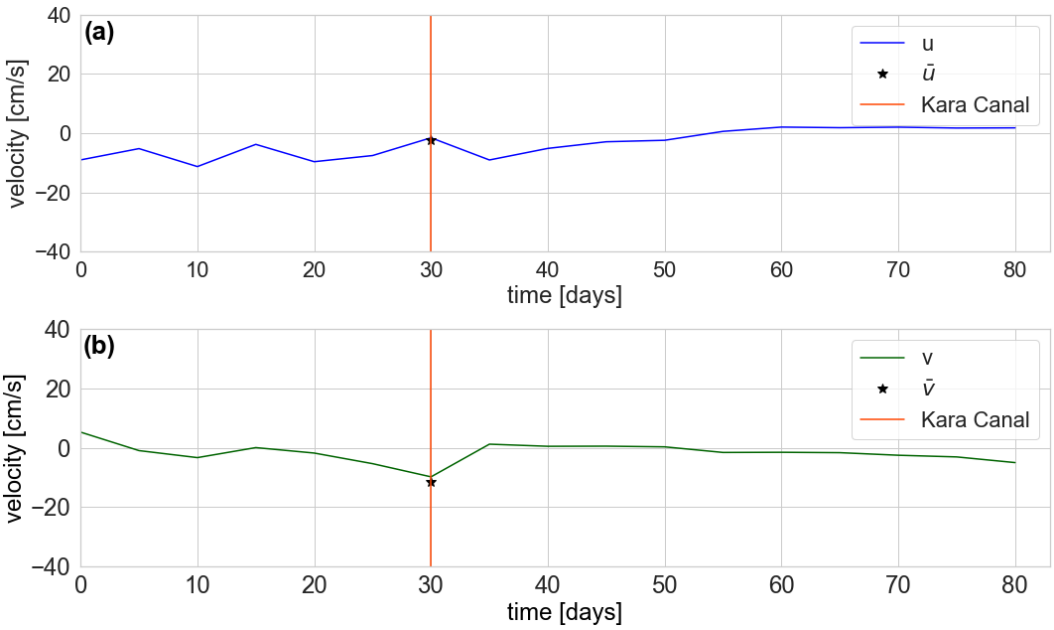

Figure 4.8: Values of velocity components u and v computed along the winter 5-days particle trajectory. The black stars represent the monthly mean velocities in the particle position at the Kara Canal.

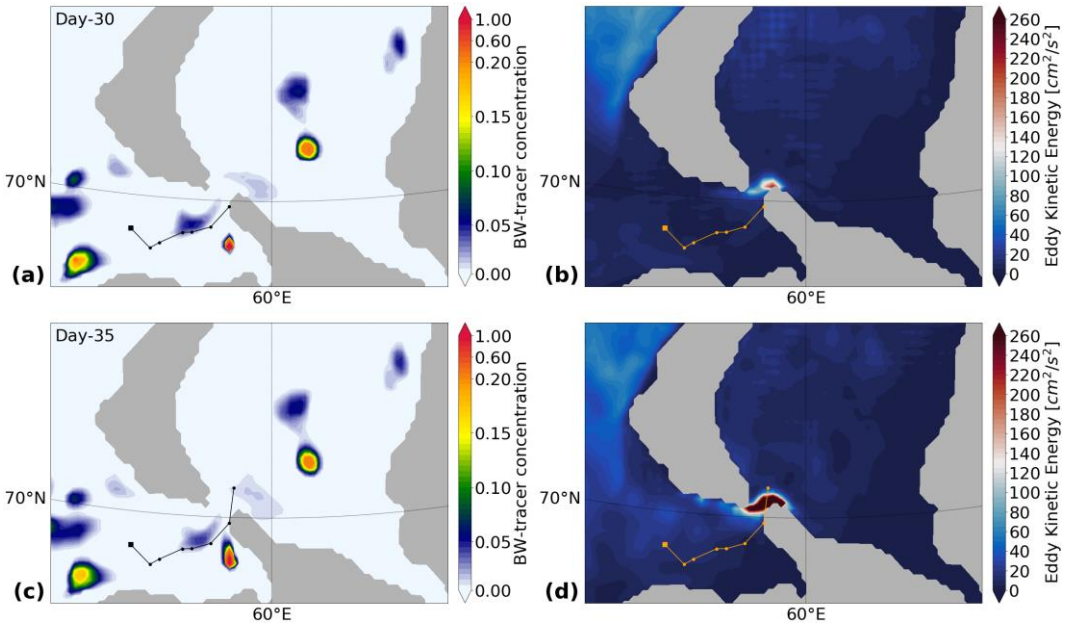

Figure 4.9: Ballast water tracer, eddy kinetic energy, and 5-days winter particle trajectory. The panels show (a, c) the ballast water tracer concentration (vertical integral values) and (b, d) eddy kinetic energy as background for the particle trajectory calculated with 5-days winter velocity field. The panels show when the particle reaches the Kara Canal on day-30 and its first position on the Kara Sea on day-35 of the trajectory.

The last particle position of the trajectory calculated with the winter 1-day velocity field is ca. 37 km from land. The particle trajectory calculated with the winter 5-days velocity field has its final position ca. 120 km from the coast. Both winter particle trajectories ended because the time selected for the experiment ends after 82 days. Figure 4.10 shows the particle trajectory pathways in separated maps.

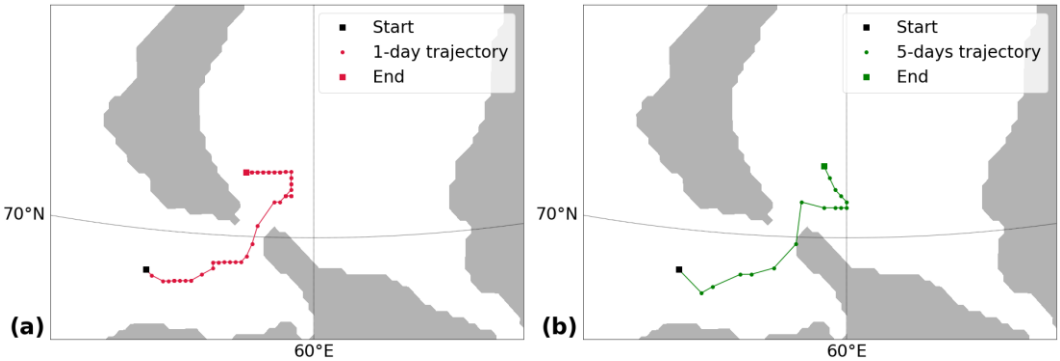

Figure 4.10: Winter particle trajectories. (a) particle trajectory calculated with 1-day, and (b) 5-days winter velocity fields.

4.1.2 Summer trajectories

The summer particle trajectories are shorter than the winter particle trajectories, and reach land. In Figure 4.11, the last particle positions presented are still on the sea; however, the next particle positions calculated after the ones shown in the figure are on land, more specific in the southern area of Novaya Zemlya. Due to computed particle displacement, these positions are not on the coast, but land, and therefore are not shown. The particle trajectories are calculated offline and do not recognize the land before the variable values are read in that position.

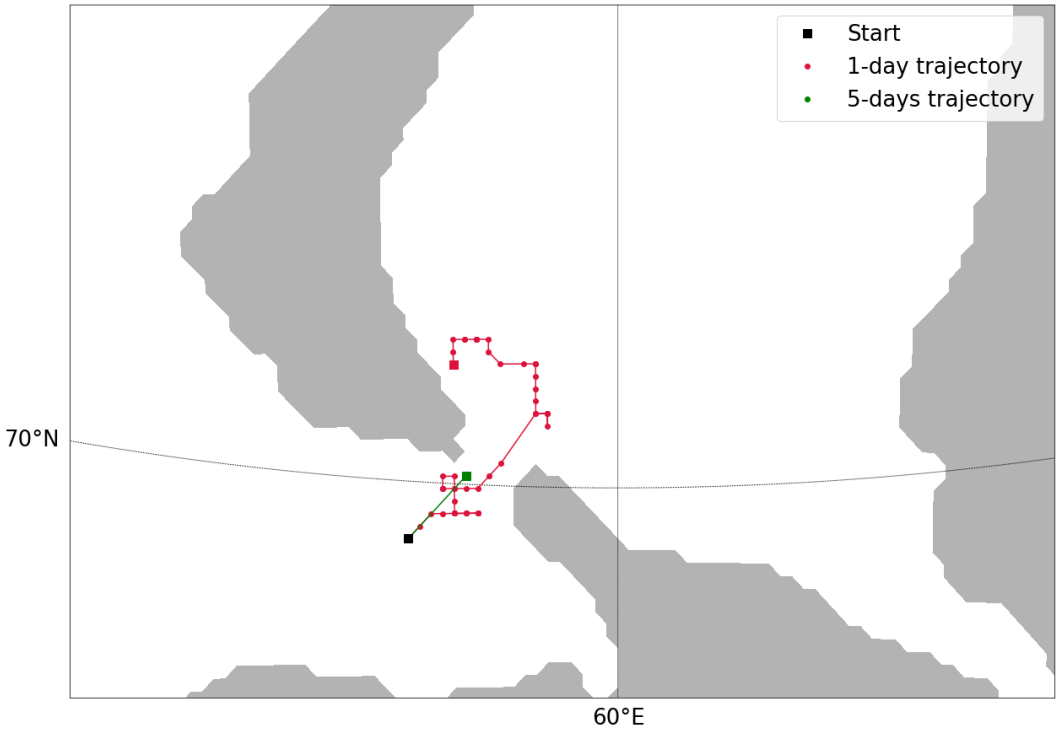

Figure 4.11: Summer particle trajectory pathways. The initial position of the trajectories is marked by a black square (i263 j489), and a square in its corresponding color, identify the last particle position on sea of each trajectory pathway.

The values of eddy kinetic energy and particle displacement are higher in summer than in winter. Table 4.4 shows the mean values of eddy kinetic energy and Table 4.5 the particle displacements, computed in the Barents Sea and the Kara Sea. Since the 5-days particle trajectory has only one particle position in the Barents Sea and one in the Kara

Canal, please note that the values are shown only for the Barents Sea computed at that particle position. The same is valid for the values of ballast water tracer concentration shown in table 4.6.

Table 4.4 – Summer averaged values of eddy kinetic energy computed from 1-day and 5-days velocities. The mean eddy kinetic energy corresponds to the time range listed in columns two and four (after no. of days) indicating the part of the trajectory being in the Barents Sea, or Kara Sea, or along the total trajectory.

EKE	**1-day trajectory**		**5-days trajectory**	
	Mean	No. days	Mean	No. days
Barents Sea	45.44	24	35.00	1
Kara Sea	35.84	25	Na	0
Trajectory	40.05	51	82.25	2

Table 4.5 – Summer averaged values of particle displacement between particle positions computed from 1-day and 5-days particle trajectories. The particle displacement values correspond to the time range listed in columns two and four (after no. of days) indicating the part of the trajectory being in the Barents Sea, or Kara Sea, or along the total trajectory.

Particle Displacement	**1-day trajectory**		**5-days trajectory**	
	Mean	No. days	Mean	No. days
Barents Sea	5.60 km	24	57.66 km	1
Kara Sea	6.04 km	25	Na	0
Trajectory	6.52 km	51	38.76 km	2

The ballast water tracer presents a steep reduction of its concentration in the first few days following the start of the particle trajectories. After discharge, the tracer spreads, and concentration reduces to ca. 0.50 in the center of the tracer. With an increase of eddy kinetic energy (i.e., turbulence), horizontal mixing becomes stronger, and it is reflected in

the concentration values of ballast water tracer computed at the first few particle positions of the trajectories. Figure 4.12 shows the values of ballast water tracer computed at the particle positions along the trajectory pathways.

Table 4.6 – Summer average values of ballast water tracer concentration along the 1-day and 5-days particle trajectories. The tracer concentration values are separately presented as vertical integral and within the surface layer. The time range correspond to the ones on table 4.4 and 4.5 (after no. of days), indicating the part of the trajectory being in the Barents Sea or the Kara Sea.

Ballast water tracer concentrations	1-day	5-day
Vertical integral of mean BW-tracer – Barents Sea	0.2049	0.3509
Vertical integral of mean BW-tracer – Kara Sea	0.1595	Na
Mean BW-tracer in surface layer – Barents Sea	0.1546	0.3047
Mean BW-tracer in surface layer – Kara Sea	0.0970	NA

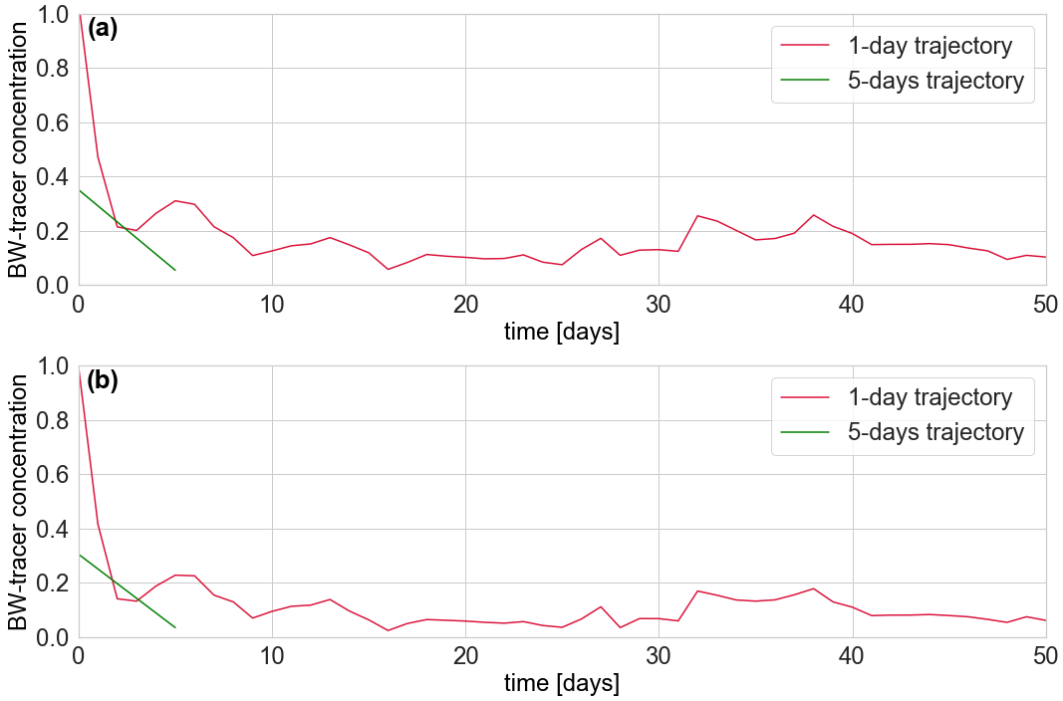

Figure 4.12: Ballast water tracer concentration along the summer trajectory pathways. The figure shows the (a) vertically integrated values of ballast water tracer, and (b) the ballast water tracer

concentration within the surface computed along both summer particle trajectories. The green line is short due to the early end of the trajectory pathway computed with 5-days summer velocity field.

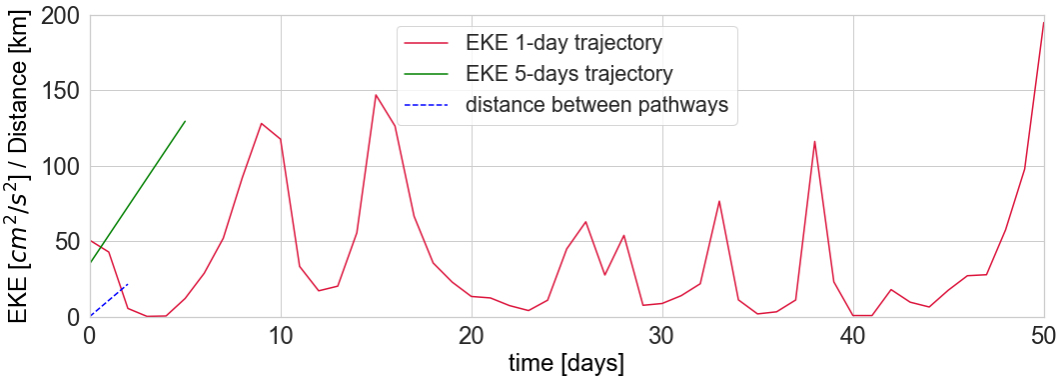

Figure 4.13: Summer eddy kinetic energy values and distance between trajectory pathways. The figure shows the eddy kinetic energy values computed at each particle position along the summer particle trajectory pathways (1-day trajectory in red and 5-days trajectory in green). The dashed blue line represents the distance between the two trajectory pathways. The green and blue lines are short due to the early end of the trajectory pathway computed with the 5-days summer velocity field.

The values of eddy kinetic energy computed along the summer particle trajectories are higher compared to winter. Figure 4.13 shows the eddy kinetic energy values computed at the particle positions along the summer particle trajectories and the distance between the trajectory path-lines.

4.1.2.1 – Summer 1-day particle trajectory

In the particle trajectory computed using 1-day velocities (u and v), the particle recirculates and remains in the Barents Sea until day-23, reaching the Kara Canal on day-24. The particle only enters the Kara Sea on day-26. High values of eddy kinetic energy are registered in the Barents Sea (on days 9, 10, 15, and 16) and the Kara Sea (on days 33, 38, and 50).

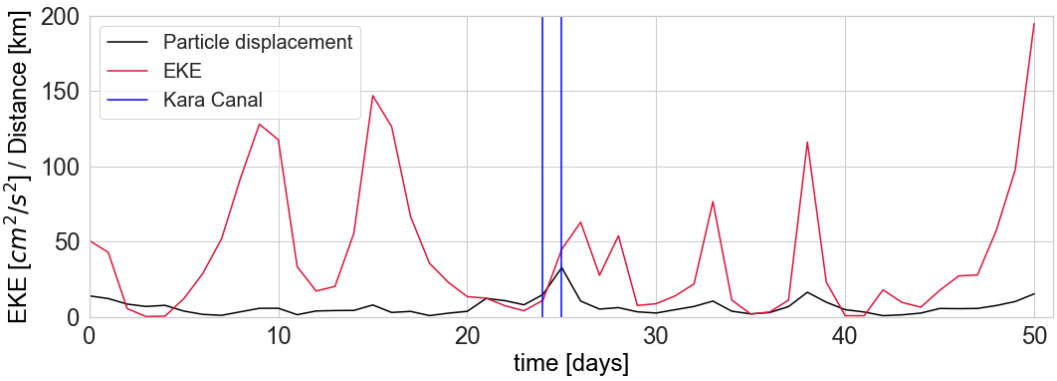

Figure 4.14: Particle displacements and eddy kinetic energy values along the particle trajectory calculated with the summer 1-day velocity field. The blue lines indicate the particle positions at the Kara Canal.

The greatest particle displacement is computed when the particle is located at the center of the Kara Canal on day-25 (August 11th). However, it does not correspond to the highest value of eddy kinetic energy computed along this trajectory, which appears at the last particle position of the trajectory on day-50 in the Kara Sea (Figure 4.14).

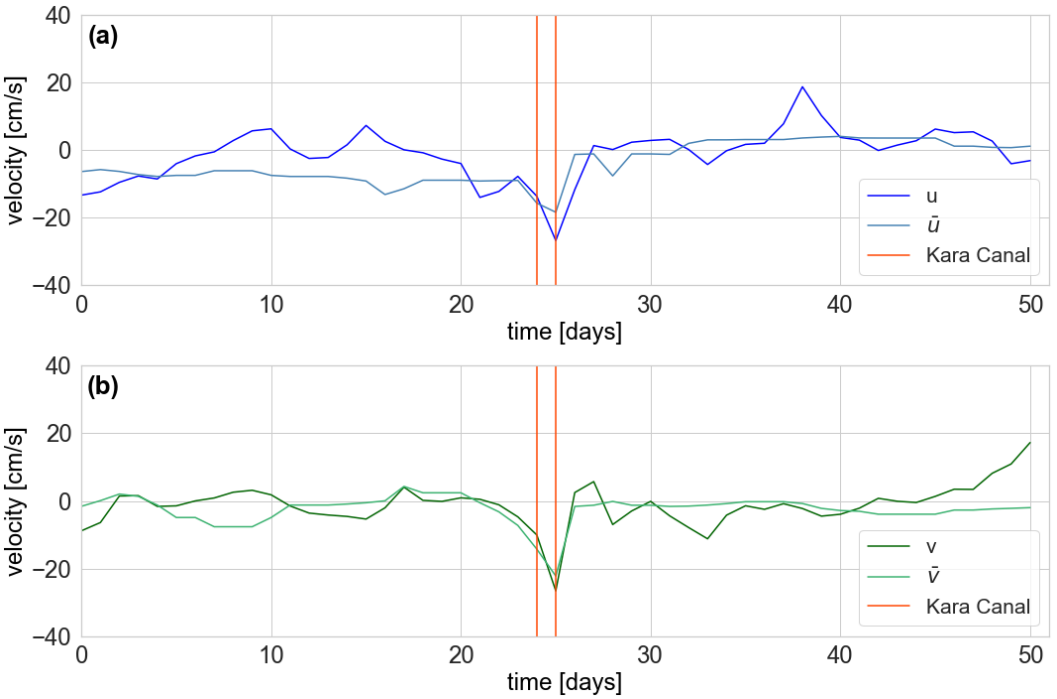

Figure 4.15: Summer 1-day velocity components (u and v) values computed along the 1-day particle trajectory and respective monthly averages represented by $\bar{u}$ and $\bar{v}$. The vertical lines (orange) indicate the days the particle is at the Kara Canal.

The particle displacement computed from the position on day-25 to the next position on day-26 is large, and due to the high values of the velocity field (u and v, Figure 4.15). The differences between the total velocities and the monthly mean velocities ($\bar{u}$ and $\bar{v}$) are not large, and so are not the returned values of perturbation velocities. Consequently, the eddy kinetic energy at the Kara Canal, on day-25, is not very high (Figure 4.16b).

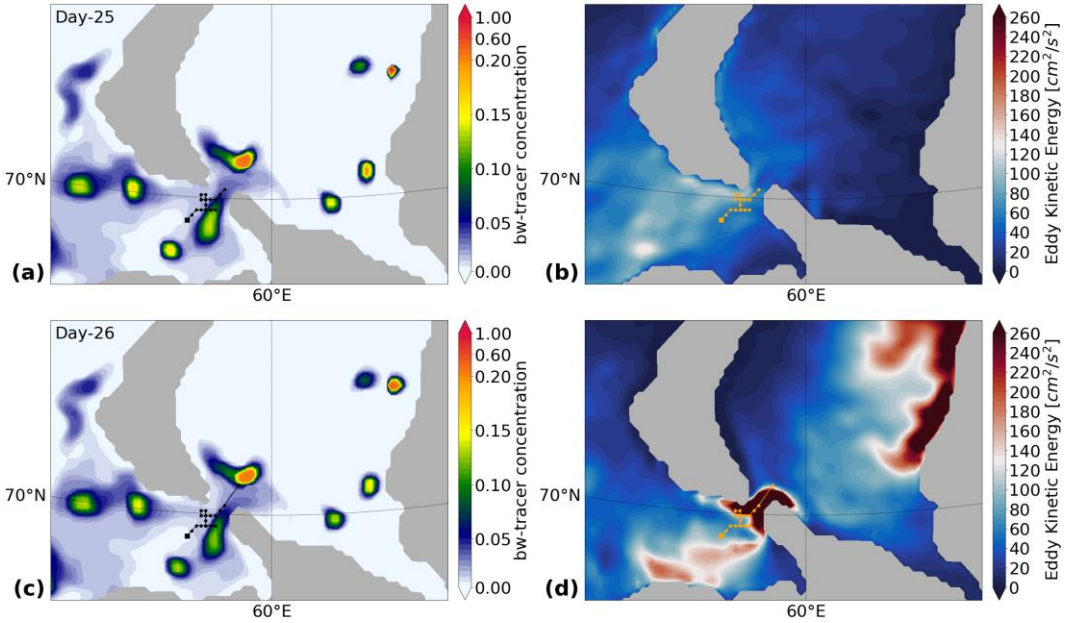

Figure 4.16: Ballast water tracer concentration, eddy kinetic energy, and 1-day summer particle trajectory. The panels show the (a, c) ballast water tracer concentration (surface layer) and (b, d) the eddy kinetic energy as background for the particle trajectory calculated with the 1-day summer velocity field.

Figure 4.16 shows the ballast water tracer concentration on the surface layer and the computed eddy kinetic energy on day-25 and day-26. In the latter, there is a substantial increase of the eddy kinetic energy in the Kara Canal and a slight increase of tracer flow into the canal from the Barents Sea. The tracer flow is subjected to the currents, and the eddy kinetic energy (turbulence) is responsible for increasing mixing. Vertical integral values of ballast water tracer concentration present an increase of tracer concentration in the Kara Canal and at the Kara Sea (shown in Figure A.07 in the thesis appendix).

4.1.2.2 – Summer 5-days particle trajectory

The particle trajectory calculated with the 5-days summer velocity field has a short pathway. The particle reaches the Kara Canal on day-5, where it ends. The next position computed is on land and not presented in Figure 4.11. The trajectory ends in the southern tip of Novaya Zemlya. This trajectory has the earliest entry to the Kara Canal among all trajectories.

Figure 4.17 shows the particle displacement from its start position to the Kara Canal in the trajectory. The time-averaging of the velocity components into 5-days smooth out the recirculation showed previously by the particle trajectory calculated with the 1-day summer velocity field. However, the mean direction of the surface velocities still carries the particle northwards, encounters land, and the path ends.

The high value of eddy kinetic energy computed at the Kara Canal particle position is high due to the difference between the total velocity u and its monthly mean value ($\bar{u}$), as presented by Figure 4.18.

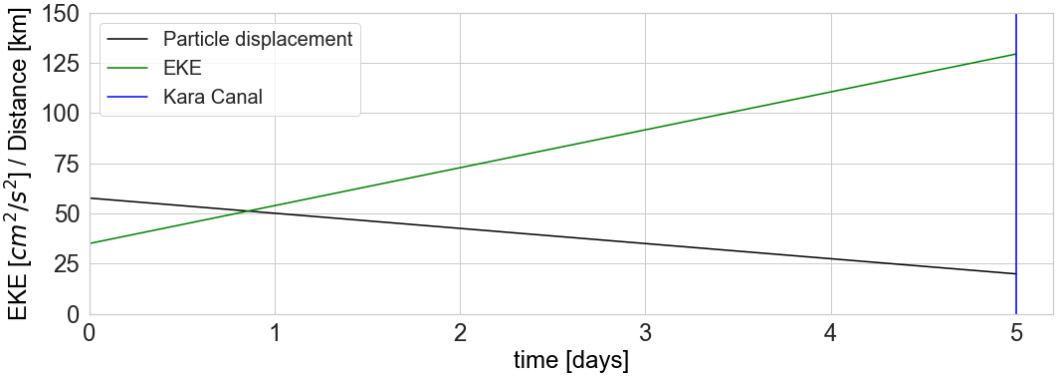

Figure 4.17: Particle displacements and eddy kinetic energy values along the particle trajectory computed with the summer 5-days velocity field. The blue line indicates the particle position at the Kara Canal.

Analysis of the ballast water tracer on the surface layer shows how much smoothed is the tracer concentration when time-averaged over 5-days. At the trajectory start position the tracer concentration is less than 0.40, i.e., less than 50% of the tracer concentration computed at the start of the particle trajectory calculated with 1-day velocities. As already described, the tracer and the particle, in the previous trajectory, showed recirculation in the

Barents Sea before entering the Kara Canal. This recirculation is 'removed' by the time-averaging, and the tracer is dislocated from the release point. The eddy kinetic energy is low in the area. The ballast water tracer concentration shows a decrease of ca. 0.05 in the center of the tracer area in the time between the start and end of the particle trajectory (Figure 4.19).

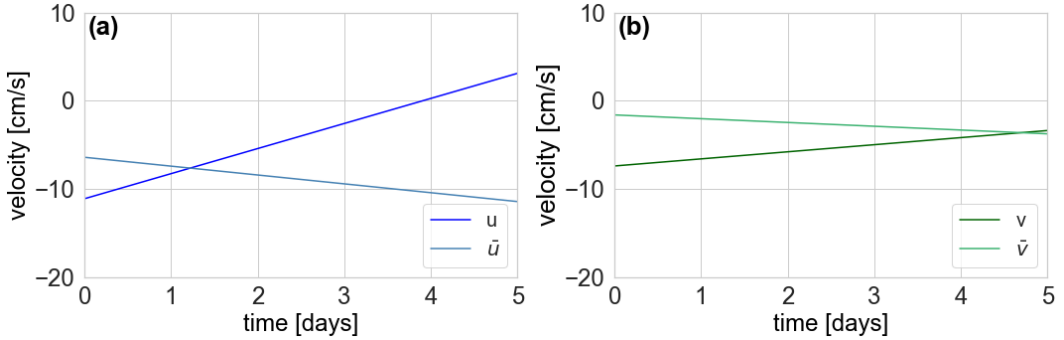

Figure 4.18: Summer 5-days velocity components (u and v) values computed along the 5-days particle trajectory and the respective monthly averages represented by $\bar{u}$ and $\bar{v}$.

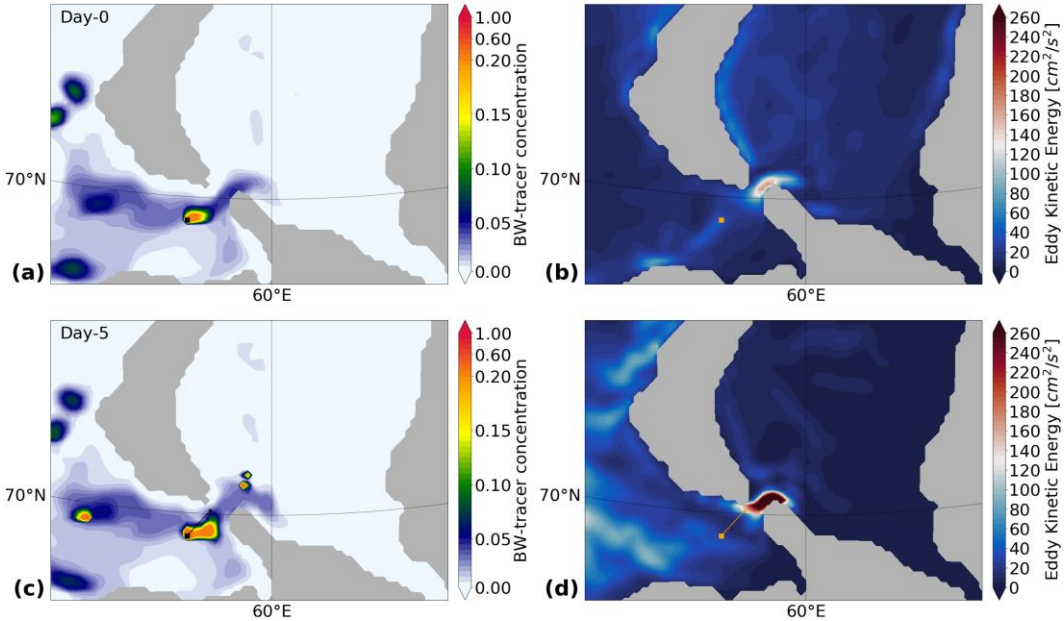

Figure 4.19: Ballast water tracer concentration, eddy kinetic energy, and 5-days summer particle trajectory. The figure shows the (a, c) ballast water tracer concentration (surface layer) and (b, d) eddy kinetic energy as background for the particle trajectory calculated with 5-days summer velocity field.

A slight increase of tracer flowing into the Kara Canal is observed in Figure 4.19 (a and c). The ballast water tracer computed at the particle position on day-5 has low surface concentration values due to the direction of the surface currents (westward) in the Kara Canal. The last particle position of the trajectory is ca. 11 km from land (southern tip of Novaya Zemlya).

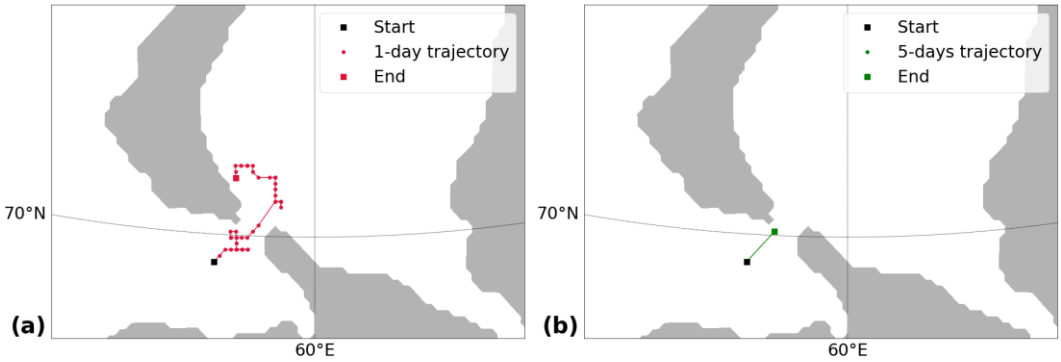

Figure 4.20: Summer particle trajectories. (a) particle trajectory calculated with 1-day, and (b) 5- days summer velocity fields.

The eddy kinetic energy is higher on day-5 than on day-0, while the particle displacement is greater on day-0 than on day-5. The high value of eddy kinetic energy is due to the difference between the total velocity component u and its monthly mean ($\bar{u}$) (Figure 4.18). The velocity component v presents a similar value to its monthly mean ($\bar{v}$). Figure 4.20 shows the summer particle trajectory pathways computed with 1-day and 5- days velocity fields.

4.2 Summary and discussion

The trajectories presented slightly different pathways from the ballast water tracer. The tracer is calculated online, and its concentration is determined by the resolved circulation, transport processes, and parameterized mixing of the model. The particle trajectories are calculated offline, using the saved velocities, and represent only the advection effects in the surface layer. Due to the different time-averaged velocities used to compute the trajectories, each has a different pathway. When the surface currents have low variability of flow direction, as in the Barents Sea in winter, the trajectories follow a similar

path. In contrast, different paths will be computed when the surface currents have higher variability of flow direction and speed, as the surface currents in the southern Barents Sea in summer. Figure 4.21 presents the winter and summer seasonal means of surface currents speed and direction in the southern Barents and Kara Seas.

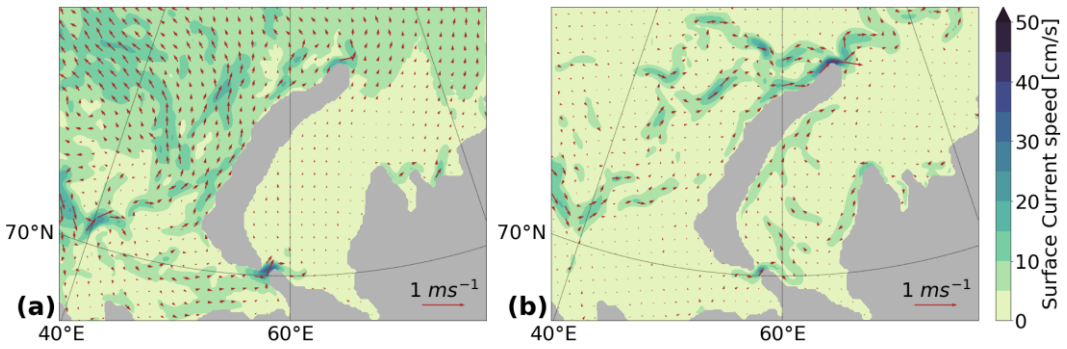

Figure 4.21: Seasonal mean surface currents direction and speed. (a) winter and (b) summer surface currents.

During winter, the ballast water tracer concentration computed along the particle trajectories presented steep reductions shortly after the trajectory started. This reduction of tracer concentration is due to convective mixing on the continental shelf and to the different paths described by the tracer and the particle trajectory. In winter, the mixed layer occupies the whole water column in coastal and shallow waters of the Barents Sea. The tracer concentration in the surface layer is close to zero by day-22 (January 31st). However, in deeper layers, the tracer remains with low concentration values until day-44 (February 22nd) in the Barents Sea near the Kara Canal. Convection carries ballast water tracer from the surface to deeper layers. The tracer is then influenced by the topography of the continental shelf (Figure 4.22), which works as a 'funnel' that guides water masses to and through the Kara Canal, with a strong flow that can be explained by the Bernoulli's principle.

Analysis of the ballast water tracer shows that the tracer spreads and diffuses from its 'center' with high concentration, to lower concentrations in the outer edges shortly after release in the Barents Sea. Mixing is enhanced due to turbulent flow that is demonstrated by the increase of the eddy kinetic energy. In other words, the tracer's initial spread is a consequence of diffusion and random walk (though not represented by the model), while turbulent transport is responsible for increased mixing. Figure 4.23 illustrates the initial

spread and diffusion of the ballast water tracer short after the release. Figure 4.24 shows tracer concentration decrease after increase of the eddy kinetic energy, i.e., turbulent flow, in the previous day (Figure 4.23d).

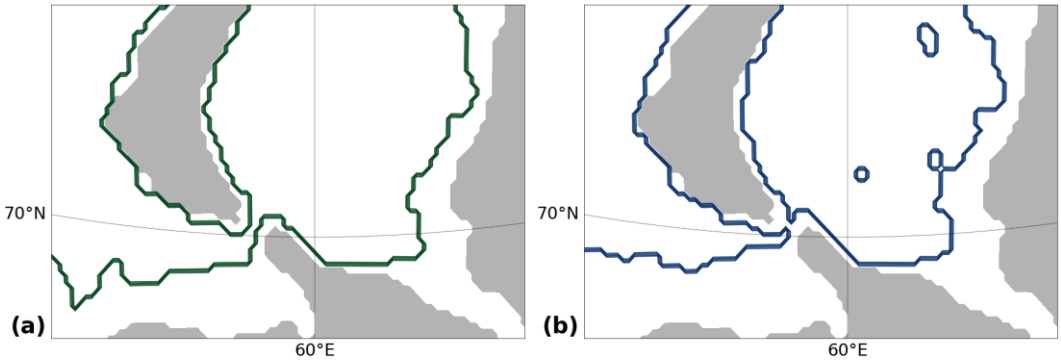

Figure 4.22 Topographic isolines. The isoline (a) of 40m depth, and (b) of 50 m depth of the model topography.

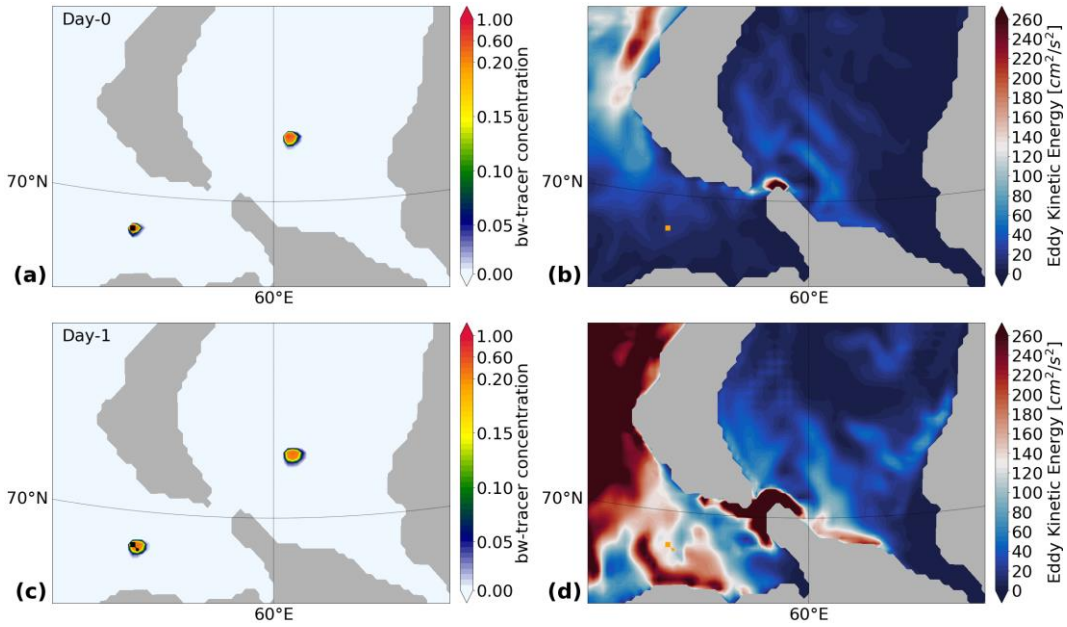

Figure 4.23: Ballast water tracer, eddy kinetic energy, and 1-day winter particle trajectory. The panels show the spread and diffusion of the tracer soon after its release in the model simulation. (a) On day-0, the tracer shows the diffusion of its low concentration around the center, and (b) the eddy kinetic energy in the area is very low. On day-1 (c), the tracer increased its area by spreading from its center, and diffusion is more pronounced on its edge. While eddy kinetic energy (d) increases, causing the mixing of the remaining tracer on the surface (Figure 4.24a).

The low amount of ballast water tracer in the Barents and Kara Sea regions during winter is partially due to the small number of vessels in the area during the season, leading to a small number of tracer releases. The model simulation also starts in January with no previous releases of the tracer. Besides that, vertical mixing, which is stronger during wintertime, decreases the tracer concentration further.

Along the winter particle trajectories, the mean eddy kinetic energy computed at the particle positions in the Barents Sea is higher (ca. 8 and 3 times for 1-day and 5-days trajectories, respectively) than the mean eddy kinetic energy computed in the Kara Sea. One factor responsible for the low eddy kinetic energy values in the Kara Sea is the presence of sea ice. During winter 2013, the southern Kara Sea was entirely sea ice-covered by the end of January, save a few coastal polynyas near the Kara Canal. In contrast, the southern Barents Sea (also known as the Pechora Sea) presented a more variable and thinner sea ice cover at the time (Figure A.08). Sea ice decreases the transfer of momentum from the atmosphere to the ocean surface, which reflects in the low surface current speed. Since wind directly forces the surface currents, the presence of sea ice cover prevents this forcing.

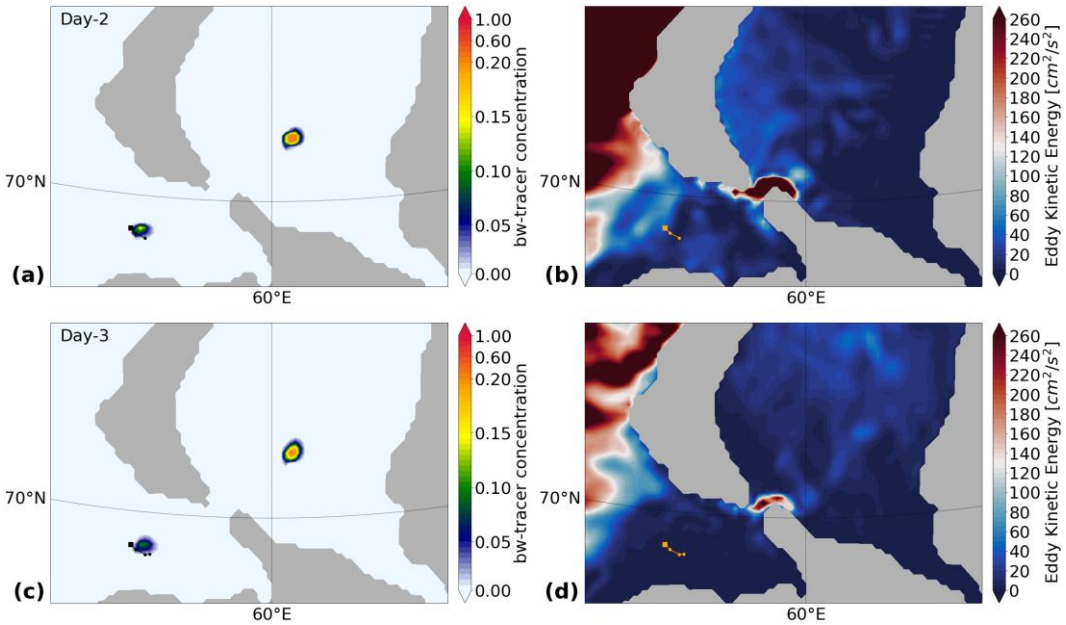

Figure 4.24: Ballast water tracer, eddy kinetic energy, and 1-day winter particle trajectory. The panels show (a) decrease of tracer concentration after the increase of eddy kinetic energy on the previous day (Figure 4.23d); (b) eddy kinetic energy on day-2; (c) tracer concentration of less than 0.10 on day-3; and (d) decrease of eddy kinetic energy on the southern Barents Sea on day-3.

The particle trajectory computed with the winter 5-days velocity field, has one particle position that reaches the southern coast of the Kara Canal (Vaygach Island); however, the trajectory does not end there. The strong currents of the Kara Canal transport the particle further into the Kara Sea. This trajectory's last particle position is ca. 120 km from the southeast coast of Novaya Zemlya. The last particle position of the trajectory computed with 1-day velocity field is closer to the land, ca. 37 km.

Organisms that are released with ballast water during winter are subjected to convection and low water temperatures. Nevertheless, organisms that may survive the voyage and discharge process, and are capable of tolerating low temperatures and seawater, will possibly follow the trajectory pathway, be advected by the surface ocean flow, and may take advantage of any nutrients that are brought to the surface by vertical convection.

Along the particle trajectories computed with the summer velocities, the 1-day particle trajectory describes recirculation in the Barents Sea. The 5-days trajectory is short, with only one particle position after the start. The values of eddy kinetic energy computed along the trajectories are high, and the highest value is computed on the last particle position of the 1-day trajectory pathway in the Kara Sea (Figure 4.14). In the 1-day particle trajectory, the highest eddy kinetic energy computed does not coincide with the largest particle displacement; however, the particle displacement on the last particle position is among the longest displacements computed on this trajectory. Both summer trajectories reach land, having their last particle positions on the coast.

July, August, and September (summer months) are characterized by an ocean surface free of sea ice in the study area. Consequently, momentum is transferred from the atmosphere directly to the ocean surface. This is visible by the high variability of the eddy kinetic energy, in Figure 4.13, and the variability of the direction of the surface currents, especially in the Barents Sea (Figure 4.21b).

The summer particle trajectories presented the largest particle displacements in the Kara Sea compared to the Barents Sea, reflecting the variability of the Barents Sea's surface currents. The particle displacement from the Kara Canal into the Kara Sea is also large when associated with turbulent flow. The strong flow through the Kara Canal together with mixing prevents high ballast water tracer concentration inside the canal.

The ballast water tracer concentration computed along the 1-day summer particle trajectory decreases to less than 0.50 a few days after the start of the trajectory. Values of ballast water tracer concentration vary along the trajectory pathway due to new tracer releases in the area. The shallow mixed layer maintains the tracer in the upper layers and prevent it from being mixed with deeper waters. In the summertime, the upper ocean is characterized by stable stratification that suppresses vertical convection in the water column and allows for a shallow mixed layer depth.

The ballast water tracer recirculates in the area south of Novaya Zemlya in the Barents Sea and is well represented by the 1-day summer particle trajectory (Figure 4.11 and 4.22a). The seasonality of atmospheric weather systems highly influences the recirculation on the ocean surface, whereas the topography of the continental shelf (Figure 4.22) plays an essential role in the tracer's recirculation in deeper layers.

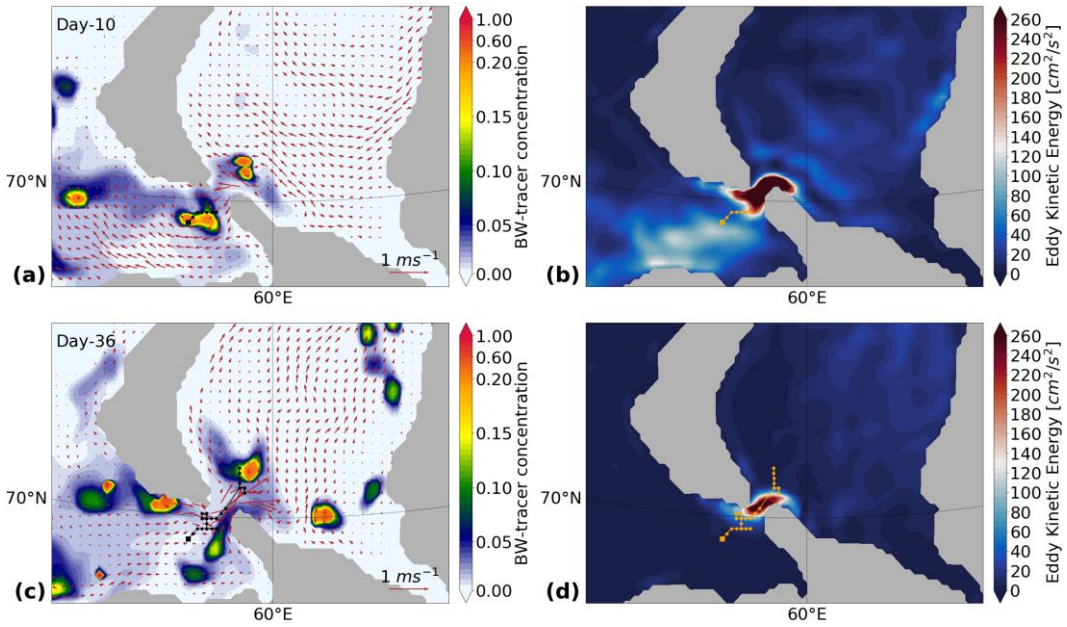

Figure 4.25: Ballast water tracer, eddy kinetic energy, and 1-day summer particle trajectory. The panels show (a, c) the surface currents and ballast water tracer concentration (surface layer), and (b, d) eddy kinetic energy as background for 1-day summer particle trajectories.

Analysis of ballast water tracer dispersion shows that the tracer spread shortly after discharge in the Barents Sea during summer is influenced by the eddy kinetic energy, i.e., by the turbulence of the flow. Due to stable stratification in summer, the tracer remains in

the surface layer (0-10 m), and the turbulent flow demonstrated by the eddy kinetic energy, enhances the spread and mixing of the tracer horizontally. In the Kara Canal, high eddy kinetic energy is correlated to the fast decrease of tracer concentration due to high speed and turbulence of the flow. However, changes in the direction of the surface flow are directly correlated to ballast water tracer transport, as shown in Figure 4.25.

Eddy kinetic energy values are higher in summer compared to winter in both the Barents Sea and the Kara Sea, by ca. 3.3 times (Figure 4.26). In summer, the surface currents are more variable in direction and speed. Analysis of daily surface currents (not shown) indicates that in winter, they have a strong tendency to flow eastwards in the Barents Sea, and the flow is stronger compared to the flow in the Kara Sea (Figure 4.21a). In summer, the surface currents presented more variability of direction (Figure 4.21b), which is observed in the trajectory pathway calculated with the 1-day velocity field (Figure 4.22a), and the ballast water tracer flow. The recirculation presented by the 1-day trajectory is smoothed out in the particle trajectory computed with the velocity field averaged over 5- days, bringing the particle directly to the Kara Canal. In the warm season, the surface currents are stronger and less variable in the Kara Sea. The seasonal mean speed and direction of the surface currents are illustrated in Figure 4.21.

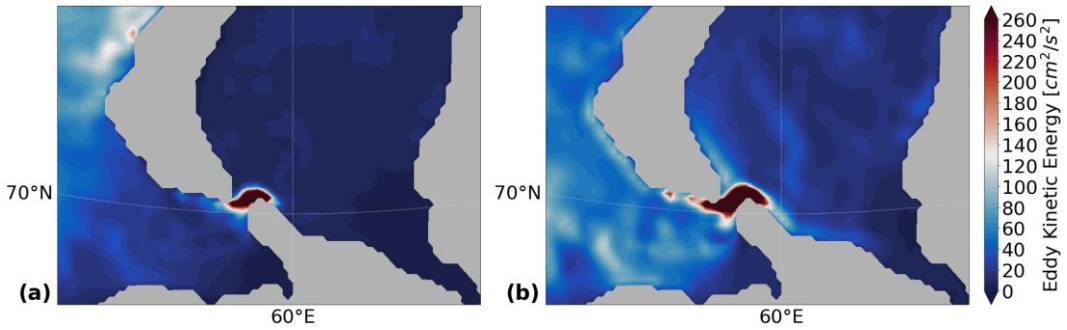

Figure 4.26: Seasonal mean eddy kinetic energy. (a) Winter and (b) summer mean eddy kinetic energy.

On average, particle displacements in the Barents Sea during summer are smaller compared to winter. On the other hand, the particle displacements in the Kara Sea are smaller in winter compared to summer. During winter, the Kara Sea surface current speeds are dampened by the sea ice cover, causing shorter displacements of the particle. As for the

Barents Sea, during summer the high variability of current speed and direction are responsible for the small particle displacements and for ballast water tracer accumulation. Accumulation of ballast water tracer indicates an increase of propagule pressure, which increases the chances for non-indigenous organisms to establish populations in the coastal ecosystems.

The winter currents in the Barents Sea present a preferential eastward flow reflected in the similar pathways drawn by the particle trajectories (Figure A.09 of the Appendix). The summer particle trajectory showed recirculation in the Barents Sea, indicating changes in the surface currents (Figure 4.20a, 4.25b, and in Figure A.10 of the Appendix). As the surface currents are forced by the transfer of momentum from the atmosphere, weather events like storms are responsible for fast changes in the surface circulation and variability of the ocean surface's eddy kinetic energy.

4.3 Conclusions

The ballast water tracer analysis combined with trajectories of advected particles in the ocean surface shows that non-indigenous organisms are able to reach shallow water and coastal environments of the Barents and Kara Seas. These organisms may be transported, like demonstrated by the tracer flow, in different depths of the water column or be advected by the surface currents, as shown with the particle trajectories.

Different pathways presented by the particle trajectories demonstrate the differences in the surface circulation patterns due to the natural variability of environmental factors. The surface currents define the particle trajectory pathways. However, the winter-summer comparison indicates that environmental factors, with fast-changing rates like sea ice and weather patterns (e.g., storms, changes in wind direction and speed), have a substantial effect on the surface currents and the ballast water tracer spread along the trajectories. That is demonstrated by the meandering of the particle and recirculation of the tracer.

Particle trajectories calculated with the 5-days velocity fields described paths with greater differences from that of the ballast water tracer. The distances between the

trajectory pathways are correlated to the eddy kinetic energy as demonstrated by its correlation to the turbulent diffusivity tensor.

Different time-averaging of the surface velocities show that the quality of tracking possible pathways of non-indigenous organisms or contaminants, may be decreased by the low time-frequency velocity field. As demonstrated by the summer trajectory computed with the surface velocity components averaged over 5-days, short and fast changes on the ocean's surface currents are not well represented.

The survivorship of non-indigenous organisms after ballast water discharge could be hindered by the sea ice cover, low seawater temperature, high salinity, and intense vertical mixing during winter. High tolerance to harsh environmental conditions by non-indigenous organisms may be an essential feature for successful adaptation in the new environment during the cold season.

Summer is considered the season with the best opportunities for non-indigenous organisms to survive discharge and establish population in the study area. Several factors are able to increase the propagule pressure and thus the opportunity for population establishment in coastal environments. These factors are the large number of vessels that navigate the Arctic waterways, the shallow mixed-layer depth, warmer temperatures, and the availability of sunlight in addition to variability of the surface currents, and tracer accumulation.

Due to the high frequency of ballast water tracer discharges in summer along with the shallow mixed-layer, tracer of different releases merge into each other, keeping a considerable amount of ballast water in the study area. The flow of the tracer is strongly dependent on the current directions. When the currents are highly variable, as they are in the Barents Sea during summer, the tracer tends to form accumulation areas. High eddy kinetic energy represents increase of turbulence in the flow, increasing mixing of the tracer, and advection of particles.

Chapter 5. Discussion and outlook

This thesis aimed to simulate the theoretical distribution and spread of ballast water discharged by cargo vessels that navigated the Arctic shipping routes in 2013. Several hypothetical experiments were performed which only can be conducted by numerical simulations. Therefore, this thesis is able to identify areas where ballast water possibly accumulates and which pathways, potentially included non-indigenous organisms or contaminant particles, may follow to reach coastal ecosystems.

For the simulations, a passive tracer was implemented in the regional ocean-sea ice coupled model NAOSIM with 1/12-degree resolution. The ballast water tracer was discharged in the model according to real ship positions selected from the dataset of the Arctic region. The ship dataset allowed identifying areas with a high density of ship tracks. The ship-track density map, illustrated by Figure 2.1, indicated that in 2013 the highest densities occurred at the western end of the Northeast Passage (i.e., West Svalbard, Barents Sea, and the Kara Sea) and at the Chukchi Sea on the eastern end.

Monthly ship-track density maps showed that cargo-shipping activities are restricted to the western part of the Northeast Passage from December to June, and expanded to the Chukchi Sea and Bering Strait from July to November. Year-round ship traffic occurred mainly in the western end (i.e., West Svalbard, Barents Sea, and the Kara Sea) of the Northeast Passage in 2013. The Northwest Passage ship-track was restricted to the Atlantic end of the route (i.e., Hudson Strait, Davis Strait and Baffin Bay), and with the exception of one month (i.e., May), presented yearlong traffic. However, only a small number of vessels navigated there in 2013. The monthly ship-track density maps are presented in Figures A.02, A.03, and A.04 of the Appendix.

The ship dataset contains vessels positions only for the year 2013. The number of vessels in the Arctic vary from year to year, as well as their navigation tracks. Compared to recent years, the Northeast Passage had a moderate navigable season with ice free corridors in 2013.

So far, there is no other work that numerically simulates ballast water distribution in the Arctic Ocean. Only a few studies exist in high latitude regions, e.g., *Brickman* [2006],

who only investigates a small area using a regional ocean circulation model of the Gulf of Maine and the Scotian Shelf (east coast of Canada). In that study, the tracer was discharged in the regional model, along ship tracks on the continental shelf. The ship tracks cover more then one grid box, which in Brickman's model have vertical resolution of 4 m in the top levels. In contrast, the simulations conducted in this thesis, a part from using a different model, releases the ballast water tracer in one grid box to compensate overestimations of tracer in the simulations, since the volume of a grid box in NAOSIM is far larger than the volume of ballast water carried by a vessel. The whole experiment setup is described in section 2.4.1.

Three experiments were designed to fulfill the objectives of this thesis. The simulations of Experiment-One had ballast water tracer released in ship positions selected from the dataset mentioned above. These positions compose the sub-dataset and were illustrated in Figure 2.4. Experiment-Two simulations released ballast water in only two of the selected ship positions (illustrated in Figure 2.5) at the beginning of each month. The tracer experiments are initialized by zero of ballast water tracer over the entire model domain. Experiment-Two was designed to estimate the time needed by the ballast water tracer of unique releases to mix into different concentration thresholds. Experiment-Three used the saved velocity field resultant from Experiment-One, with an offline approach to compute trajectory pathways of particles in the ocean surface layer of the model. From this velocity field, the surface eddy kinetic energy was computed. The experiment was designed to analyze surface horizontal advection of particles as representatives of organisms or contaminants that can be discharged within the ballast water, and the role of the eddy kinetic energy, representing turbulent flow, on the mixing of the tracer.

The number of vessels in the Arctic region is small in winter, increases towards summer, and starts to decrease in autumn. The presence of sea ice is a strong limiting factor for navigation in the Arctic. The third chapter of this thesis shows that the spread and accumulation of the ballast water tracer are strongly influenced by seasonality.

During winter, physical oceanographic aspects such as deepening of the mixed-layer depth and vertical convection, are responsible for carrying ballast water tracer released in the ocean surface layer to greater depths where the tracer is mixed with the surrounding waters. As described in Chapter 3, in deep regions of the Arctic Ocean, the mixed-layer depth can

reach ca. 200-350 m in winter. On the shallow seas of the continental shelf, the mixed-layer can occupy the whole water column. The horizontal spread of the ballast water tracer, as shown in Chapter 3, is strongly dependent of the ocean currents. However, as shown in Chapter 4, increase of eddy kinetic energy, i.e., turbulent flow, plays an important role in increasing the mixing rate of the ballast water tracer on the surface with the surrounding waters.

In spring, when sea ice starts to melt, freshwater is returned to the ocean surface. The now open water, absorbs more heat from solar radiation, and increases the water temperature. By the beginning of summer, the water column is stably stratified and the mixed-layer occupies only a few meters of the upper ocean.

During summer, the number of tracer releases in the model simulation is large compared to winter. With a shallow mixed-layer, most of the ballast water tracer remains on the surface layers. As shown in Chapter 3, both deep sea and shallow shelf areas presented similar stratification of the water column, with tracer remaining in the upper 10-20 m, and mostly mixed horizontally, high tracer concentration and accumulation areas are formed. Without the sea ice cover and the upper ocean being forced directly by the atmosphere, the variability of the atmospheric circulation and short events like storms are reflected in the uppermost ocean circulation as shown in Chapter 4 through the variability of the particle trajectory pathways, and the high values of the eddy kinetic energy computed along the trajectories. The recirculation of the ballast water tracer showed in Chapter 3 is also described by the particle trajectories in Chapter 4.

The experiments reveal three areas with substantial ballast water tracer accumulation. Two of these areas have topographic features that induce water recirculation and thus lead to tracer accumulation. As these topographic features remain constant in time, the results of this thesis are not limited to the year 2013 with its specific distribution and variability of sea ice concentration and weather patterns. Features such as the variability of wind and ocean currents are able to change, especially by possible future climate changes.

From those two areas, one is located between Bear Island and southern Spitsbergen. Recirculation in this area was already described in studies by *Loeng et al.* [1997] and *Timofeev* [1963]. The recirculation is caused by the steep slopes of the two islands along with the in- and outflow of water in the Storfjord sea channel. The second

area is located south of Novaya Zemlya in the southern Barents Sea. Here, depth increases northwards towards the south coast of Novaya Zemlya, which along with the surface currents by the end of summer, created an accumulation area. Towards the Kara Canal, the continental shelf starts to shallow, influencing the strong eastward flow through the canal.

The West Spitsbergen Current played an essential role transporting ballast water tracer northwards and along Spitsbergen's west coast. The ballast water tracer is further transported southwards by the East Greenland Current. Autumn was the season with the highest concentration of tracer in this sector, which occupies a considerable large area of the Fram Strait. Overall, autumn is a season marked by high tracer concentration despite instabilities in the water column.

The Ballast Water Management Convention guidelines suggest a minimum water depth for ballast water exchange due to the believe that most coastal, brackish, and freshwater organisms usually do not tolerate open ocean salinity. However, organisms that tolerate a wide range of temperature and salinity may survive discharge on deep waters. In spring and summer, due to the shallow mixed-layer, the ballast water tracer does not show differences of vertical mixing between the deep west Spitsbergen sector and shallow shelf southern Barents Sea. The differences between the chosen areas in the warmer season are related to the ocean surface circulation. During summer, when ship density in the Arctic is highest, the water column is stably stratified, the mixed layer is thin and thus prevents vertical mixing of the ballast water tracer, and non-indigenous organisms that survive discharge, may remain in the upper layers of the ocean.

The results presented in the previous chapters demonstrate that:

i. Ballast water tracer and particles are able to reach coastal ecosystems;
ii. In spring and summer ballast water tracer remains in the ocean surface layer, forming accumulation areas, regardless of water depth;
iii. Ballast water tracer accumulation occurs due to circulation patterns induced by topographic features, atmospheric circulation, and seasonality of the water column, along with the number of tracer releases.
iv. The ocean currents govern the flow of the ballast water, and increases of eddy kinetic energy (i.e., turbulent flow) increases mixing.

Phytoplankton starts blooming in spring. It is also in spring that the number of vessels in the Northeast Passage starts to increase, which in turn increases the discharges of ballast water tracer. Tracer simulations showed that during summer, when non-indigenous organisms have the most favorable conditions in the Arctic, is also the season with the highest number of individual vessels, and consequently, the largest amount of ballast water tracer. The shallow mixed-layer depth, defines the extension of vertical mixing, and allows for tracer accumulation. Accumulation of ballast water tracer represents the risk of propagule pressure increase, as the number of individuals of the same species may increase, creating the opportunity for reproduction and population establishment.

The diversity of organisms with different buoyancy and migration patterns, make it impracticable to conduct experiments to include all behaviors. Some organisms can swim, others will sink in the water column. On the other hand, some organisms, in early life stages (e.g., eggs, cysts), can be advected by the surface currents, and eventually reach coastal ecosystems, as presented by the ballast water tracer simulation and the by particle trajectories.

Invasive species were already identified in some of the Arctic seas [*Chan et al.*, 2019]. As the sea ice retreats, other Arctic shelf seas may become suitable for non-indigenous species, and areas that already have a small number of invasive species may become suitable for other non-indigenous organisms. Organisms classified as invasive in ecosystems like the North Sea, and are adapted to harsh environmental conditions, may survive the voyage in ballast water tanks and the discharge, and will possibly establish a population in the host environment.

In the near future, it is expected that most vessels will be equipped with ballast water treatment systems. These systems are not 100% effective in eliminating all organisms in the ballast tanks. Studies show regrowth of organisms after treatment with UV radiation and electro chlorination (e.g., *Casas-Monroy et al.* [2018]; *Jang et al.* [2020]; *Stehouwer et al.* [2015]. Ballast water treatment system still are considered as a solution to reduce aquatic invasions and their negative impact on ecosystems. However, the impact of treated ballast water on the aquatic ecosystems is not yet known.

The summer of 2020 recorded the second minimum Arctic sea ice extent of the satellite era. This summer also presented the longest navigable season of the Northeast

Passage with a total of 88 days[11]. The Northeast Passage was navigable from August to October. Arctic sea ice is expected to decrease during summer even more due to future climate changes, which in turn can lead to extended navigable seasons with increased number of individual vessels and voyages in the Arctic region, and thus to an increased number of ballast water discharges and accumulation areas. While years with less sea ice cover will attract ship traffic, and more resources are expected to be exported, the decrease of sea ice cover will possibly also influence changes in the ocean surface circulation, influencing ballast water accumulation and mixing patterns.

The results of this study demonstrated that ballast water discharged by cargo vessels in the Arctic shipping routes can accumulate in different areas, and can be harmful to coastal ecosystems. It also demonstrated that particles discharged with the ballast water can be advected to coastal ecosystems.

The Northwest Passage was not investigated in this thesis due to the small number of vessels in transit, limited to Hudson Strait, Davis Strait, and Baffin Bay. However, due to the recent increase in ship transits in this region, as well as a decrease in sea ice extent [*Goldsmit et al.*, 2019; *Guy and Lasserre*, 2016; *Pizzolato et al.*, 2016], it is worth prolongating model simulations with ship positions from the year 2014 onwards, especially in the Norwest Passage. With the opening of the Mary River Mine on Baffin Island, there was an increase in the seasonal traffic of bulkers in the Baffin Bay [*PAME*, 2020]. The Arctic Shipping Status Report (ASSR#1[*PAME*, 2020]) reported that the sailed distance of bulkers increased by 160% inside the Arctic Polar Code area between 2013 and 2019.

Due to low seawater temperatures, it is expected that non-indigenous organisms from mid and low latitudes that are released in the Northwest Passage have minimal chances of survival [*Goldsmit et al.*, 2019]. However, with a further decreased sea ice extent and increased navigation, non-indigenous species can be transported in ballast tanks into this environment. New studies concerning ballast water and non-indigenous species are necessary to understand and mitigate possible harm to the Northwest Passage ecosystem.

[11] https://global.weathernews.com/wp-content/uploads/2020/12/20201215-2.pdf

References

Aagaard, K., and E. C. Carmack (1989), The role of sea ice and other fresh water in the Arctic circulation, *Journal of Geophysical Research: Oceans*, *94*(C10), 14485-14498, doi:10.1029/JC094iC10p14485.

Aagaard, K., and L. Coachman (1975), Toward an ice-free Arctic Ocean, *Eos, Transactions American Geophysical Union*, *56*(7), 484-486.

Aagaard, K., L. K. Coachman, and E. Carmack (1981), On the halocline of the Arctic Ocean, *Deep Sea Research Part A. Oceanographic Research Papers*, *28*(6), 529-545, doi:https://doi.org/10.1016/0198-0149(81)90115-1.

Albaina Vivanco, A., I. Uriarte Capetillo, A. I. Aguirre Escobal, D. Abad García, M. A. Iriarte Gabicagogeascoa, L. F. Villate Guinea, and M. A. Estomba Recalde (2016), Insights on the origin of invasive copepods colonizing Basque estuaries; a DNA barcoding approach.

Amante, C., and B. Eakins (2009), ETOPO1 1 Arc-Minute Global Relief Model: Procedures, Data Sources and Analysis. NOAA Technical Memorandum NESDIS NGDC-24. National Geophysical Data Center, *Biblioteca Digital ILCE*, *1*.

An Open University Course, T. (1989), CHAPTER 3 - OCEAN CURRENTS, in *Ocean Circulation*, edited by T. An Open University Course, pp. 31-72, Butterworth-Heinemann, Oxford, doi:https://doi.org/10.1016/B978-0-7506-3716-9.50007-7.

Arrigo, K. R., G. van Dijken, and S. Pabi (2008), Impact of a shrinking Arctic ice cover on marine primary production, *Geophysical Research Letters*, *35*(19).

Blanke, B., and S. Raynaud (1997), Kinematics of the Pacific Equatorial Undercurrent: An Eulerian and Lagrangian Approach from GCM Results, *Journal of Physical Oceanography*, *27*(6), 1038-1053, doi:10.1175/1520-0485(1997)027<1038:Kotpeu>2.0.Co;2.

Brandon, M. A., F. R. Cottier, F. Nilsen, D. Thomas, and G. Dieckmann (2010), Sea ice and oceanography, *Sea Ice*, 79-111.

Brickman, D. (2006), Risk assessment model for dispersion of ballast water organisms in shelf seas, *Canadian Journal of Fisheries and Aquatic Sciences*, *63*(12), 2748-2759.

Brickman, D., and P. C. Smith (2007), Variability in invasion risk for ballast water exchange on the Scotian Shelf of eastern Canada, *Mar Pollut Bull*, *54*(7), 863-874, doi:10.1016/j.marpolbul.2007.03.015.

Briski, E., L. E. Allinger, M. Balcer, A. Cangelosi, L. Fanberg, T. P. Markee, N. Mays, C. N. Polkinghorne, K. R. Prihoda, and E. D. Reavie (2013), Multidimensional approach to invasive species prevention, *Environmental Science & Technology*, *47*(3), 1216-1221.

Brodie, P. (2014), *Commercial shipping handbook*, CRC Press.

Brubaker, R. D., and W. Østreng (1999), The Northern Sea Route Regime: Exquisite Superpower Subterfuge?, *Ocean Development & International Law*, *30*(4), 299-331, doi:10.1080/009083299276131.

Bryan, K. (1969), A numerical method for the study of the circulation of the world ocean, *Journal of computational physics*, *4*(3), 347-376.

Brylinski, J.-M., E. Antajan, T. Raud, and D. Vincent (2012), First record of the Asian copepod Pseudodiaptomus marinus Sato, 1913 (Copepoda: Calanoida: Pseudodiaptomidae) in the southern bight of the North Sea along the coast of France, *Aquat Invasions*, *7*(4).

CABI (2020), Compendium, Invasive Species, in *Wallingford, UK: CAB International*, edited.

Casas-Monroy, O., R. D. Linley, P.-S. Chan, J. Kydd, J. V. Byllaardt, and S. Bailey (2018), Evaluating efficacy of filtration+ UV-C radiation for ballast water treatment at different temperatures, *Journal of Sea Research*, *133*, 20-28.

Chan, F. T., K. Stanislawczyk, A. C. Sneekes, A. Dvoretsky, S. Gollasch, D. Minchin, M. David, A. Jelmert, J. Albretsen, and S. A. Bailey (2019), Climate change opens new frontiers for marine species in the Arctic: Current trends and future invasion risks, *Global Change Biology*, *25*(1), 25-38, doi:10.1111/gcb.14469.

Comiso, J. C. (2002), A rapidly declining perennial sea ice cover in the Arctic, *Geophysical Research Letters*, *29*(20), 17-11-17-14, doi:10.1029/2002gl015650.

Comiso, J. C. (2010), Variability and trends of the global sea ice cover, *Sea ice*, *2*, 205-246.

Comiso, J. C., and D. K. Hall (2014), Climate trends in the Arctic as observed from space, *Wiley Interdisciplinary Reviews: Climate Change*, *5*(3), 389-409.

Comiso, J. C., W. N. Meier, and R. Gersten (2017), Variability and trends in the Arctic Sea ice cover: Results from different techniques, *Journal of Geophysical Research: Oceans*, *122*(8), 6883-6900, doi:10.1002/2017jc012768.

Council, A. (2009), Arctic marine shipping assessment 2009 report, edited.

David, M. (2015), Vessels and ballast water, in *Global Maritime Transport and Ballast Water Management*, edited, pp. 13-34, Springer.

David, M., and S. Gollasch (2015), Ballast water management systems for vessels, in *Global Maritime Transport and Ballast Water Management*, edited, pp. 109-132, Springer.

David, M., S. Gollasch, B. Elliott, and C. Wiley (2015), Ballast water management under the ballast water management convention, in *Global maritime transport and ballast water management*, edited, pp. 89-108, Springer.

de Olazabal, A., and V. Tirelli (2011), First record of the egg-carrying calanoid copepod Pseudodiaptomus marinus in the Adriatic Sea, *Marine Biodiversity Records*, *4*.

de Rivera, C. E., B. P. Steves, P. W. Fofonoff, A. H. Hines, and G. M. Ruiz (2011), Potential for high-latitude marine invasions along western North America, *Diversity and Distributions*, *17*(6), 1198-1209, doi:10.1111/j.1472-4642.2011.00790.x.

Deschutter, Y., G. M. Vergara Grandes, J. Mortelmans, K. Deneudt, K. De Schamphelaere, and M. De Troch (2018), Distribution of the invasive calanoid copepod Pseudodiaptomus marinus (Sato, 1913) in the Belgian part of the North Sea, *Bioinvasions records*, *7*(1), 33-41.

DiBacco, C., D. B. Humphrey, L. E. Nasmith, and C. D. Levings (2012), Ballast water transport of non-indigenous zooplankton to Canadian ports, *Ices J Mar Sci*, *69*(3), 483-491, doi:10.1093/icesjms/fsr133.

Dieckmann, G. S., and H. H. Hellmer (2010), The importance of sea ice: an overview, *Sea ice*, *2*, 1-22.

Drinkwater, K. F. (2011), The influence of climate variability and change on the ecosystems of the Barents Sea and adjacent waters: Review and synthesis of recent studies from the NESSAS Project, *Progress in Oceanography*, *90*(1-4), 47-61.

Emami, K., V. Askari, M. Ullrich, K. Mohinudeen, A. C. Anil, L. Khandeparker, J. G. Burgess, and E. Mesbahi (2012), Characterization of Bacteria in Ballast Water Using MALDI-TOF Mass Spectrometry, *PLOS ONE*, *7*(6), e38515, doi:10.1371/journal.pone.0038515.

Endresen, O., H. L. Behrens, S. Brynestad, A. B. Andersen, and R. Skjong (2004), Challenges in global ballast water management, *Mar Pollut Bull*, *48*(7-8), 615-623, doi:10.1016/j.marpolbul.2004.01.016.

Epstein, P. R. (1995), The role of algal blooms in the spread and persistence of human cholera, *Harmful marine algal blooms. Edited by P. Lassus et al. Lavoisier, Paris*, 846.

Ferrari, R., and C. Wunsch (2009), Ocean circulation kinetic energy: Reservoirs, sources, and sinks, *Annual Review of Fluid Mechanics*, *41*.

Fieg, K., R. Gerdes, E. Fahrbach, A. Beszczynska-Moller, and U. Schauer (2010), Simulation of oceanic volume transports through Fram Strait 1995-2005, *Ocean Dynam*, *60*(3), 491-502, doi:10.1007/s10236-010-0263-9.

Galil, B. S., F. Boero, M. L. Campbell, J. T. Carlton, E. Cook, S. Fraschetti, S. Gollasch, C. L. Hewitt, A. Jelmert, and E. Macpherson (2015), 'Double trouble': the expansion of the Suez Canal and marine bioinvasions in the Mediterranean Sea, *Biological Invasions*, *17*(4), 973-976.

Gascard, J.-C., K. Riemann-Campe, R. Gerdes, H. Schyberg, R. Randriamampianina, M. Karcher, J. Zhang, and M. Rafizadeh (2017), Future sea ice conditions and weather forecasts in the Arctic: Implications for Arctic shipping, *Ambio*, *46*(3), 355-367.

Gerdes, R., M. Karcher, F. Kauker, and C. Köberle (2001), Predicting the spread of radioactive substances from the Kursk, *Eos, Transactions American Geophysical Union*, *82*(23), 253-257.

Gerdes, R., M. J. Karcher, F. Kauker, and U. Schauer (2003), Causes and development of repeated Arctic Ocean warming events, *Geophysical Research Letters*, *30*(19).

Goldsmit, J., P. Archambault, G. Chust, E. Villarino, G. Liu, J. V. Lukovich, D. G. Barber, and K. L. Howland (2018), Projecting present and future habitat suitability of ship-mediated aquatic invasive species in the Canadian Arctic, *Biological Invasions*, *20*(2), 501-517, doi:10.1007/s10530-017-1553-7.

Goldsmit, J., S. H. Nudds, D. B. Stewart, J. W. Higdon, C. G. Hannah, and K. L. Howland (2019), Where else? Assessing zones of alternate ballast water exchange in the Canadian eastern Arctic, *Mar Pollut Bull*, *139*, 74-90.

Gollasch, S., D. Minchin, and M. David (2015), The Transfer of Harmful Aquatic Organisms and Pathogens with Ballast Water and Their Impacts, in *Global Maritime Transport and Ballast Water Management: Issues and Solutions*, edited by M. David and S. Gollasch, pp. 35-58, Springer Netherlands, Dordrecht, doi:10.1007/978-94-017-9367-4_3.

Gregg, M. D., and G. M. Hallegraeff (2007), Efficacy of three commercially available ballast water biocides against vegetative microalgae, dinoflagellate cysts and bacteria, *Harmful Algae*, *6*(4), 567-584, doi:10.1016/j.hal.2006.08.009.

Gregory, G. J., and P. A. Quijón (2011), The impact of a coastal invasive predator on infaunal communities: Assessing the roles of density and a native counterpart, *Journal of Sea Research*, *66*(2), 181-186.

Griffiths, R. W., D. W. Schloesser, J. H. Leach, and W. P. Kovalak (1991), Distribution and dispersal of the zebra mussel (Dreissena polymorpha) in the Great Lakes region, *Canadian Journal of Fisheries and Aquatic Sciences*, *48*(8), 1381-1388.

Guy, E., and F. Lasserre (2016), Commercial shipping in the Arctic: new perspectives, challenges and regulations, *Polar Record*, *52*(3), 294-304, doi:10.1017/S0032247415001011.

Hallegraeff, G. M., and C. J. Bolch (1992), Transport of Diatom and Dinoflagellate Resting Spores in Ships Ballast Water - Implications for Plankton Biogeography and Aquaculture, *J Plankton Res*, *14*(8), 1067-1084, doi:DOI 10.1093/plankt/14.8.1067.

Hanzlick, D., and K. Aagaard (1980), Freshwater and Atlantic water in the Kara Sea, *Journal of Geophysical Research: Oceans*, *85*(C9), 4937-4942.

Haug, T., B. Bogstad, M. Chierici, H. Gjøsæter, E. H. Hallfredsson, Å. S. Høines, A. H. Hoel, R. B. Ingvaldsen, L. L. Jørgensen, and T. Knutsen (2017), Future harvest of living resources in the Arctic Ocean north of the Nordic and Barents Seas: a review of possibilities and constraints, *Fisheries Research*, *188*, 38-57.

Hibler, W. D. (1979), A Dynamic Thermodynamic Sea Ice Model, *Journal of Physical Oceanography*, *9*(4), 815-846, doi:10.1175/1520-0485(1979)009<0815:ADTSIM>2.0.CO;2.

Ho, J. (2010), The implications of Arctic sea ice decline on shipping, *Marine Policy*, *34*(3), 713-715.

Horton, T., et al. (2017), Improving nomenclatural consistency: a decade of experience in the World Register of Marine Species, *European Journal of Taxonomy*, *389*, 1-24, doi:10.5852/ejt.2017.389.

Ichikawa, S., Y. Wakao, and Y. Fukuyo (1992), Extermination Efficacy of Hydrogen-Peroxide against Cysts of Red Tide and Toxic Dinoflagellates, and Its Adaptability to Ballast Water of Cargo-Ships, *Nippon Suisan Gakk*, *58*(12), 2229-2233.

Jakobsson, M., A. Grantz, Y. Kristoffersen, R. Macnab, R. MacDonald, E. Sakshaug, R. Stein, and W. Jokat (2004), The Arctic Ocean: Boundary conditions and background information, in *The organic carbon cycle in the Arctic Ocean*, edited, pp. 1-32, Springer.

Jang, P.-G., B. Hyun, and K. Shin (2020), Ballast Water Treatment Performance Evaluation under Real Changing Conditions, *Journal of Marine Science and Engineering*, *8*(10), 817.

Jha, U., A. Jetter, J. A. Lindley, L. Postel, and M. Wootton (2013), Extension of distribution of Pseudodiaptomus marinus, an introduced copepod, in the North Sea, *Marine Biodiversity Records*, *6*, e53, doi:10.1017/S1755267213000286.

Jing, L., B. Chen, B. Zhang, and H. Peng (2012), A review of ballast water management practices and challenges in harsh and arctic environments, *Environmental Reviews*, *20*(2), 83-108.

Jørgensen, L. L., and V. Spiridonov (2013), Effect from the king-and snow crab on Barents Sea benthos. Results and conclusions from the Norwegian-Russian Workshop in Tromsø 2010.

Kaiser, B. A., M. Kourantidou, and L. Fernandez (2018), A case for the commons: the snow crab in the Barents, *Journal of environmental management*, *210*, 338-348.

Kalnay, E., M. Kanamitsu, R. Kistler, W. Collins, D. Deaven, L. Gandin, M. Iredell, S. Saha, G. White, and J. Woollen (1996), The NCEP/NCAR 40-year reanalysis project, *Bulletin of the American meteorological Society*, *77*(3), 437-471.

Karcher, M., J. N. Smith, F. Kauker, R. Gerdes, and W. M. Smethie (2012), Recent changes in Arctic Ocean circulation revealed by iodine-129 observations and modeling, *Journal of Geophysical Research: Oceans*, *117*(C8).

Katsanevakis, S., K. Bogucarskis, F. Gatto, J. Vandekerkhove, I. Deriu, and A. C. Cardoso (2012), Building the European Alien Species Information Network (EASIN): a novel approach for the exploration of distributed alien species data, *BioInvasions Record*, *1*(4).

Kauker, F., R. Gerdes, M. Karcher, C. Köberle, and J. L. Lieser (2003), Variability of Arctic and North Atlantic sea ice: A combined analysis of model results and observations from 1978 to 2001, *Journal of Geophysical Research: Oceans*, *108*(C6).

Kelly, S., E. Popova, Y. Aksenov, R. Marsh, and A. Yool (2018), Lagrangian Modeling of Arctic Ocean Circulation Pathways: Impact of Advection on Spread of Pollutants, *Journal of Geophysical Research: Oceans*, *123*(4), 2882-2902, doi:10.1002/2017jc013460.

Khon, V., I. Mokhov, M. Latif, V. Semenov, and W. Park (2010), Perspectives of Northern Sea Route and Northwest Passage in the twenty-first century, *Climatic Change*, *100*(3-4), 757-768.

Kideys, A. E. (2002), Fall and rise of the Black Sea ecosystem, *Science*, *297*(5586), 1482-1484.

Klassen, G. J., and A. Locke (2007), *A biological synopsis of the European green crab, Carcinus maenas*, Fisheries and Oceans Canada Moncton, New Brunswick, Canada.

Köberle, C., and R. Gerdes (2003), Mechanisms Determining the Variability of Arctic Sea Ice Conditions and Export, *Journal of Climate*, 16, doi:https://doi.org/10.1175/1520-0442(2003)016<2843:MDTVOA>2.0.CO;2.

Kovács, T. (2019), Wind stress forcing of the freshwater distribution in the Arctic and North Atlantic Oceans, IRC-Library, Information Resource Center der Jacobs University Bremen.

Larson, M. R., M. G. G. Foreman, C. D. Levings, and M. R. Tarbotton (2003), Dispersion of discharged ship ballast water in Vancouver Harbour, Juan De Fuca Strait, and offshore of the Washington Coast, *J Environ Eng Sci*, *2*(3), 163-176, doi:10.1139/S03-014.

Lenoir, S., G. Beaugrand, and E. Lecuyer (2011), Modelled spatial distribution of marine fish and projected modifications in the North Atlantic Ocean, *Global Change Biology*, *17*(1), 115-129.

Levitus, S., and T. Boyer (1994), World Ocean Atlas 1994, vol. 4, Temperature, NOAA Atlas NESDIS 4, edited, Natl. Oceanic and Atmos. Admin., Silver Spring, Md.

Levitus, S., R. Burgett, and T. Boyer (1994), World Ocean Atlas 1994, vol. 3, Salinity, NOAA Atlas NESDIS 3, *US Department of Commerce, Washington, DC*.

Liebich, V., P. P. Stehouwer, and M. Veldhuis (2012), Re-growth of potential invasive phytoplankton following UV-based ballast water treatment, *Aquat Invasions, 7*(1), 29-36, doi:10.3391/ai.2012.7.1.004.

Lind, S., R. B. Ingvaldsen, and T. Furevik (2018), Arctic warming hotspot in the northern Barents Sea linked to declining sea-ice import, *Nature Climate Change*, *8*(7), 634-639, doi:10.1038/s41558-018-0205-y.

Lockwood, J. L., P. Cassey, and T. Blackburn (2005), The role of propagule pressure in explaining species invasions, *Trends in ecology & evolution*, *20*(5), 223-228.

Loeng, and Drinkwater (2007), An overview of the ecosystems of the Barents and Norwegian Seas and their response to climate variability, *Deep Sea Research Part II: Topical Studies in Oceanography*, *54*(23-26), 2478-2500.

Loeng, Ozhigin, and Adlandsvik (1997), Water fluxes through the Barents Sea, *Ices J Mar Sci*, *54*(3), 310-317.

Lu, D., G.-K. Park, K. Choi, and S. Oh (2014), An economic analysis of container shipping through Canadian Northwest Passage, *International Journal of e-Navigation and Maritime Economy*, *1*, 60-72.

Lučić, D., P. MOZETič, J. France, P. Lučić, and L. Lipej (2015), Additional record of the non-indigenous copepod Pseudodiaptomus marinus (Sato, 1913) in the Adriatic Sea, *Acta Adriatica*, *56*(2), 275-282.

Luitjens, L. (2015), Study on the distribution of ballast water through shipping in the Arctic Ocean, 86 pp, Jade University of Applied Sciences, Elsfleth, Germany.

Mack, R. N., D. Simberloff, W. Mark Lonsdale, H. Evans, M. Clout, and F. A. Bazzaz (2000), Biotic invasions: causes, epidemiology, global consequences, and control, *Ecological applications*, *10*(3), 689-710.

Martínez-Moreno, J., A. M. Hogg, A. E. Kiss, N. C. Constantinou, and A. K. Morrison (2019), Kinetic energy of eddy-like features from sea surface altimetry, *arXiv preprint arXiv:1906.01929*.

Mauritzen, C., and S. Häkkinen (1997), Influence of sea ice on the thermohaline circulation in the Arctic-North Atlantic Ocean, *Geophysical Research Letters*, *24*(24), 3257-3260, doi:10.1029/97gl03192.

McCarthy, S. A., and F. M. Khambaty (1994), International dissemination of epidemic Vibrio cholerae by cargo ship ballast and other nonpotable waters, *Applied and environmental microbiology*, *60*(7), 2597-2601.

Meier, W. N., et al. (2014), Arctic sea ice in transformation: A review of recent observed changes and impacts on biology and human activity, *Reviews of Geophysics*, *52*(3), 185-217, doi:10.1002/2013rg000431.

Miller, A. W., and G. M. Ruiz (2014), Arctic shipping and marine invaders, *Nature Climate Change*, *4*(6), 413-416.

Molnar, J. L., R. L. Gamboa, C. Revenga, and M. D. Spalding (2008), Assessing the global threat of invasive species to marine biodiversity, *Frontiers in Ecology and the Environment*, *6*(9), 485-492.

Olbers, D., J. Willebrand, and C. Eden (2012), *Ocean dynamics*, Springer Science & Business Media.

Ostreng, W., K. M. Eger, B. Fløistad, A. Jørgensen-Dahl, L. Lothe, M. Mejlænder-Larsen, and T. Wergeland (2013), *Shipping in Arctic waters: a comparison of the Northeast, Northwest and trans polar passages*, Springer Science & Business Media.

Pacanowski, R. (1995), MOM 2 Documentation, users guide and reference manual, GFDL Ocean Group Technical Report 3, Geophys, *Fluid Dyn. Lab., Princeton University, Princeton, NJ*.

PAME (2020), Arctic Shipping Status Report #1*Rep.*

Perovich, D. K., J. A. Richter-Menge, K. F. Jones, and B. Light (2008), Sunlight, water, and ice: Extreme Arctic sea ice melt during the summer of 2007, *Geophysical Research Letters*, *35*(11), doi:10.1029/2008gl034007.

Perry, A. L., P. J. Low, J. R. Ellis, and J. D. Reynolds (2005), Climate change and distribution shifts in marine fishes, *science*, *308*(5730), 1912-1915.

Petersen, G. H. (1999), Five recent Mya species, including three new species and their fossil connections, *Polar Biology*, *22*(5), 322-328.

Petrich, C., and H. Eicken (2010), Growth, structure and properties of sea ice, *Sea ice*, *2*, 23-77.

Pharand, D. (2007), The Arctic waters and the Northwest Passage: A final revisit, *Ocean Development & International Law*, *38*(1-2), 3-69.

Pizzolato, L., S. E. Howell, J. Dawson, F. Laliberté, and L. Copland (2016), The influence of declining sea ice on shipping activity in the Canadian Arctic, *Geophysical Research Letters*, *43*(23), 12,146-112,154.

Proshutinsky, A. Y., and M. A. Johnson (1997), Two circulation regimes of the wind-driven Arctic Ocean, *Journal of Geophysical Research: Oceans*, *102*(C6), 12493-12514, doi:10.1029/97jc00738.

Reise, K., S. Gollasch, and W. J. Wolff (1998), Introduced marine species of the North Sea coasts, *Helgoländer Meeresuntersuchungen*, *52*(3), 219-234.

Rey, F. (2004), Phytoplankton: the grass of the sea, *The Norwegian Sea Ecosystem*, *6*(1), 97-136.

Ricciardi, A., et al. (2017), Invasion Science: A Horizon Scan of Emerging Challenges and Opportunities, *Trends in Ecology & Evolution*, *32*(6), 464-474, doi:https://doi.org/10.1016/j.tree.2017.03.007.

Richardson, P. L. (1983), Eddy kinetic energy in the North Atlantic from surface drifters, *Journal of Geophysical Research: Oceans*, *88*(C7), 4355-4367.

Ricker, R., S. Hendricks, L. Kaleschke, X. Tian-Kunze, J. King, and C. Haas (2017), A weekly Arctic sea-ice thickness data record from merged CryoSat-2 and SMOS satellite data, *Cryosphere*, *11*(4), 1607-1623.

Rosenhaim, I. L., K. Riemann-Campe, H. Sumata, C. Koeberle, R. Brauner, A. Herber, and R. Gerdes (2019), Simulated ballast water accumulation along Arctic shipping routes, *Marine Policy*, *103*, 9-18, doi:https://doi.org/10.1016/j.marpol.2019.02.013.

Roy-Barman, M., and C. Jeandel (2016), *Marine geochemistry: ocean circulation, carbon cycle and climate change*, Oxford University Press.

Rudels, B. (2009), Arctic Ocean Circulation A2 - Steele, John H, in *Encyclopedia of Ocean Sciences (Second Edition)*, edited, pp. 211-225, Academic Press, Oxford, doi:https://doi.org/10.1016/B978-012374473-9.00601-9.

Rudels, B. (2015), Arctic Ocean circulation, processes and water masses: A description of observations and ideas with focus on the period prior to the International Polar Year 2007–2009, *Progress in Oceanography*, *132*, 22-67, doi:https://doi.org/10.1016/j.pocean.2013.11.006.

Rudels, B. (2019), Arctic Ocean Circulation☆, in *Encyclopedia of Ocean Sciences (Third Edition)*, edited by J. K. Cochran, H. J. Bokuniewicz and P. L. Yager, pp. 262-277, Academic Press, Oxford, doi:https://doi.org/10.1016/B978-0-12-409548-9.11209-6.

Rudels, B., H. J. Friedrich, and D. Quadfasel (1999), The arctic circumpolar boundary current, *Deep-Sea Res Pt Ii*, *46*(6-7), 1023-1062.

Rudels, B., E. P. Jones, U. Schauer, and P. Eriksson (2004), Atlantic sources of the Arctic Ocean surface and halocline waters, *Polar Research*, *23*(2), 181-208, doi:10.1111/j.1751-8369.2004.tb00007.x.

Ruiz, G. M., J. T. Carlton, E. D. Grosholz, and A. H. Hines (1997), Global invasions of marine and estuarine habitats by non-indigenous species: mechanisms, extent, and consequences, *American zoologist*, *37*(6), 621-632.

Ruiz, G. M., P. W. Fofonoff, J. T. Carlton, M. J. Wonham, and A. H. Hines (2000), Invasion of coastal marine communities in North America: apparent patterns, processes, and biases, *Annual review of ecology and systematics*, *31*(1), 481-531.

Ruiz, G. M., and C. Hewitt (2009), Latitudinal patterns of biological invasions in marine ecosystems: a polar perspective.

Sabia, L., G. Zagami, M. Mazzocchi, E. Zambianchi, and M. Uttieri (2015), Spreading factors of a globally invading coastal copepod, *Mediterranean Marine Science*, *16*(2), 460-471.

Saloranta, T. M., and P. M. Haugan (2001), Interannual variability in the hydrography of Atlantic water northwest of Svalbard, *J Geophys Res-Oceans*, *106*(C7), 13931-13943.

Scriven, D. R., C. DiBacco, A. Locke, and T. W. Therriault (2015), Ballast water management in Canada: A historical perspective and implications for the future, *Marine Policy*, *59*, 121-133, doi:10.1016/j.marpol.2015.05.014.

Semtner, A. J. (1976), Model for Thermodynamic Growth of Sea Ice in Numerical Investigations of Climate, *Journal of Physical Oceanography*, *6*(3), 379-389.

Spreen, G., L. Kaleschke, and G. Heygster (2008), Sea ice remote sensing using AMSR-E 89-GHz channels, *Journal of Geophysical Research: Oceans*, *113*(C2).

Stehouwer, P. P., A. Buma, and L. Peperzak (2015), A comparison of six different ballast water treatment systems based on UV radiation, electrochlorination and chlorine dioxide, *Environmental technology*, *36*(16), 2094-2104.

Stevens, D. P. (1991), The open boundary condition in the United Kingdom fine-resolution Antarctic model, *Journal of Physical Oceanography*, *21*(9), 1494-1499.

Stroeve, J., and W. Meier (2018), Sea Ice Trends and Climatologies from SMMR and SSM/I-SSMIS, Version 3., edited, Boulder, Colorado USA. NASA National Snow and Ice Data Center Distributed Active Archive Center, doi: https://doi.org/10.5067/IJ0T7HFHB9Y6.

Takahashi, C. K., N. G. G. S. Lourenco, T. F. Lopes, V. L. M. Rall, and C. A. M. Lopes (2008), Ballast water: A review of the impact on the world public health, *J Venom Anim Toxins*, *14*(3), 393-408.

Talley, L. D. (2011), *Descriptive physical oceanography: an introduction*, Academic press.

Tamburri, M. N., K. Wasson, and M. Matsuda (2002), Ballast water deoxygenation can prevent aquatic introductions while reducing ship corrosion, *Biol Conserv*, *103*(3), 331-341, doi:Doi 10.1016/S0006-3207(01)00144-6.

Taylor, A., G. Rigby, S. Gollasch, M. Voigt, G. Hallegraeff, T. McCollin, and A. Jelmert (2002), Preventive treatment and control techniques for ballast water, in *Invasive Aquatic Species of Europe. Distribution, Impacts and Management*, edited, pp. 484-507, Springer.

Thresher, R. E., and A. M. Kuris (2004), Options for managing invasive marine species, *Biological Invasions*, *6*(3), 295-300.

Timofeev, V. (1963), Water interaction between the Arctic, Atlantic and Pacific oceans, *Oceanology*, *3*, 569-578.

Vallis, G. K. (2017), *Atmospheric and oceanic fluid dynamics*, Cambridge University Press.

Van Dokkum, K. (2003), Ship Knowledge–A modern encyclopedia, *Published by: DOKMAR, PO Box 360, 1600 AJ Enkhuizen, ISBN: 90-806330-2-X, Copyright 2003, DOKMAR*.

Vermeij, G. J., and P. D. Roopnarine (2008), The coming Arctic invasion, *Science*, *321*(5890), 780-781.

Volkov, V. A. (2002), *Polar seas oceanography : an integrated case study of the Kara Sea*, xxxvii, 450 p. pp., Springer ;

Praxis Pub., London ; New York

Chichester, UK.

Wadhams, P. (2000), *Ice in the Ocean*, CRC Press.

Wagner, P., S. Rühs, F. U. Schwarzkopf, I. M. Koszalka, and A. Biastoch (2019), Can Lagrangian Tracking Simulate Tracer Spreading in a High-Resolution Ocean General Circulation Model?, *Journal of Physical Oceanography*, *49*(5), 1141-1157, doi:10.1175/jpo-d-18-0152.1.

Wang, Q., N. V. Koldunov, S. Danilov, D. Sidorenko, C. Wekerle, P. Scholz, I. L. Bashmachnikov, and T. Jung (2020), Eddy Kinetic Energy in the Arctic Ocean From a Global Simulation With a 1-km Arctic, *Geophysical Research Letters*, *47*(14), e2020GL088550, doi:https://doi.org/10.1029/2020GL088550.

Ware, C., J. Berge, J. H. Sundet, J. B. Kirkpatrick, A. D. M. Coutts, A. Jelmert, S. M. Olsen, O. Floerl, M. S. Wisz, and I. G. Alsos (2014), Climate change, non-indigenous species and shipping: assessing the risk of species introduction to a high-Arctic archipelago, *Diversity and Distributions*, *20*(1), 10-19, doi:10.1111/ddi.12117.

Weeks, W. F., and S. F. Ackley (1986), The growth, structure, and properties of sea ice, in *The geophysics of sea ice*, edited, pp. 9-164, Springer.

Wells, M. G., S. A. Bailey, and B. Ruddick (2011), The dilution and dispersion of ballast water discharged into Goderich Harbor, *Mar Pollut Bull*, *62*(6), 1288-1296, doi:10.1016/j.marpolbul.2011.03.005.

Wilson, K. J., J. Falkingham, H. Melling, and R. De Abreu (2004), Shipping in the Canadian Arctic: other possible climate change scenarios, paper presented at IGARSS 2004. 2004 IEEE International Geoscience and Remote Sensing Symposium, IEEE.

Wisz, M. S., O. Broennimann, P. Grønkjær, P. R. Møller, S. M. Olsen, D. Swingedouw, R. B. Hedeholm, E. E. Nielsen, A. Guisan, and L. Pellissier (2015), Arctic warming will promote Atlantic–Pacific fish interchange, *Nature Climate Change*, *5*(3), 261-265, doi:10.1038/nclimate2500.

Wolfram, P. J., and T. D. Ringler (2017), Quantifying residual, eddy, and mean flow effects on mixing in an idealized circumpolar current, *Journal of Physical Oceanography*, *47*(8), 1897-1920.

Appendix

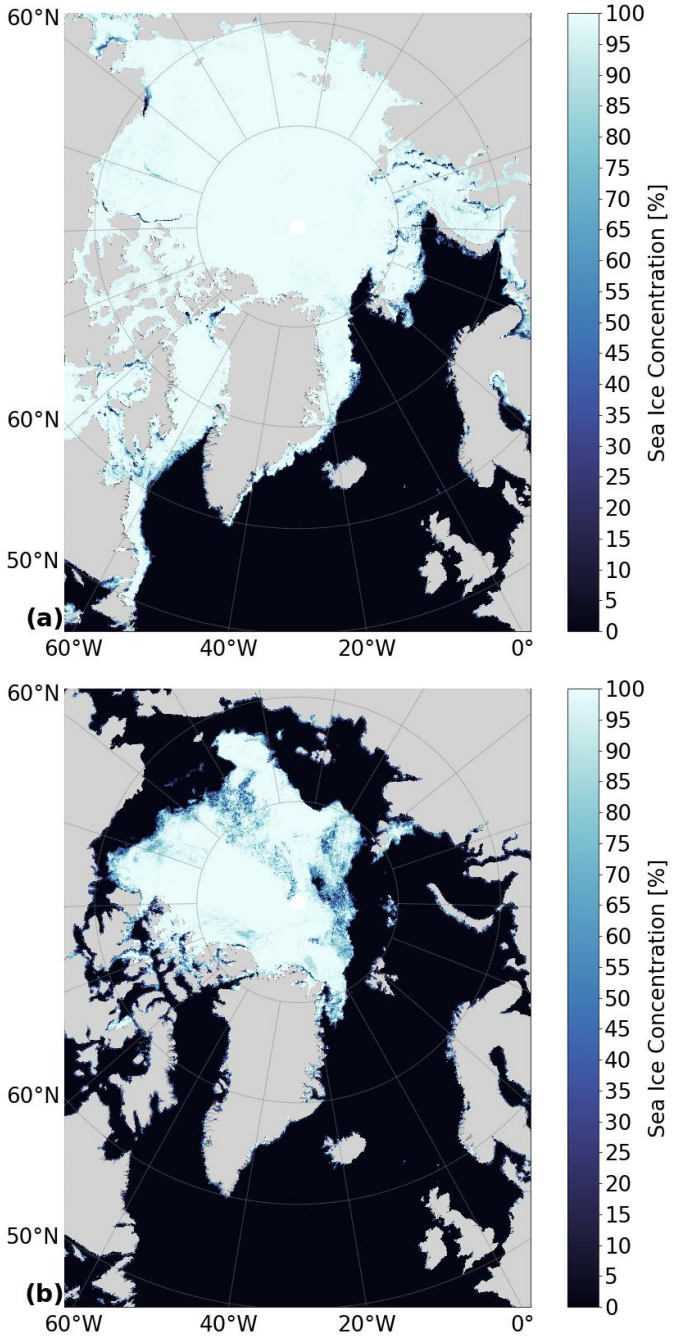

Figure A.01: Maximum (a) and minimum (b) average sea ice concentrations AMSR2 from Meereisportal [*Spreen et al.*, 2008]. (a) maximum average sea ice concentration in March and (b) minimum average sea ice concentration in September, 2013.

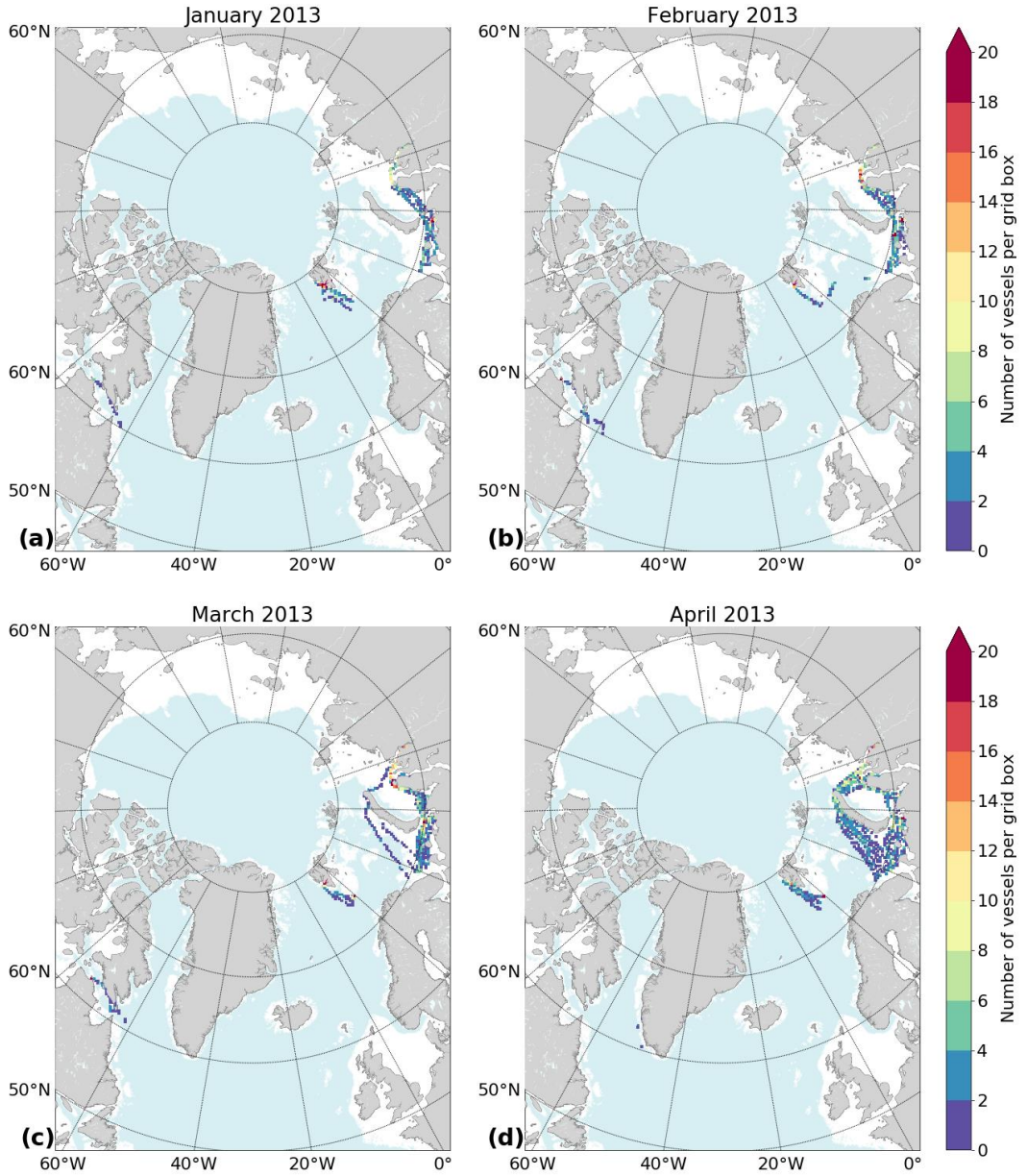

Figure A.02: Monthly ship-track density. (a) January, (b) February, (c) March, and (d) April 2013.

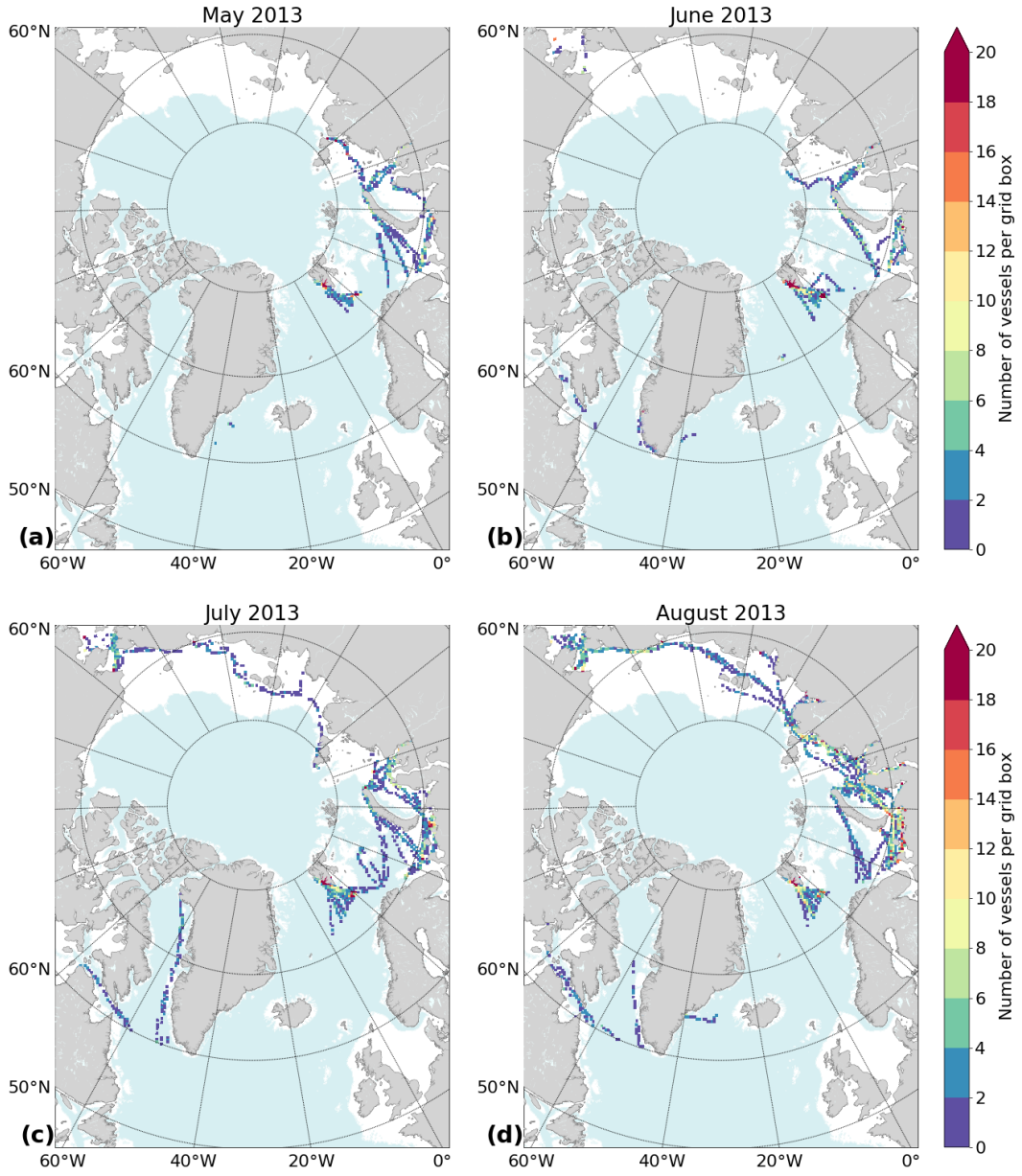

Figure A.03: Monthly ship-track density. (a) May, (b) June, (c) July, and (d) August 2013.

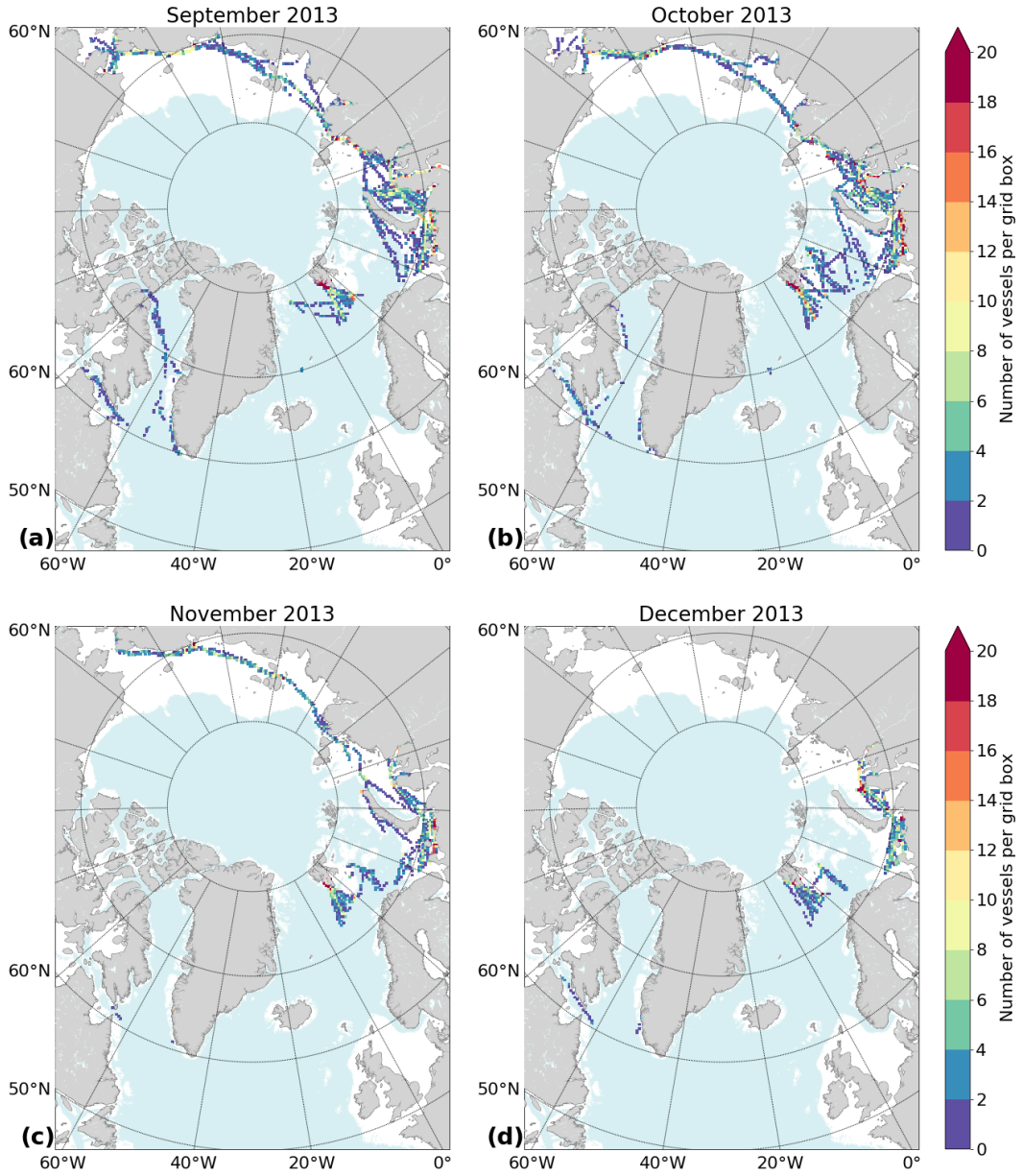

Figure A.04: Monthly ship-track density. (a) September, (b) October, (c) November, and (d) December 2013.

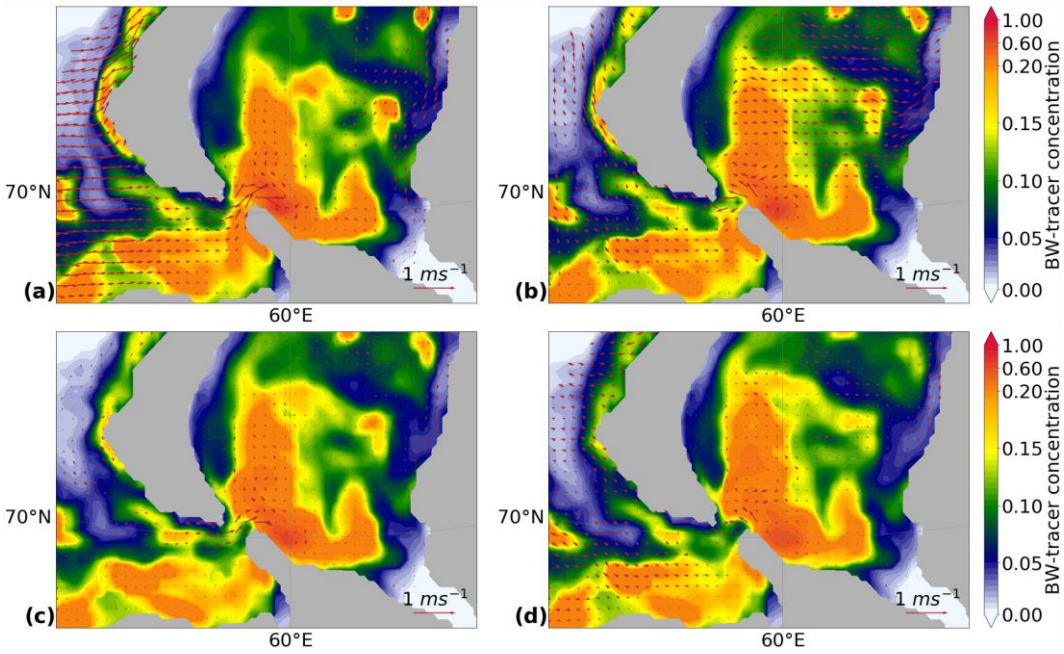

Figure A.05: Ballast water tracer in January 2014. (a) January 1st, (b) January 7th, (c) January 14th, and (d) January 25th, 2014.

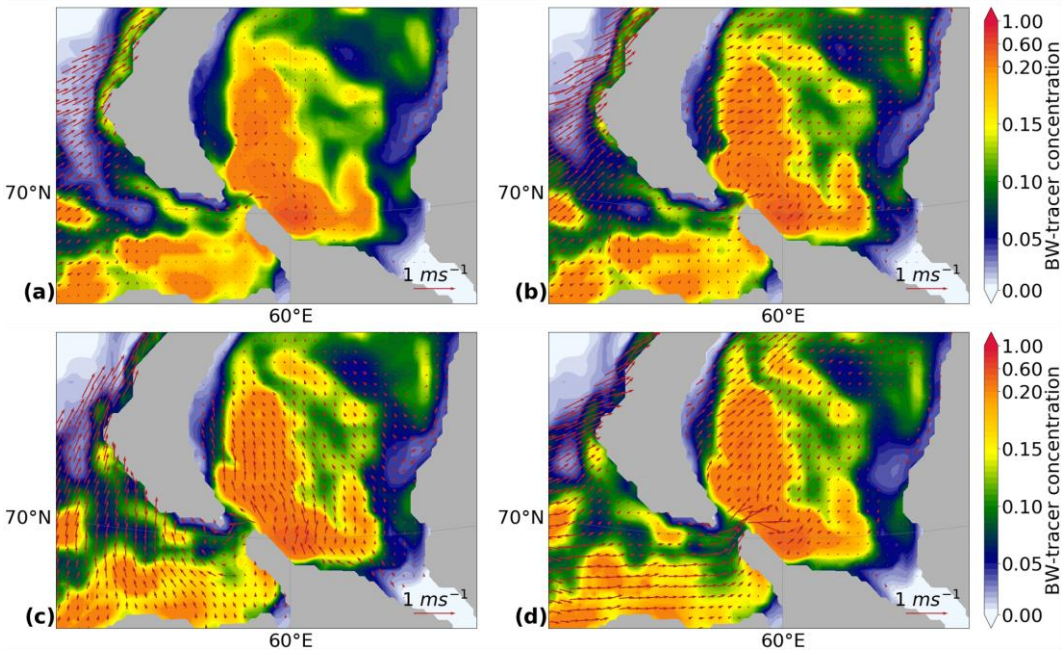

Figure A.06: Ballast water tracer in February 2014. (a) February 1st, (b) February 7th, (c) February 15th, and (d) February 21st, 2014.

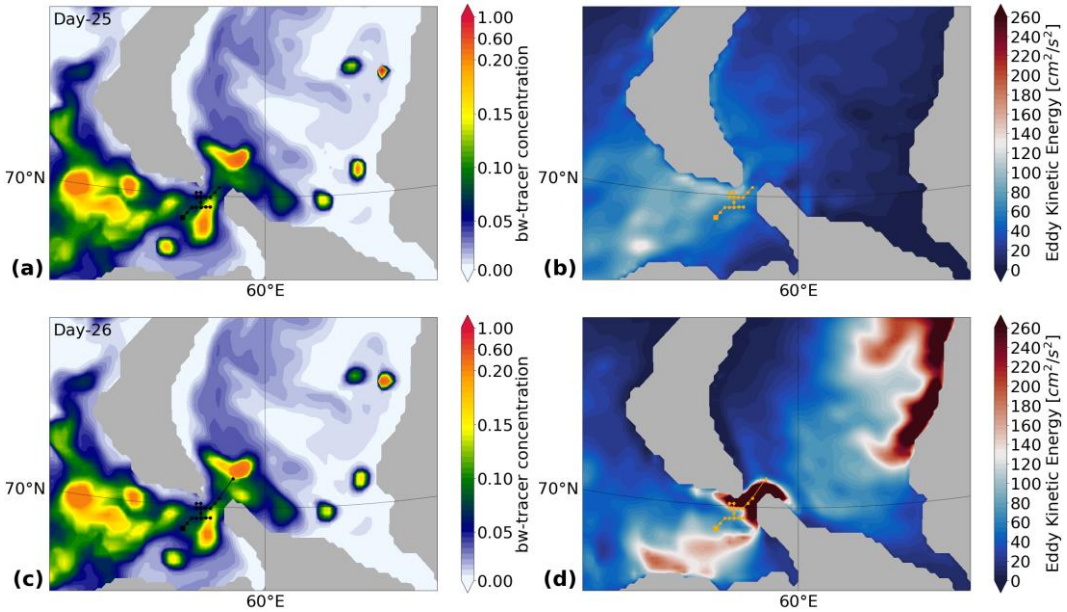

Figure A.07: Ballast water tracer concentration, eddy kinetic energy, and 1-day summer particle trajectory. The panels show the (a, c) ballast water tracer concentration (vertical integral) and (b, d) the eddy kinetic energy as background for the particle trajectory calculated with the 1-day summer velocity field.

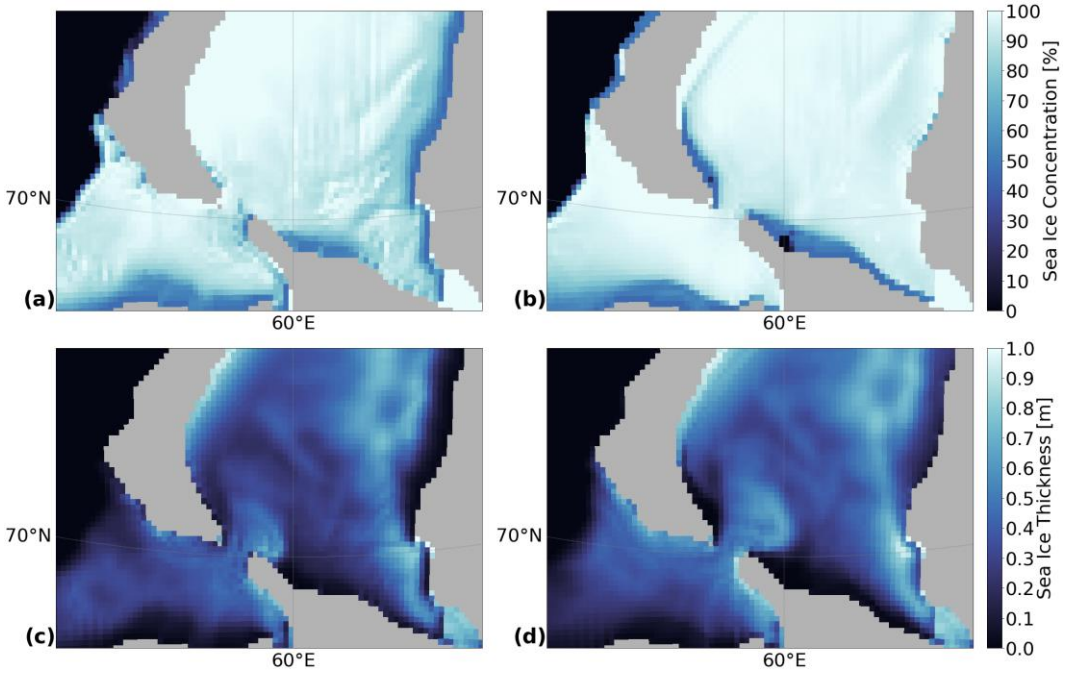

Figure A.08: Sea ice concentration in (a) January 21st and (b) January 31st. Sea ice thickness in (c) January 21st and (d) January 31st.

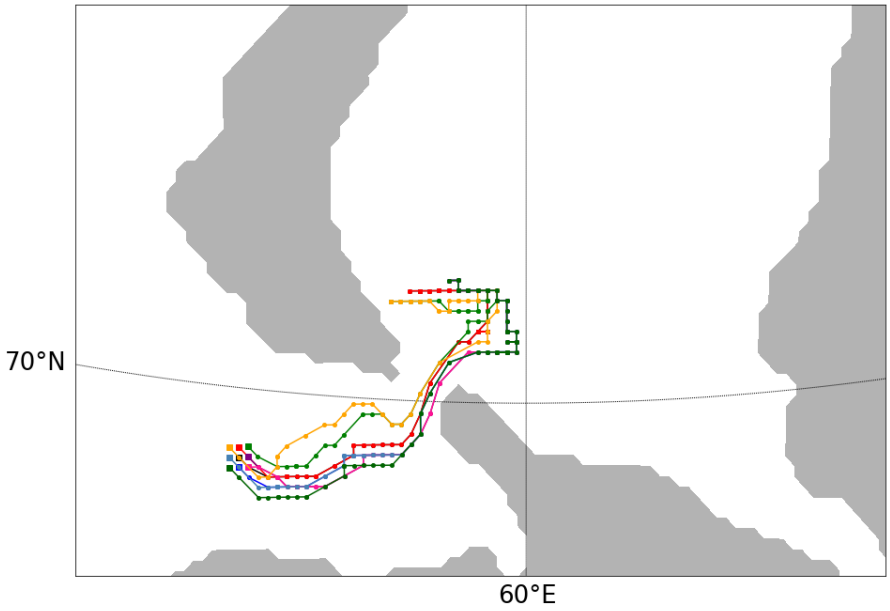

Figure A.09: Winter particle trajectories. Particle trajectories computed with 1-day velocity components. The trajectories have start positions around the main trajectory described in Chapter 5. The figure shows a total of nine different particle trajectory pathways.

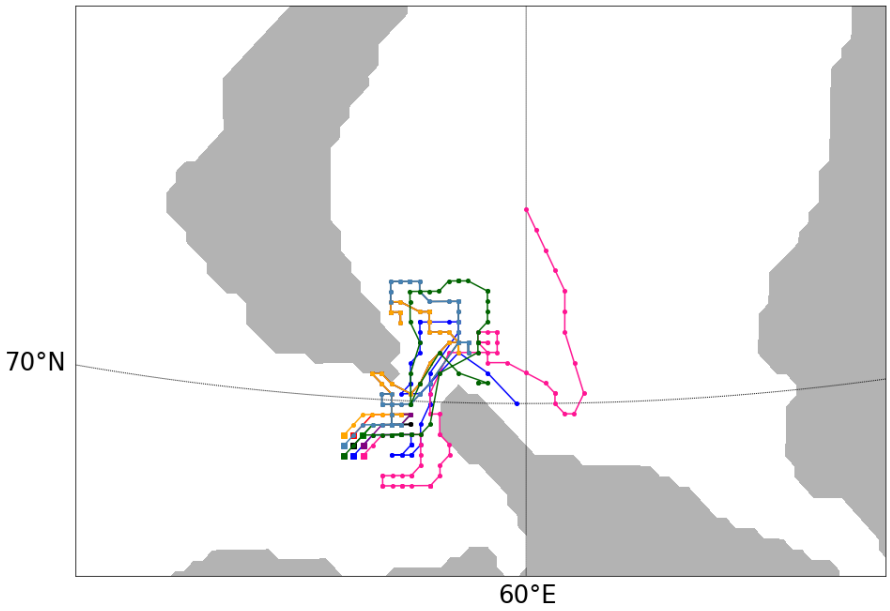

Figure A.10: Winter particle trajectories. Particle trajectories computed with 1-day velocity components. The trajectories have start positions around the main trajectory described in Chapter 5. The figure shows a total of nine different particle trajectory pathways.

Acknowledgements

Through the development and writing of this dissertation I have received a great deal of support and assistant.

I would like to thank my supervisor, Prof. Dr. Rüdiger Gerdes, for accepting me as his Ph.D. student and for receiving me at the Alfred Wegener Institute. Thank you for our scientific talks, for encouraging me and pushing me to keep learning, and for your guidance along this journey. I also would like to thank, my second supervisor, Prof. Dr. Laurenz Thomsen, for being part of my Dissertation Committee.

I would like to thank the members of my Dissertation Committee for all their support, help, and encouragements. Prof. Ralf Brauner, Dr. Andreas Herber, Dr. Hiroshi Sumata, and Dr. Kathrin Riemann-Campe.

I would like to thank the person that introduced me to NAOSIM, Cornelia Köberle. Thank you for showing me how the model works, for all the help, especially with the tracer, and for all the patience. And thank you for the gardening tips.

I would like to thank Lisa Marie Luitjens for preparing the ship dataset so thoroughly, but especially for your friendship.

I would like to thank the Environmental Research and Development department of DNVGL for making the ship data available for Lisa, and myself.

I would like to thank the Reederei Drevin from Cuxhaven for the opportunity to travel with Thetis-D from Bremerhaven to St. Petersburg and back, for the opportunity of learning how the work in a container ship is done. The Baltic Sea from the bridge of a ship, is incredible.

I would like to thank the colleagues and friends of the Sea Ice Physics section (AWI), Dr. Michael Karcher and especially Dr. Frank Kauker, for dealing with my stupid questions, but always taking time for helping me. My long-time office colleagues, Dr. Tamas Kovacs, and Behnam Zamani, for the friendship, support, and laughs. Dr. Hiroshi Sumata thank you for all the Fortran instructions, Python conversation, and modelling tips. Dr. Kathrin

Riemann-Campe, thank you for never letting me down, for all the support, for teaching me Python, and sharing knowledge.

I would like to thank POLMAR. The Claudias and Dörte, for their support along this journey to its end, for organizing and offering incredible workshops, and for the PhD Days giving us the opportunity to present our work, and network with our fellow PhD students.

I am grateful for all the people that I met along these years. Thank you for the good times, and for your friendship.

I have a few special thanks. To my friend Kathrin, my first friend in Bremerhaven, to my dear Mariam, to Estelle, Antonia, Jörg, Kristina, Madlen, Dragos, Rafael, Bruno, Claudia, Jenny, Anja, Lera, Nok, Steffi, Giulia, Michael, Paul, Christopher, Myriel, Ralf, Miriam, and so many others. Thank you for your friendship.

I would like to thank my old friends, too. The ones that are part of my journey for so long, and even being so far physically, are always with me. Thank you Patrícia and Luiz Felipe. For all the support, for this long friendship, and for being the best friends any one could have. Without you two I don't know who or where I would be. Thank you.

I am grateful for the love and support my family has given me my whole life. To my parents, Margareth and Paulo, to my brother, Henery, to my niece, Bia, and to Dinda Mila. And also, to my extended family, the Pinkernells. Thank you all for loving, accepting, supporting, and believing in me.

I am grateful, for the best boyfriend, the best man, the best partner, Stefan. Thank you for loving me, for inspiring me to be a better person. Thank you for your unconditional support and for believing in me. I love you.

This Ph.D. study was financed by the Brazilian National Council for Scientific and Technological Development CNPq/Brazil in the form of a scholarship (grant no.: 248432/2013-3). Thank you for the financial support.

The sea ice concentration data from DATE to DATE were obtained from http://www.meereisportal.de (grant: REKLIM-2013-04).

The merging of CryoSat-2 und SMOS data was funded by the ESA project SMOS+ Sea Ice (4000101476/10/NL/CT and 4000112022/14/I-AM) and data from DATE to DATE were obtained from http://www.meereisportal.de (grant: REKLIM-2013-04).